LA-13439-C
Conference

UC-714
Issued: April 1998

Proceedings of the Nuclear Criticality Technology Safety Project

San Diego, California
May 16-17, 1995

Compiled by
Rene G. Sanchez

Los Alamos
NATIONAL LABORATORY
Los Alamos, New Mexico 87545

DISCLAIMER

DISCLAIMER

Portions of this document may be illegible in electronic image products. Images are produced from the best available original document.

TABLE OF CONTENTS

Proceedings of the Nuclear Criticality Technology Safety Project

May 16 – 17, 1995

Abstract

This document contains summaries of most of the papers presented at the 1995 Nuclear Criticality Technology Safety Project (NCTSP) meeting, which was held May 16 and 17 at San Diego, Ca. The meeting was broken up into seven sessions, which covered the following topics: (1) Criticality Safety of Project Sapphire; (2) Relevant Experiments For Criticality Safety; (3) Interactions with the Former Soviet Union; (4) Misapplications and Limitations of Monte Carlo Methods Directed Toward Criticality Safety Analyses; (5) Monte Carlo Vulnerabilities of Execution and Interpretation; (6) Monte Carlo Vulnerabilities of Representation; and (7) Benchmark Comparisons.

Agenda

Nuclear Criticality Technology Safety Project Workshop
May 16-17, 1995

Tuesday, May 16 (Kon Tiki Ballroom)

Registration		0730-0830
Introduction & Opening Remarks	Burton Rothleder (DOE/EH-31)	0830-0840
Keynote Speaker	Neal Goldenberg (DOE/HQ)	0840-0910
Announcements & Break		0910-0930
Session I, Chair - Dennis Tollefson (ORNL) Criticality Safety of Project Sapphire		
Speaker	Topic	
Richard G. Taylor (ORNL)	Overview of Project Sapphire	0930-1000
Allan W. Krass (ORNL)	Case Studies of U(100)-Be-H_2O Systems in Support of Project Sapphire	1000-1030
Kenneth D. Lewis (ORNL)	Dose Rate Estimates for Uranium-Beryllium Compounds in the Sapphire Project	1030-1100
Dennis A. Tollefson/ R . Chris Robinson/ Joseph C. Turner/ Gary R. Smolen (ORNL)	Nuclear Criticality Safety Evaluation of the Project Sapphire U/Be Alloys and Compounds for International Shipment	1100-1130
Lunch		1130-1300

Session II, Chair -
Richard Anderson (LANL)
Relevant Experiments For Criticality Safety

Speaker	Topic	
David K. Hayes (DNFSB)	Design of a Critical Assembly for Testing Integral Properties of Materials	1300-1320
Rene Sanchez (LANL)	Critical Mass of Np-237	1320-1340
John T. Mihalczo (ORNL)	Small Beryllium and Graphite Reflected Critical Experiments	1340-1400
Ken Butterfield (LANL)	SHEBA Experiments	1400-1420
Robert Kimpland (LANL)	Dynamic Modeling of SHEBA Excursions	1420-1440
John T. Mihalczo (ORNL)	Bias in Calculated k_{eff} from Subcritical Measurements by the Cf-252 Source Driven Method	1440-1500
Peter Jaegers (LANL)	Comparison of Numerical and Experimental Multiplications in Subcritical Systems	1500-1520
Charles A. Goulding (LANL)	Proposed Source Jerk Measurements	1520-1540
Announcements & Break		1540-1600

Session II, Chair -
Thomas McLaughlin(LANL)
Interactions with the Former Soviet Union

Richard E. Anderson (LANL)	LANL Activities for Lab-to-Lab	1600-1630
Thomas McLaughlin (LANL)	Criticality Safety Issues	1630-1700

Stuart Vessard (LANL)	Determining Small delta-K-effectives Using Standard Monte Carlo Techniques	1130-1150
Todd J. Urbatsch/ Edward Larsen (University of Michigan)	Acceleration of Monte Carlo Criticality Calculations	1150-1210
	Discussion	1210-1230
Lunch		1230-1400

Session III, Co-Chairs-
R. Michael Westfall (ORNL)/Robert Roussin CSEWG (ORNL)
Monte Carlo Vulnerabilities of Representation

Speaker	Topic	
L. C. Leal/W. C. Jordan/ R. Q. Wright (ORNL)	Nuclear Data for Criticality Safety---- Current Issues	1400-1425
R. Michael Westfall/L. C. Leal (ORNL)	Multigroup Cross Section Representation	1425-1450
P. J. Collins/S. E. Aumeier (ANL)	Utilization of VIM Monte Carlo Calculations for Fast Reactor Experimental Data Analysis	1450-1515
R. E. McFarlane/S. C. Frankle (LANL)	Testing of the ENDF/B-VI Neutron Data Library ENDF60 for Use with MCNP™	1515-1540
	Discussion/Break	1540-1600

Session IV, Co-Chairs-
Burton Rothleder (DOE/EH-31)/ Richard E. Anderson (LANL)
Benchmark Comparisons

Speaker	Topic	
S. M. Bowman/W. C. Jordan/ D. F. Hollenbach (ORNL)	Validation of SCALE ENDF/B-V and ENDF/B-VI Cross Section Libraries	1600-1625
R. W. Schaefer/R. D. McKnight/ P. J. Collins (ANL)	Lessons Learned from Applying VIM to Fast Reactor Critical Experiments	1625-1650
Roger N. Blomquist (ANL)	Monte Carlo Analysis a of Loosely Coupled Reactor	1650-1715

Wednesday, May 17 (Kon Tiki Ballroom)

Embedded Topical Meeting
Misapplications and Limitations of Monte Carlo
Methods Directed Toward Criticality Safety Analyses

Speaker	Topic	
Burton Rothleder (DOE/HQ)	Introduction-Deterministically and Stochastically Based Solutions	0800-0810
Session I, Co-Chairs- R. Arthur Forster (LANL)/ Edward Fujita (ANL) The K-effective of the World		
G. Elliott Whitesides (ORNL, Retired)	A Difficulty in Computing the K-effective of the World, Revisited	0810-0835
Ely M. Gelbard (ANL)	Pitfalls in Criticality Safety Monte Carlo Computations: "The K-effective of the World"	0835-0900
Nigel R. Smith (AEA Technology)	Experiences with the Superhistory Powering Algorithm in MONK	0900-0925
G. Elliott Whitesides (ORNL, Retired)/ Ely M. Gelbard (ANL)/ Nigel R. Smith (AEA Technology)	Panel Discussion	0925-0950
	General Discussion	0950-1015
Break		1015-1030
Session II, Co-Chairs- R. Arthur Forster (LANL)/ Edward Fujita (ANL) Monte Carlo Vulnerabilities of Execution and Interpretation		
Speaker	Topic	
Daniel. F. Hollenbach/ Lester. M. Petrie (ORNL)	Assurances Associated with Monte Carlo Code Results	1030-1050
R. Arthur Forster/ Thomas E. Booth (LANL)	New MCNP Statistical Analyses for Criticality	1050-1110
Todd J. Urbatsch/R. Arthur Forster/ Richard E. Prael/ Richard J. Beckman (LANL)	Estimation and Interpretation of k_{eff} Confidence Intervals in MCNP	1110-1130

Agenda

Working Group Sessions
May 15, 1995

Monday, May 15, 1995	Chairperson	Meeting Room	Time
Registration		Aviary Foyer	0730 - 0800
Physics Criteria for Benchmarks	M. Westfall/ N. Landers	Toucan	0800 - 1000
Evaluation Techniques	J. Bazley	Macaw	0800 - 1000
Parametric Studies	H. Toffer	Toucan	1000 - 1200
Lunch			1200 - 1300
Experimental Needs	D. Rutherford	Toucan	1300 - 1500
Training	M. Crowell	Macaw	1300 - 1500
Rules, Regulations, and Standards	B. Rothleder	Toucan	1500 - 1700

TUESDAY, MAY 16, 1995

SESSION I

CRITICALITY SAFETY OF PROJECT SAPPHIRE

DESCRIPTION OF PROJECT SAPPHIRE

R. G. Taylor

SUMMARY

The mission of Project Sapphire was to repackage approximately 600 kg of highly enriched uranium (HEU) in the Republic of Kazakhstan into internationally acceptable shipping packages and transport the material to a storage location in the United States. There were four material types to be repackaged: metal; oxide; uranium/beryllium (U/Be) alloy; and residues from U/Be alloy production. Seven major steps were necessary for successful execution of the project: planning and training; readiness assessment; deployment; set up; process; take down; and transport. Nuclear criticality safety especially affected several of these steps.

Planning and Training

During this initial phase of the project, it was necessary to determine the size and composition of the team necessary to accomplish the mission over a period of approximately six weeks. It was also necessary to define the process and determine all the equipment and supplies necessary for the team to be essentially self-sufficient, identify and resolve issues, and train the team.

The team decided upon included 31 persons as shown in Table 1. The expertise of the personnel selected is also indicated in the table. The shipping package selected was the U. S. Department of Transportation (DOT) Specification 6M under Certificate USA/0002/B( )F, Revision 13.

The use of 6M packaging raised two issues of nuclear criticality safety concern. The packaging has mass limits and hydrogen moderation limits depending upon the material form. Depending upon the Transportation Index desired, there are mass limits for metal or alloy with a hydrogen to ^{235}U atomic ratio ($H/^{235}U$) = 0 and for compounds with either $H/^{235}U = 0$ or $H/^{235} \leq 3$. Much of the material to be repackaged contained beryllium, which is considered to be a moderator, and it was suspected that any original nuclear criticality safety analyses done to establish container loading limits had not contemplated the presence of beryllium. It was thus necessary to perform extensive calculations to demonstrate the safety of 6M packages for a variety of U/Be loadings. The second issue, which affected the equipment taken and the repackaging process design, was the need to verify that $H/^{235}U \leq 3$ in the residues. The planned repackaging process flow had to include sampling steps and the equipment taken had to include a laboratory induction furnace and support equipment and supplies for the measurement of hydrogen so the $H/^{235}U$ ratio could be calculated.

During this phase of the project, it was also necessary to generate subcritical limit data for U/Be systems for use in evaluating the safety of the process. Extensive calculations were done to

develop limits for mass, volume, infinite length cylinder diameter, and infinite extent slab thicknesses as a function of uranium concentration for HEU/Be and HEU/Be/water systems. These parameters are analogous to the limits data shown in reference 1 and the developed limits were used to analyze the nuclear criticality safety of the process as project planning proceeded.

Table 1. Project Sapphire Team Size and Composition

25 Lockheed Martin Energy Systems Persons
- 2 Project Management
- 8 Material Processing
- 2 Nondestructive Analysis
- 1 Nuclear Material Control & Accountability
- 3 Health Physics
- 3 Nuclear Criticality Safety
- 1 Industrial Hygiene
- 2 Packaging
- 3 Maintenance

1 OAK RIDGE INSTITUTE FOR SCIENCE AND EDUCATION PERSON
Medical Doctor

1 EG&G MEASUREMENTS INC. PERSON
Communications

4 ON SITE INSPECTION AGENCY PERSONS
- 3 Interpreters
- 1 Liaison with Embassy

The process which ultimately evolved included two repackaging glovebox lines, one sampling glovebox line, a hydrogen measurement station, a nondestructive analysis (NDA) measurement station, two accountability scales stations, and a 6M container loading area. Ventilation of the glovebox lines was through multiple High Efficiency Particulate Air (HEPA) filters. The process work area available was approximately 6 meters by 18 meters.

Major administrative issues which had to be addressed included indemnification by the U. S. Department of Energy because civilian employees of a contractor to the government would be performing hands-on nuclear work in another country and modifications to National Environmental Policy Act (NEPA) documents to accommodate the storage of HEU not of U. S. origin. It was also necessary to produce operating procedures and emergency procedures.

The actual hands-on repackaging of fissile material was to be done by the Lockheed Martin personnel indicated in Table 1 except for the three maintenance persons. Background training of these hands-on persons in subjects such as Fissile Material Worker/Supervisor, Radiation Worker, Beryllium Worker, and Respiratory Protection was accomplished by classroom instruction and practical demonstration. Process operation training was accomplished using operating procedures and a mock-up of the process facility. The mock-up was somewhat crude in that cardboard boxes on tables were used to simulate gloveboxes and hoods, but it was valuable in providing realism and did result in several procedure changes as problems were found. It did also emphasize that the actual facility would be somewhat cramped.

Readiness Assessment

Near the end of the planning and training phase, a small, proficient, and tough Readiness Assessment Team (RAT) was formed to examine every aspect of the project (they were affectionately called RATs after their team acronym). The RATs raised issues and made recommendations and were the final authority on their resolution. The process was agonizing but valuable and several changes were made because of the issues raised by the RATs.

Deployment

Beginning 7 October 1994, the 31 team members and 130 tons of equipment were deployed. Transport to Ust Kamenogorsk, Kazakhstan, was via three U. S. Air Force C-5 transport aircraft which proceeded separately from Knoxville, Tennessee, with two intermediate refueling stops. After arrival at Ust Kamenogorsk, equipment was off-loaded onto Ulba Metallurgical Plant vehicles and transported to the work site at the Ulba Metallurgical Plant. Team members were transported to the Hotel Irtysh which was to be home for the next month and a half.

Set-Up

Process and process support equipment were uncrated and set up over a 4 day period. At the work site, tents and hutments were erected, two diesel powered generators were set up along with their electrical grid, and a field office/command center with communications equipment was established. The repackaging and sampling glovebox lines were constructed along with the process ventilation system, hydrogen analysis, and NDA stations. Two portable criticality accident alarm monitors were emplaced to supplement the host's fixed system and they were tested using a radiation source. Personal protective equipment such as clothing, a variety of gloves, and respirators was unpacked and issued. Health physics and industrial hygiene monitoring equipment was made ready for use. After the process and process support equipment was set up and shown to be functional, several emergency drills were conducted to demonstrate evacuation routes and procedures.

Process

Typical repackaging involved receipt of requested process containers from the host followed by opening of the containers and transfer of the contents into packing cans. Packing cans were stainless steel cans of 120 mm diameter and were available in two lengths, 127 mm and 178 mm. Process container opening and contents transfer were conducted within connected gloveboxes. Limits for packing cans had been established and the packing can being loaded was on a scale during loading. Following loading, a lid was crimped on in a hood which was part of each repackaging glovebox line and the packing can was decontaminated before removal to the accountability scales and NDA station.

After NDA determination, each can was taken to the container loading area for placement into the Specification 2R inner containment vessel which was located within each 6M container. Up to three of the 178 mm length packing cans or four of the 127 mm packing cans could be placed within the payload volume of the Specification 2R inner container. Depending upon the material being packaged and the desired transport index, it was sometimes necessary to include empty packing cans within the 2R vessel because the mass was contained within fewer packing cans than the 2R vessel could hold. Padding between the packing cans and between the packing cans and the ends of the 2R vessel was provided by stainless steel wool pads. After eight 6M containers had been packed, they were assembled into Cargo Restraint Transporters (CRTs) which were turned over to the host for storage.

The four main material types were individually campaigned for repackaging to minimize the opportunities for error. The order in which materials were repackaged was: (1) metal; (2) oxide; (3) U/Be alloy; and (4) U/Be alloy production residues.

Concurrent with repackaging, selected containers of residues were sampled and the samples analyzed to determine hydrogen content. The trend which emerged was that low uranium equity residues had enough hydrogen (or too little uranium) to exceed the $H/^{235}U \leq 3$ specification. It was necessary to thermally process these materials. Thermal processing in the work area using a laboratory muffle furnace proved to be hopelessly optimistic and the materials were processed by the host. The thermally processed materials were returned as relatively large fused pieces and it was necessary to break them up using hammers in the gloveboxes to obtain acceptable packing can loading levels.

The contents of approximately 1200 of the host's process containers were transferred into approximately 1400 packing cans which were packaged into approximately 450 6M containers. Twenty five working days were required to complete the repackaging. The typical work day was nominally 12 hours and the typical work week was 6 days, Sunday through Friday. During the repackaging process effort, a startup crew left the hotel for the work site about an hour ahead of the rest of the team to prepare the process lines for production. The full team returned to the hotel together at the end of the work day. One meal was provided at the work site each working day

and it was a military Meal, Ready-to-Eat (MRE) which had been brought with the equipment and supplies for the project.

Take-Down

After repackaging was completed, process and support equipment was taken down, inspected, crated, and sealed in preparation for transport. Most of the contaminated process equipment was left with the host and some training was provided in its use. Personal protective equipment was also left with our host. Two and one half days were required to take down the process, break the work camp, and prepare for transport.

Transport

For transport, CRTs were convoyed from storage in the Ulba Metallurgical Plant to the Ust Kamenogorsk airport and loaded aboard C-5 aircraft. Approximately half the containers were aboard the first aircraft which departed on 20 November with the remainder aboard a second aircraft departing 21 November. Approximately half the team rode on each aircraft and each aircraft proceeded nonstop from Ust Kamenogorsk to Dover Air Force Base in Dover, Delaware. Two aerial refuelings and about 20 hours flying time were required. After arrival, the CRTs were loaded aboard Safe, Secure Trailers (SSTs), which are used for domestic transport of safeguardable quantities of special nuclear material, and transported to storage at the Oak Ridge Y-12 Plant.

Conclusion

Participation in Project Sapphire was a challenging and valuable experience because it permitted nuclear criticality safety personnel to perform hands-on work with fissile materials and to experience real life, real time operating problems. Project Sapphire itself was complex because it required coordination with three Cabinet Departments and it was unique and unprecedented in that no similar activity is known to have been conducted before. It was also conducted safely with no one hurt.

References

1. J. T. Thomas, Editor, "Nuclear Criticality Safety Guide TID-7016 Revision 2," NUREG/CR-0095, ORNL/NUREG/CSD-6, Union Carbide Corporation, Nuclear Division, Oak Ridge, Tennessee (June 1978).

NUCLEAR CRITICALITY SAFETY EVALUATION OF THE PROJECT SAPPHIRE U/BE ALLOYS AND COMPOUNDS FOR INTERNATIONAL SHIPMENT

Dennis A. Tollefson
Joseph C. Turner
R. Chris Robinson, Kenneth D. Lewis,
Richard G. Taylor, Larry C. Masters, Allan W. Krass
Martin Marietta Energy Systems, Inc.

Beth E. McKenzie
Pinkerton Government Services

1.0 BACKGROUND

In the early days of 1994, while news stories of nuclear materials allegedly being smuggled out of former Soviet Union republics were focusing attention on nuclear non-proliferation issues, President Bill Clinton was actively doing something to eliminate one such potential source of nuclear weapons grade materials. By early summer, negotiations between the USA and the Republic of Kazakhstan for the removal (by the USA) of several hundred kilograms of highly enriched uranium had reached such a high probability of success that full-scale planning activities for Project Sapphire were put into high gear. The mission of Project Sapphire was to remove almost 600 hundred kilograms of highly enriched uranium materials from storage containers at the Ulba Metallurgical Plant in Ust-Kamenogorsk in the Republic of Kazakhstan, repack the materials into steel cans, package these cans into shipping containers, and then transport these materials safely to the Oak Ridge Y-12 Plant for safeguarded temporary storage. This operation was directed by the United States Departments of Energy, Defense, and State, with the cooperation of the government of the Republic of Kazakhstan. Personnel from Martin Marietta Energy Systems, Inc. (MMES), and the Oak Ridge Department of Energy (DOE/OR) planned the packing and packaging operations, including life-size mock-ups of operating glove box packing lines, and conducted extensive training for both the physical packing process and the general hazards problems associated with uranium, beryllium, and other hazardous materials which could have been involved. Additional personnel who participated were a medical doctor from Radiation Emergency Assistance Center/Training Site (REAC/TS), operated by the Oak Ridge Institute for Science and Education/Oak Ridge Associated Universities (ORISE/ORAU), language translators from the On Site Inspection Agency (OSIA), and a communications specialist from EG&G Energy Measurement Corporation, Nevada. All together, 31 scientists, engineers, nuclear material operators, and other specialists were deployed on October 7th to pack the uranium into cans and transport these materials to the Oak Ridge Y-12 Plant in Oak Ridge, Tennessee, USA, using internationally approved shipping containers.

2.0 DISCUSSION AND RESULTS

The purpose of this evaluation was to confirm that the Authorized Contents for a 55-gallon Spec 6M drum-type container (Certificate USA/0002/B()F, Revision 13, which contains the DOT Spec 6M loading limits table from 49 CFR 173.417[1]) was applicable and appropriate for uranium/beryllium mixtures ranging from 1 to 67 percent by weight uranium.

Per Certificate USA/0002/()F, Rev. 13, the Fissile Class I packages are limited to 1.6 kg of U-235. The maximum ratio of hydrogen to fissile material must not exceed three, including all of the sources of hydrogen within the DOT Spec 2R inner container. The maximum authorized quantities of uranium-235 for Fissile Class II are given in Table 1.

The mass limits in Table 1 were evaluated in this study and shown to be applicable for uranium/beryllium mixtures ranging from 1 to 67 weight percent uranium although space limitations prevented inclusion of all tables of results. Tables 2 and 3 show the uranium/ beryllium loadings compared to the allowable loadings for compounds at a hydrogen to U-235 ratio of zero and less than or equal to three. (NOTE: Some of the loadings are limited by density of the material and the volume of the 2R (i.e., loading limits can not be reached as weight percent of uranium decreases and the material density decreases).

The results show that the generic uranium-235 loadings for a DOT Spec 6M/2R container will work for the range of uranium/beryllium mixtures evaluated.

3.0 FUEL AND PACKAGE SPECIFICATIONS

The package fuel loadings consisted of uranium/beryllium mixtures ranging from 1 to 67 percent uranium by weight and having a hydrogen to fissile ratio of 0 or 3. Table 4 shows fuel specifications used in this evaluation.

The theoretical densities assumed throughout this evaluation are based on a volume additive determination and increased five percent for additional conservatism. The exception to this is for 10 and 67 weight percent uranium in the uranium/beryllium mixture. For the 10 weight percent mixture the density was increased approximately 7 percent in order to achieve the 1.6 kg uranium-235 loading allowed for a transport index of zero. For the 67 weight percent uranium in the uranium/beryllium compound (UBe_{13}), a reference density exists and was used.

For calculations having a hydrogen to uranium-235 ratio of three, the density was held constant. Therefore, the mass of uranium and beryllium remained constant and the only change was to disperse a sufficient amount of water throughout the system to obtain the desired hydrogen to uranium-235 ratio.

Operationally, the mixtures were loaded into 4.75-inch diameter by 5- or 7-inch tall stainless steel cans. (However, all calculations assumed that the fuel loading homogeneously filled the 2R inner container.) The weight of the hydrogenous packing material used for taping and sealing the cans was such that the hydrogen to fissile ratio limit was not exceeded.

The 2R inner container has dimensions of 5.05-inches inside diameter, 5.56-inches outside diameter, 22.5-inches inside height, and 23.81-inches outside height. The available fuel loading volume is 7.4 liters. The outer container evaluated is a 55-gallon Spec 6M shipping container. Dimensions are 24-inches outside diameter, 34.62-inches outside height, and wall and bottom thicknesses of 0.1087 cm. The inner container is fixed within the outer container by machined discs and rings of specified materials (normally Celotex™) which provide thermal and impact protection.

4.0 METHOD OF CALCULATION AND MODEL SPECIFICATIONS

The multigroup Monte Carlo criticality program KENO V.a with the SCALE 27 energy group ENDFIB-IV neutron cross section library was used to calculate k_{eff} values for containers under Normal Conditions of Transport and Hypothetical Accident Conditions. All cases used 50,000 neutron histories with 500 neutrons per generation. All calculations were performed with the CSA25 control sequence of the CSAS4 control module of SCALE using the configuration controlled version (NCSSHP) on the Y-12 Plant Nuclear Criticality Safety Department's HP 9000/Series 700 Workstation.

The array configurations and mass loadings (see Table 2 and 3) evaluated were based on authorized quantities of fissile material, as well as other packaging restrictions, as given in the Certificate. Table 5 shows the transport index (TI) versus array configurations used throughout this evaluation.

The inner container (2R) was modeled as a stainless steel straight-wall cylinder having an inside diameter of 5.05 inches, an inside height of 22.5 inches, wall thickness of 0.255 inches, and top and bottom thicknesses of 0.04 inches. The steel in the bolt flange and bolts (for the leak-testable version) were not included in the model.

For Normal Conditions of Transportation, the thermal insulation (assumed as cellulose, $C_6H_{10}O_5$) and plywood was not modeled explicitly in the calculational model. In these calculations, water at 0.1 gram per cubic centimeter was substituted for insulation as a calculational technique for simplification.

For Hypothetical Accident Conditions, the principal material change that results from testing is to the thermal insulation and plywood. The significance of insulation damage in terms of criticality safety is the reduction in the amount of hydrogenous material available for interstitial moderation. This loss is a result of the high temperature of the thermal tests which will

effectively drive off some of the hydrogen and oxygen. Conversely, the insulation and plywood could become fully saturated with water during water immersion conditions. These variations in the amount of interstitial moderation were incorporated in the calculations by modeling the thermal insulation region, the plywood regions, and the space between the drums as variable density water ranging from 0 to 0.9982 gram per cubic centimeter.

The drum model differs from the actual drum in the treatment of the drum wall, which was taken to be a straight-wall cylinder without the rolling hoops or chimes and without the top and bottom heads inset into the drum wall. The outside diameter of the drum was modeled as 56.6928 centimeters; this is a 7-percent reduction in the actual outside diameter of 60.96 centimeters. The 7-percent reduction in diameter produces an array density equivalent to drums in a tight-packed, triangular pitched configuration, while actual calculations utilized a square pitch configuration. The inside dimensions of the drum model were determined by using the outside dimensions while maintaining a uniform steel thickness for the wall, bottom, and lid. The wall, bottom, and lid thicknesses used in the model was the minimum value for 18-gauge sheet steel as defined in 49 CFR 178.118-6(b)[1]. The resulting wall, bottom, and lid thickness was 0.1087 centimeter (0.0428 inch); the corresponding inside dimensions of the drum were 56.4754 centimeters in diameter and 87.7174 centimeters in height.

5.0 CRITICALITY CALCULATIONS

5.1 Calculational Method

The computer program modules used in this evaluation are part of the Standardized Computer Analysis for Licensing Evaluation (SCALE) code system. The CSAS25 control sequence of the CSAS4 control module of SCALE was used for all computations. The CSAS25 control sequence activates the functional modules BONAMI-S, NITAWL-S, and KENO V.a. The control sequence and functional modules are summarized in the following paragraphs. The 27 group ENDF/B-IV cross section library in SCALE was utilized for all calculations.

KENO V.a is a multigroup Monte Carlo computer code employed to determine the k_{eff} for multidimensional systems. The basic geometrical bodies allowed for defining a model are cuboids, spheres, cylinders, hemispheres, and hemicylinders. KENO V.a has the following major characteristics: an enhanced geometry package that allows arrays to be defined and positioned throughout the model; a P_a scattering treatment; an extended use of differential albedo reflection; printer plots for checking the input model; the capability of supergrouping of energy dependent data; a restart capability; and origin specifications for spheres, cylinders, hemicylinders, and hemispheres.

The CSAS4 control module, the associated functional modules, cross sections, and data bases used in this evaluation reside in a version (NCSSHP) that is under configuration control on an HP 9000/Series 700 Workstation maintained by the Oak Ridge Y-12 Plant Nuclear Criticality Safety Department.

5.2 Code Validation and Establishment of Calculational Safety Limit

The computer code validation for uranium/beryllium systems is the subject of other papers not yet published. However, the calculations that were performed included systems which include highly enriched uranium cylinders and spheres reflected by different beryllium systems, highly enriched uranium disks separated by beryllium blocks, and compressed ceramic pellets of intermediate enrichment uranium mixed with beryllium oxide latticed in water. These benchmark experiments demonstrated the ability of the KENO V.a code and the CSAS25 control sequence with the 27 energy group library to accurately predict k_{eff} for the geometries encountered in the shipping package evaluation.

5.3 Calculational Results

Due to space limitations, only one set of representative results of the calculations performed for the criticality safety evaluation of U/Be in a 55-gallon 6M is presented in Table 6. The calculated neutron multiplication factor with one standard deviation ($k_{eff} \pm \sigma$) is listed. The table provides the case designator, a case description, the calculational result ($k_{eff} \pm \sigma$), and the average energy group of neutrons causing fission (AEG) for each case evaluated.

For the purpose of making comparisons of academic interest, the range of interspersed moderation evaluated in the array cases represent extreme conditions that are more severe than required for analysis of the Hypothetical Accident Conditions (10 CFR 71.73[2]), In terms of criticality safety, the results of evaluations for these severe conditions, if used, would be no more restrictive than the results actually given in Table 2 and 3.

Table 6 lists the calculational results for packages with an H/X of zero and a transport index of zero which allows a maximum uranium-235 loading of 1.6 kilograms. In this series of calculations, the 2R inner vessel was filled at theoretical density for each mixture. For all cases evaluated (for all TIs and both H/X values) for both Normal Conditions of Transport and Hypothetical Accident Conditions, calculational results were all subcritical.

REFERENCES

1. "Transportation," Title 49, *Code of Federal Regulations,* Parts 100-179, Washington, D.C.

2. "Packaging and Transportation of Radioactive Material," Title 10, *Code of Federal Regulations,* Part 71, Washington, D.C.

Table 1. Authorized U-235 Contents for Fissile Class II in a DOT Specification 6M Package.

Uranium-235 (quantity in kilograms) Compounds		Transport Index
H/X=0	H/X≤3	
7.6	5.3	0.1
9.6	6.4	0.2
13.9	8.3	0.5
16.0	10.1	1.0

Table 2. U/Be Loadings for H/X=0 in 55 gal 6M/2R Container.

TI	CFR Limit (kg) for U-235 H/X=0	U-235 Loading (kg) for 6M/2R versus TI wt% U in U(100)/Be Mixture								
		1	5	10	20	30	40	50	60	67
0	1.6	0.145	0.75	1.6	1.6	1.6	1.6	1.6	1.6	1.6
0.1	7.6				3.5	5.8	7.6	7.6	7.6	7.6
0.2	9.6						8.9	9.6	9.6	9.6
0.5	13.9							13.0	13.9	13.9
1	16.0								16.0	16.0

Table 3. U/Be Loadings for H:X ≤ 3 in 55 gal 6M/2R Container.

TI	CFR Limit (kg) for U-235 H/X≤3	U-235 Loading (kg) for 6M/2R versus TI								
		wt% U in U(100)/Be Mixture								
		1	5	10	20	30	40	50	60	67
0	1.6	0.145	0.75	1.6	1.6	1.6	1.6	1.6	1.6	1.6
0.1	5.3				3.5	5.3	5.3	5.3	5.3	5.3
0.2	6.4					5.8	6.4	6.4	6.4	6.4
0.5	8.3						8.3	8.3	8.3	8.3
1	10.1						8.9	10.1	10.1	10.1

Table 4. Densities used for U(100) mixtures.

Density (g/cm^3) (lower value)								
wt% U in U(100)/Be Mixture (upper value)								
1	5	10	20	30	40	50	60	67
1.96	2.03	2.17	2.37	2.66	3.04	3.53	4.23	4.37

Table 5. Transport index versus array configurations.

Transport Index	Max. No. of Packages in Array per Certificate: NCT (HAC)	Array Size for NCT (HAC)	Actual No. of Units in Calc. Arrays: NCT (HAC)
0	Infinite (250)	Infinite (8 x 8 x 4)	Infinite (256)
0.1	2500 (1000)	14 x 14 x 13 (10 x 10 x 10)	2548 (1000)
0.2	1250 (500)	11 x 11 x 11 (8 x 8 x 8)	1331 (512)
0.5	500 (200)	8 x 8 x 8 (6 x 6 x 6)	512 (216)
1	250 (100)	8 x 8 x 4 (5 x 5 x 4)	256 (100)

Table 6

Case Name	wt% U in alloy	TI	kg ^{235}U	Mod ρ	k_{eff}	AEG
ρ_{mix} = 4.373 g/cc						
NCT k_{eff} = 0.79771(0.00293) AEG = 15.35						
hac_67Ube_ti0_mdo_td	67	0	21.64	0.0	0.7493(0.0035)	11.60
mdp001	67	0	21.64	0.001	0.7464(0.0031)	11.69
mdp005	67	0	21.64	0.005	0.7589(0.0030)	11.85
mdp01	67	0	21.64	0.01	0.7714(0.0033)	12.25
mdp03	67	0	21.64	0.03	0.8076(0.0036)	13.65
mdp05	67	0	21.64	0.05	0.8039(0.0037)	14.39
mdp07	67	0	21.64	0.07	0.7747(0.0032)	14.68
mdp1	67	0	21.64	0.1	0.7169(0.0036)	14.59
mdp3	67	0	21.64	0.3	0.5956(0.0030)	12.68
md1	67	0	21.64	1.0	0.6799(0.0030)	13.38
ρ_{mix} = 4.2276 g/cc						
NCT k_{eff} = 0.79372(0.00328) AEG = 15.53						
hac_60Ube_ti0_mdo_td	60	0	18.73	0.0	0.7449(0.0033)	11.98
mdp001	60	0	18.73	0.001	0.7455(0.0033)	12.01
mdp005	60	0	18.73	0.005	0.7583(0.0032)	12.16
mdp01	60	0	18.73	0.01	0.7704(0.0036)	12.54
mdp03	60	0	18.73	0.03	0.8062(0.0035)	13.93
mdp05	60	0	18.73	0.05	0.7590(0.0032)	14.73
mdp07	60	0	18.73	0.07	0.7873(0.0032)	14.98
mdp1	60	0	18.73	0.1	0.7156(0.0030)	14.81
mdp3	60	0	18.73	0.3	0.5891(0.0036)	12.94
md1	60	0	18.73	1.0	0.6809(0.0033)	13.68
ρ_{mix} = 3.5335 g/cc						
NCT k_{eff} = 0.72756(0.00319) AEG = 16.65						
hac_50Ube_ti0_mdo_td	50	0	13.05	0.0	0.6679(0.0029)	12.97
mdp001	50	0	13.05	0.001	0.6739(0.0027)	13.07
mdp005	50	0	13.05	0.005	0.6839(0.0031)	13.32
mdp01	50	0	13.05	0.01	0.6997(0.0033)	13.59
mdp03	50	0	13.05	0.03	0.7389(0.0032)	15.04
mdp05	50	0	13.05	0.05	0.7271(0.0035)	15.75
mdp07	50	0	13.05	0.07	0.7005(0.0032)	16.07
mdp1	50	0	13.05	0.1	0.6457(0.0035)	16.02
mdp3	50	0	13.05	0.3	0.5302(0.0029)	14.12
md1	50	0	13.05	1.0	0.6297(0.0030)	14.80

Table 6 (cont.)

Case Name	wt% U in alloy	TI	kg ^{235}U	Mod ρ	k_{eff}	AEG
ρ_{mix} = 3.0351 g/cc						
NCT k_{eff} = .067243(0.00289) AEG = 17.74						
hac_40Ube_ti0_mdo_td	40	0	8.97	0.0	0.6051(0.0035)	14.12
mdp001	40	0	8.97	0.001	0.6005(0.0032)	14.11
mdp005	40	0	8.97	0.005	0.6217(0.0032)	14.35
mdp01	40	0	8.97	0.01	0.6331(0.0031)	14.74
mdp03	40	0	8.97	0.03	0.6748(0.0030)	16.18
mdp05	40	0	8.97	0.05	0.6734(0.0035)	16.89
mdp07	40	0	8.97	0.07	0.6451(0.0031)	17.07
mdp1	40	0	8.97	0.1	0.5882(0.0035)	17.08
mdp3	40	0	8.97	0.3	0.4826(0.0035)	15.34
md1	40	0	8.97	1.0	0.5671(0.0033)	15.96
ρ_{mix} = 2.6599 g/cc						
NCT k_{eff} = 0.61621(0.00316) AEG = 18.72						
hac_30Ube_ti0_mdo_td	30	0	5.89	0.0	0.5367(0.0029)	15.22
mdp001	30	0	5.89	0.001	0.5460(0.0028)	15.31
mdp005	30	0	5.89	0.005	0.5553(0.0029)	15.51
mdp01	30	0	5.89	0.01	0.5752(0.0034)	15.91
mdp03	30	0	5.89	0.03	0.6094(0.0031)	17.29
mdp05	30	0	5.89	0.05	0.6129(0.0036)	18.04
mdp07	30	0	5.89	0.07	0.5915(0.0031)	18.24
mdp1	30	0	5.89	0.1	0.5390(0.0028)	18.24
mdp3	30	0	5.89	0.3	0.4257(0.0026)	16.50
md1	30	0	5.89	1.0	0.5251(0.0033)	17.22
ρ_{mix} = 2.3673 g/cc						
NCT k_{eff} = 0.55097(0.00263) AEG = 19.87						
hac_20Ube_ti0_mdo_td	20	0	3.50	0.0	0.4739(0.0027)	16.68
mdp001	20	0	3.50	0.001	0.4692(0.0027)	16.71
mdp005	20	0	3.50	0.005	0.4817(0.0030)	17.00
mdp01	20	0	3.50	0.01	0.5034(0.0028)	17.36
mdp03	20	0	3.50	0.03	0.5448(0.0030)	18.63
mdp05	20	0	3.50	0.05	0.5451(0.0033)	19.23
mdp07	20	0	3.50	0.07	0.5182(0.0029)	19.42
mdp1	20	0	3.50	0.1	0.4816(0.0027)	19.49
mdp3	20	0	3.50	0.3	0.3760(0.0025)	18.00
md1	20	0	3.50	1.0	0.4676(0.0030)	18.61

Table 6 (cont.)

Case Name	wt% U in alloy	TI	kg ^{235}U	Mod ρ	k_{eff}	AEG
ρ_{mix} = 2.1666 g/cc						
NCT k_{eff} = 0.46269(0.00281) AEG = 21.39						
hac_10Ube_ti0_mdo_td	10	0	1.6	0.0	0.3829(0.0027)	18.75
mdp001	10	0	1.6	0.001	0.3808(0.0028)	18.77
mdp005	10	0	1.6	0.005	0.3941(0.0029)	19.04
mdp01	10	0	1.6	0.01	0.4163(0.0030)	19.39
mdp03	10	0	1.6	0.03	0.4572(0.0028)	20.36
mdp05	10	0	1.6	0.05	0.4588(0.0025)	20.81
mdp07	10	0	1.6	0.07	0.4395(0.0032)	21.03
mdp1	10	0	1.6	0.1	0.4045(0.0029)	20.94
mdp3	10	0	1.6	0.3	0.3041(0.0027)	19.98
md1	10	0	1.6	1.0	0.3967(0.0026)	20.42
ρ_{mix} = 2.0230 g/cc						
NCT k_{eff} = 0.3742(0.0024) AEG = 22.47						
hac_5Ube_ti0_mdo_1p75	5	0	0.75	0.0	0.2950(0.0021)	20.36
md001	5	0	0.75	0.001	0.3020(0.0023)	20.46
md005	5	0	0.75	0.005	0.3090(0.0022)	20.68
md01	5	0	0.75	0.01	0.3278(0.0025)	20.95
md03	5	0	0.75	0.03	0.3636(0.0027)	21.71
md05	5	0	0.75	0.05	0.3706(0.0027)	22.12
md07	5	0	0.75	0.07	0.3483(0.0025)	22.21
mdp1	5	0	0.75	0.1	0.3237(0.0025)	22.22
mdp3	5	0	0.75	0.3	0.2385(0.0021)	21.47
md1	5	0	0.75	1.0	0.3299(0.0022)	21.88
ρ_{mix} = 1.9581 g/cc						
NCT k_{eff} = 0.1793(0.0015) AEG = 23.88						
hac_1Ube_ti0_mdo_1	1	0	0.145	0.0	0.1356(0.0014)	22.70
md001	1	0	0.145	0.001	0.1373(0.0012)	22.76
md005	1	0	0.145	0.005	0.1432(0.0015)	22.89
md01	1	0	0.145	0.01	0.1519(0.0014)	23.01
md03	1	0	0.145	0.03	0.1723(0.0014)	23.49
md05	1	0	0.145	0.05	0.1734(0.0013)	23.67
md07	1	0	0.145	0.07	0.1646(0.0013)	23.71
mdp1	1	0	0.145	0.1	0.1539(0.0014)	23.75
mdp3	1	0	0.145	0.3	0.1238(0.0015)	23.39
md1	1	0	0.145	1.0	0.1691(0.0015)	23.67

TUESDAY, MAY 16, 1995

SESSION II
RELEVANT EXPERIMENTS FOR CRITICALITY SAFETY

DESIGN OF A CRITICAL ASSEMBLY FOR TESTING INTEGRAL PROPERTIES OF MATERIALS

David K. Hayes
DNFSB/LACEF

INTRODUCTION:

Implementation of the Defense Nuclear Facilities Safety Board (DNFSB) Recommendation 93-2 (Critical Experiment Capability) includes "improving the information base underlying prediction of criticality." To that end, the Nuclear Criticality Experiments Steering Committee (NCESC) has compiled and prioritized a list of experiments solicited from the criticality community. In response to the NCESC list, a critical assembly is being designed at the Los Alamos Critical Experiments Facility (LACEF) to incorporate elements of several experiments. Specifically, the design will include elements from the following experiments:

1. Experiment 102 - Large Array of Small Units,
2. Experiment 501 - Assessment Program for Materials Used to Transport and Store Discrete Items and Weapons Components,
3. Experiment 502a - Absorption Properties of Waste Matrices and
4. Experiment 609 - Validation of Calculational Methodology in the Intermediate Energy Range.

DESCRIPTION:

Design of the assembly centers around the fuel elements, which are five-liter right circular cylinders filled with $U(93.1)O_2(NO_3)_2 * 6H_2O + HNO_3 + H_2O$ (U(93. l)NH). The cylinders are 0.25 cm thick 304SS with a height to diameter ratio of one. Initially, four elements, in a square lattice reflected by 10 cm of polyethylene, will be utilized. Future modifications include fuel changes (to UO_2, PuO_2, ...) and increases in the array size (to 2x2x2, 3x3x3, ...)(Experiment 102).

OPERATION:

Honeycomb, a horizontal split table, serves as the platform for the assembly. Two fuel elements will be placed on the "movable" side and two will be placed on a jackscrew table mounted on the "stationary" side. Closure is achieved by hydraulic ram ("movable" side) and the jackscrew table, using a 1/M approach. The hydraulic ram and jackscrew also serve as scram mechanisms.

Non-fissile materials will be introduced interstitially and externally to the fuel elements to determine their integral properties as moderators, reflectors and absorbers. Materials of interest include: Al_2O_3, CaCl, cellulose, celotex, concrete, depleted uranium, expanded borated polyfoam, Fe_2O_3, kerosene, lead, plexiglass, polyethylene, PVC, SiO_2, TBP, ... etc (Experiments 501, 502a).

Concrete (building material) will be used as a reflector at varying distances from the fuel elements to investigate room return effects.

Varying the spacing of fuel elements and the size and position of non-fissile materials results in a varying neutron energy spectrum. Thus, the spectrum may be adjusted to a specific energy range for evaluating material properties (Experiment 609).

EXPECTED RESULTS:

Critical dimensions of the various systems will be measured, yielding information on the physics of interacting fuel elements and materials. The data will be evaluated to determine the effects of fuel element size, geometry and fuel type. Integral measurements of non-fissile material properties will be used to evaluate computer models (MCNP, KENO, ...), associated cross-sections and thermal treatments ($S(\alpha, \beta)$).

DESIGN PROGRESS:

Budget concerns and time constraints control the design of this assembly. As a result, the design requires use of existing equipment and on hand fissile materials. Thus, HONEYCOMB and U(93.1)NH from the WINCO Slab Tank Experiment will be utilized.

For simplicity, four fuel elements compose the initial assembly. This necessitates use of a reflector to achieve delayed critical. Ten centimeters of polyethylene serve as the reflector, with the added benefit of isolating the assembly from room return. Figures 1 and 2 show the side and top view of the assembly with a fuel element spacing of 10cm and 3cm separation from the polyethylene walls.

MCNP k_{eff}-calculations have been performed to determine appropriate geometries. Preliminary calculations used 3000 neutrons per cycle, 15 inactive cycles, 200 active cycles and the ENDF/B-VI continuous energy cross sections. Based on the k_{eff}-calculations and mechanical simplicity, polyethylene was placed adjacent to the top and bottom of the fuel elements. To determine critical geometries, the distance between the fuel elements (face to face separation) and the polyethylene walls was varied.

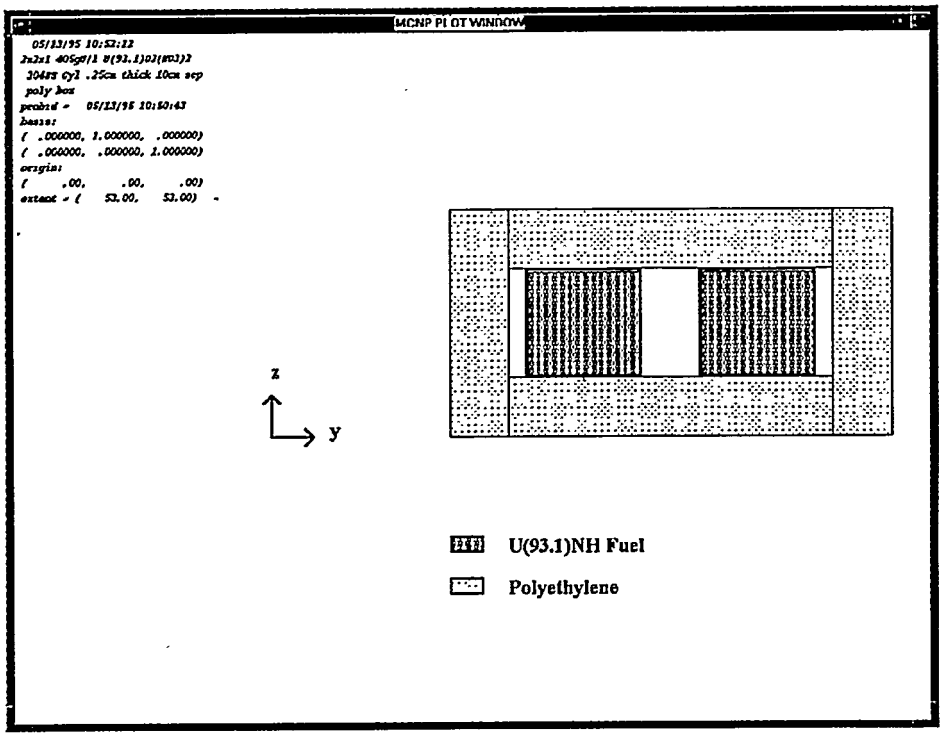

Figure 1. Assembly side view.

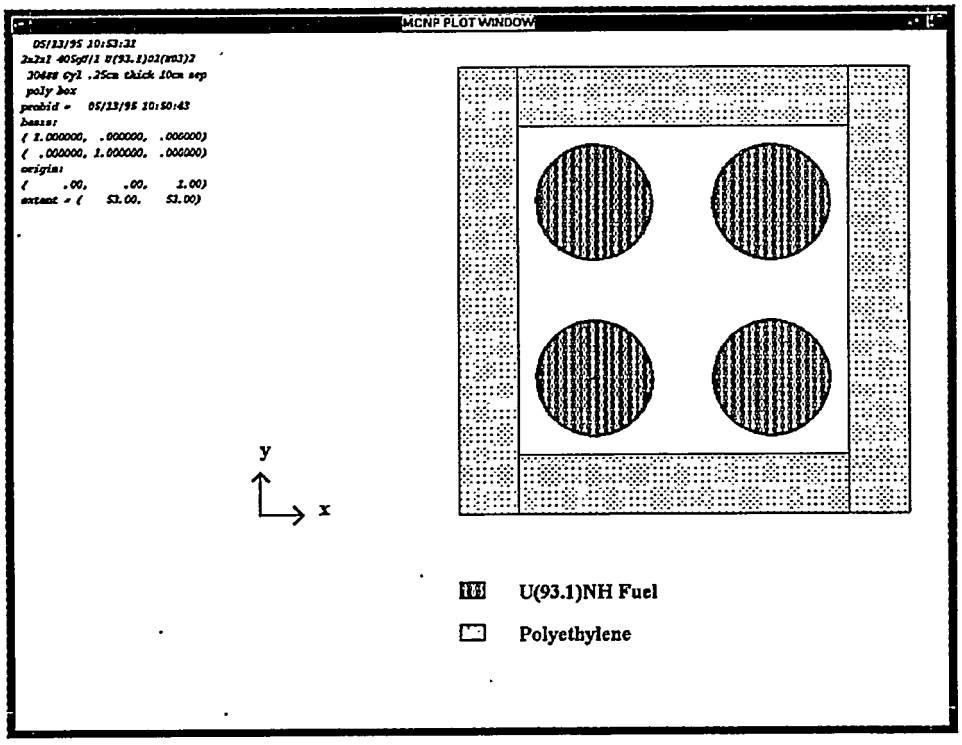

Figure 2. Assembly top view.

Fuel element spacing of 10cm was selected to facilitate placement of materials interstitially. Figure 3 depicts the results of varying the separation to the polyethylene walls from 25cm to 0cm. Since this fuel spacing precludes reaching delayed critical, fuel element spacing in the "y" direction was decreased while the "x" separation was maintained at 10cm (Figure 4, polyethylene adjacent to fuel elements). Distance from the fuel to the polyethylene walls was then varied for the 10cm "x", 0cm "y" separation of fuel elements (Figure 5).

K_{eff} has been calculated for two configurations of half the assembly. First, polyethylene was placed adjacent to two fuel elements (0 cm separation), resulting in a k_{eff} of 0.96421± 0.00125. One end wall was then removed, decreasing k_{eff} to 0.9076 ± 0.00118.

Additional k_{eff}-calculations have been performed for a single unreflected fuel element using TWODANT and compared with MCNP. A significant difference exists between the calculations. The results are tabulated in Table 1.

Results from the dimension searches were evaluated using different cross-sections/codes. The Hansen-Roach (HR16) anomaly is being investigated.

FUTURE EFFORT:

MCNP calculations of increased detail, including interstitial materials, will be performed to support control system, mechanical design, and administrative operational requirements. A Design Requirements Document and Experiment Plan will be developed.

HONEYCOMB modifications include removal of the box tubes, installation of new fixtures and installation of a digital control system.

Fuel elements require the addition of vents for radiolytic gas production. A positioning system will also be incorporated for precise spacing adjustments of the fuel.

Table 1. Single Unit k_{eff} Calculations

Case	k_{eff} from MCNP	k_{eff} from TWODANT-MENDF30	k_{eff} from TWODANT-HR 16
Bare 5L Cylinder	0.62262 ± 0.00095	0.62485	0.60581
TWODANT-HR16 Dimension Search	1.02033 ± 0.00115	1.01796	1.00000
TWODANT-MENDF30 Dimension Search	1.00085 ± 0.00116	1.00000	0.98181
Bare 5L Sphere	0.61981 ± 0.00096	0.62603	0.61057

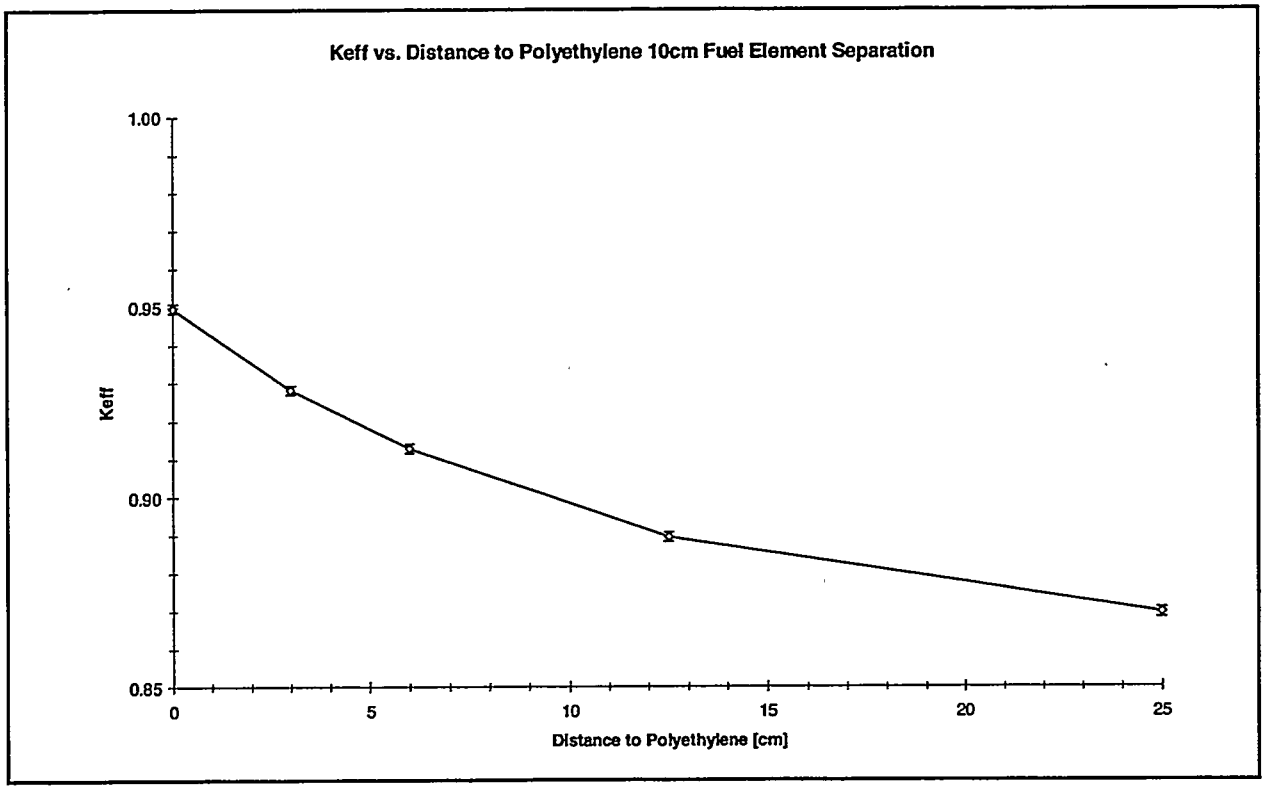

Figure 3

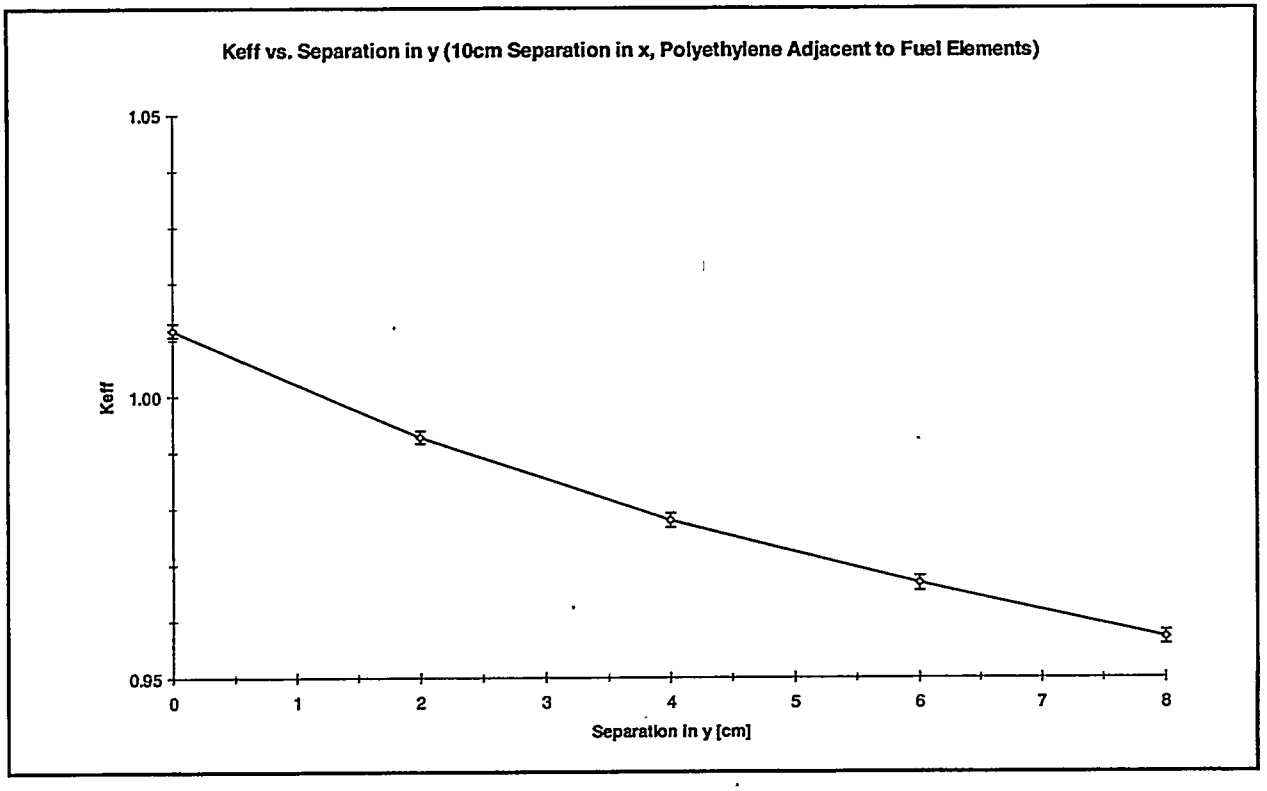

Figure 4

This page cannot be converted.

Please view the native document

for the original page.

CRITICAL MASS OF NP-237

Rene Sanchez

INTRODUCTION

The criticality of Np-237 is governed by several factors. For instance, it is well known that nuclides with an even number of neutrons, such Np-237, exhibit a sharp threshold in their fission cross section. For Np-237, the threshold occurs at approximately 500 keV. Above this neutron energy, the fission cross section is comparable to that of U-235. On the other hand, below this energy threshold, the fission cross section is quite low. Thus, the criticality of Np-237 can only occur in a fast neutron spectrum. Another factor that affects the critical mass of this element is the inelastic scattering cross section of Np-237. A low inelastic scattering cross section in a fast spectrum will enhance criticality, since fewer neutrons will scatter below the fission threshold where they will be unable to cause more fissions.

DESCRIPTION OF EXPERIMENT AND COMPUTER MODELS

The experiment consists of replacing small samples of neptunium, 93.2% U-235 (Oralloy), or empty aluminum cans in the center of a fast-critical reflected assembly, known as Flattop.[1] This critical assembly is operated above delayed-critical by inserting three control rods to their full-in position. The worth of each sample is estimated through the measured asymptotic reactor period and the inhour equation. The worth measurements were also corrected for temperature changes in the assembly.

The Flattop assembly consists of a driver core of fissile material that sits in the center of a 48-cm-diameter natural uranium reflector. There are two driver cores available for the Flattop assembly. The Oralloy core weighs approximately 16.22 kg and has a 1.27-cm- diameter glory hole where mass adjustment buttons and the Np-237, Oralloy, or empty aluminum can samples are placed. The second available core is made of delta-phase plutonium (95% Pu-239, 5% Pu-240) and weighs approximately 5.9 kg. It also has a glory hole where mass adjustment buttons and the different sample can be placed. All the plutonium pieces are clad with nickel. The calculated effective delayed neutron fractions for the Oralloy and plutonium Flattop cores are 0.00664 and 0.00276, respectively.[2] Table I shows the dimensions, weights, and isotopic composition of the samples used for these experiments.

A computer model was developed with the help of TWODANT[3] to simulate Flattop and the different samples that were placed in the center of this assembly. The TWODANT code used the 16-group Hansen-Roach and 30-group MENDF5 neutron cross section libraries. TWODANT calculated the keff of the system based on the different samples placed in the assembly.

RESULTS

Table II lists the experimental and calculated results. The experiments show that when the oralloy core is present in the Flattop assembly, the oralloy sample is worth 3.41 ± 0.4 cents more than the neptunium sample. The TWODANT calculations show that the oralloy sample is worth 2.16 cents more than the neptunium sample when Hansen-Roach cross sections are used and 2.19 cents more when the MENDF5 cross section library is used.

When the plutonium core is present, the worth of the oralloy sample is 6.41 ± 0.4 cents more than the neptunium sample. TWODANT predicts a worth of 5.31 cents when Hansen-Roach cross sections are used and 7.85 cents when using MENDF5 30 group cross sections. These comparisons are in somewhat good agreement. The differences between experimental and calculated values are due to the uncertainty associated with the inelastic cross section of Np-237.[4] The ONEDANT code was then used to estimate the critical mass of Np-237. The code yielded a value of 56 kg for a bare sphere with an uncertainty of ± 10 kg based on a 30 g sample and the uncertainty of the Np-237 inelastic cross section.

Table I. Properties of the replacement samples.

	Uranium sample	Np-237 sample	Empty Al can
Weight of metal	29.909 g	28.393 g	------
Weight of can	-------	0.773 g	0.476 g
Dimensions			
Length (in.)	0.5015	0.4890	0.4975
Outside Diameter (in.)	0.4990	0.4865	0.4865
Thickness		Nickel clad	Al wall thickness
Ends (in.)	-----	0.0035	0.010
Sides (in.)	-----	0.0057	0.010
Isotopic composition, wt%			
Uranium		Neptunium	
U-234	1.1	Np-237	99.87
U-235	93.2	Other elements	0.13
U-236	0.2		
U-238	5.5		

Table II. Experimental and computational results.

Experimental Results	
Oralloy (Oy) Core	**Pu Core**
$\Delta\rho$ (Oy-Np) = 3.41 ± 0.39 cents	
$\Delta\rho$ (Oy-Al) = 22.44 ± 0.22 cents	$\Delta\rho$ (Oy-Np) = 6.41 ± 0.40 cents
$\Delta\rho$ (Np-Al) = 18.95 ± 0.32 cents	
Computational Results	
TWODANT (Oy Core)	**TWODANT (Pu Core)**
Hansen-Roach Cross Sections	**Hansen-Roach Cross Sections**
$\Delta\rho$ (Oy-Np) = 2.16 cents	
$\Delta\rho$ (Oy-Al) = 23.95 cents	$\Delta\rho$ (Oy-Np) = 5.31 cents
$\Delta\rho$ (Np-Al) = 21.78 cents	
MENDF5	**MENDF5**
$\Delta\rho$ (Oy-Np) = 2.19 cents	
$\Delta\rho$ (Oy-Al) = 22.66 cents	$\Delta\rho$ (Oy-Np) = 7.85 cents
$\Delta\rho$ (Np-Al) = 20.48 cents	

References

1. R. Paternoster et al., Safety Analysis Report for the Los Alamos Critical Experiments Facility (LACEF) and the Hillside Vault (PL-26), LA-CP-92-235, (1994).
2. Personal communication with Gordon Hansen Los Alamos National Laboratory (November 1994).
3. R. Alcouffe, et al., "User's Guide for TWODANT: A Code Package for Two-Dimensional, Diffusion-Accelerated, Neutral-Particle Transport," Los Alamos National Laboratory report LA-10049-M (1992).
4. G. Hansen, et al., Los Alamos National Laboratory Memorandum, "Uncertainty in the Np-237 Critical Mass," T-2-M-1388; May 27, 1983.

COMPUTER SIMULATION OF SHEBA EXCURSIONS

Robert Kimpland
Los Alamos National Laboratory

A computer model, which simulates the dynamic behavior of the SHEBA assembly during excursions, has been developed at LACEF. This model is a simple lumped parameter model, which combines the neutron point kinetics equations with simple thermodynamic expressions for temperature and density. In addition, a radiolytic gas model has been developed to simulate the production and migration of radiolytic gas bubbles in an aqueous fissile solution. The results produced by this model have been compared with experimental data from the SHEBA assembly.

The goal of this work is a better understanding of the basic physics of aqueous fissile solutions, in particular, the reactivity feedback mechanisms present during an excursion and the phenomena of radiolytic gas formation and migration. It is anticipated that information gained from this work will be of use in other areas such as criticality accident analysis and in the design of the medical isotope production reactor (MIPR).

The effect of radiolytic gas on an aqueous fissile solution can be quite significant. During slow excursions, the radiolytic gas can provide a large negative reactivity insertion. During fast excursions above prompt critical, the radiolytic gas can produce a transient compression of the fissile solution. Radiolytic gas is formed by the process of radiation nucleation during high-power operation. Fission fragments slowing down in the aqueous medium dissociate water into dissolved hydrogen and oxygen gas. At some threshold point, enough dissolved gas exists so that the radiation nucleation process can occur along fission tracks. On the macroscopic level, this process is not well understood. An equation for the amount of radiolytic gas in an assembly after some threshold point is given by

$$\frac{dV_g}{dt} = C\frac{dE}{dt} - \frac{V_g}{1}$$

where the rate of gas production is proportional to the rate of energy being dumped into the system multiplied by an adjustable parameter, and the mitigation of gas bubbles out of the assembly is modeled by giving the bubbles a mean bubble lifetime.

The neutron point kinetics equations are coupled through reactivity feedback with an energy equation and an equation of state given by

$$\frac{dE}{dt} = MC_p\frac{dT}{dt}$$

and

$$\frac{d\rho_1}{dt} = -\rho_1 \alpha \frac{dT}{dt}$$

where ρ_1 is the solution density, α is the isobaric compressibility, and T is the solution temperature.

Three reactivity feedback mechanisms have been identified for the SHEBA assembly. The first is a neutron temperature feedback, which accounts for hardening of the thermal neutron spectrum with increasing solution temperature. The second is volumetric expansion, which accounts for the decrease in density of the solution with increasing temperature. The third is radiolytic gas feedback, which accounts for the radiolytic gas displacing fuel from regions of high importance to regions of low importance. An expression for the reactivity of the SHEBA assembly is given by

$$\rho = \rho_O - \alpha\Delta T - \phi\Delta V - \psi V_g$$

where ρ_o is a step insertion of reactivity and α,ϕ, and ψ are the neutron temperature, volumetric, and radiolytic gas feedback coefficients. A series of transport calculations, using the discrete transport code TWODANT, was performed to determine these feedback coefficients.

Figure 5.1 shows the model's prediction for a \$0.29 step insertion in the SHEBA assembly. The model has the ability to track the core-height change due to liquid expansion as well as expansion due to the radiolytic gas. The effect of these expansions can be seen clearly from the reactivity and power curves. A comparison between the model and experimental data from a \$0.29 free run in SHEBA is shown in Fig. 5.2(a and b).

The model demonstrates all the main features of the SHEBA free runs. The results of the comparison between the model and the experimental data are encouraging. Future work will concentrate on the radiolytic gas formation and migration mechanisms. Also, new methods for calculating reactivity feedback effects will be considered.

Figure 5.1. Model's predicxtion of a \$0.29 excursion in SHEBA.

Figure 5.2(a and b). Comparison between the model and experimental data from a \$0.29 free-run in SHEBA.

WEDNESDAY, MAY 17, 1995

EMBEDDED TOPICAL MEETING

MISAPPLICATIONS AND LIMITATIONS OF MONTE CARLO METHODS DIRECTED TOWARD CRITICALITY SAFETY ANALYSES

MISAPPLICATIONS AND LIMITATIONS OF MONTE CARLO METHODS DIRECTED TOWARD CRITICALITY SAFETY ANALYSES

Burton Rothleder
DOE/HQ

INTRODUCTION

Deterministically and Stochastically Based Solutions

Some years ago, Eugene Wigner made the comment, which I can only paraphrase, that it is surprising that the equations of mathematical physics work as well as they do. He was certainly referring to the deterministic differential equations, and possibly to the related stochastic methods, that provide solutions to describe the behavior of physical systems. I think that his surprise, and ours in agreement, stems from the successful reification of Analysis (i.e., calculus) as Physics. In a sense, however, it should not be surprising that stochastic methods work as well as they do, since they imitate natural processes directly and do not work better than their statistical precision. But both deterministic methods and stochastic methods can fail completely to "capture" the physical problem if they are misused and misapplied, independent of the accuracy of their representation of the physical problem. (Accuracy of representation of the physical (e.g., geometry, materials, data base) affects both methods equivalently.)

For deterministic codes, selection of mesh, convergence, and quadrature to capture the physical problem can usually be evaluated, *a priori*, in terms of the physical behavior required of the solution. For stochastic codes, such selections are not relevant. Instead, selections of number of histories, random number generation method, sampling method, and source generation method are made to capture the physical problem. These selections cannot be easily evaluated in terms of the physical behavior required of the solution, if they can be evaluated in such terms at all, and as such their selection presents a subtlety, and poses a concomitant challenge, to the user of stochastic codes.

This Embedded Topical Meeting is directed toward exposing this subtlety and meeting its challenge.

This meeting was made possible by the efforts of members of the Methodology and Experiments Subcommittee of the Nuclear Criticality Experiments Steering Committee, established by DOE to address DNFSB Recommendation 93-2; by the efforts of the authors who are making the technical presentations; by the efforts of the session chairmen who assisted by organizing the meeting; and by the support of the U.S. Department of Energy.

Sessions and Topics

The papers to be presented are grouped into four sessions. The sessions are listed below with their intended topics. The session grouping and topic lists do not preclude overlapping. The topic lists are incomplete in principle, but are overly ambitious in the expectation of their complete inclusion in the formal presentations. More completeness and greater inclusion will be left to author and listener comments and questions during the discussion periods.

Session 1 The K-effective of the World

Topics: Sampling,
.
.
.

Session 2 Monte Carlo Vulnerabilities of Execution and Interpretation

Topics: Sampling,
Number of Histories,
Random Number Generation
Methods of Source Generation,
Method of Library Generation,
Proper Convergence of Fission Source,
Bias in Estimated Eigenvalue from Criticality Algorithm,
Interpretation of Error Band,
Proper Use of Variance Reduction Techniques,
Role of Sensitivity Studies,
.
.
.

Session 3 Monte Carlo Vulnerabilities of Representation

Topics: Cross Section Library,
Resonance Modeling,
Scattering Kernel,
Neutron Energy Population Distribution,
Geometry Limitations,
.
.
.

Session 4 Benchmark Comparisons

Topics: Continuous Energy Stochastic Codes vs. Measurements,
Discrete Energy Stochastic Codes vs. Measurements,
Deterministic Codes vs. Measurements,
Intercomparisons of Stochastic Codes and Deterministic Codes,
Deep Penetration Problems Related to Nuclear Criticality,
.
.
.

WEDNESDAY, MAY 17, 1995

SESSION I
THE K-EFFECTIVE OF THE WORLD

A DIFFICULTY IN COMPUTING THE k_{eff} OF THE WORLD, REVISITED

G. E. Whitesides

NOTE: This paper was originally presented in 1971 at an American Nuclear Society Meeting. With a new generation of criticality safety specialists making calculations, it is important that lessons learned from the past not be forgotten. Time has not diminished the importance of the topic discussed in this paper. In fact, as the geometrical capabilities expand in our Monte Carlo computer programs the likelihood of encountering the difficulties discussed are greatly enhanced. Hence, the need to repeat this paper.

In the course of applying Monte Carlo programs in the solution of criticality safety problems, a difficulty in correctly computing certain types of systems has arisen. In view of the increasing use of Monte Carlo-type programs, it is important that some statement be made about the type of systems in which the difficulty is likely to be encountered, since when one attempts to compute the multiplication factor for such a system, the result will almost always yield a low, and hence for criticality safety purposes, nonconservative result. This can occur with no hint that the computed result is in error.

The extreme example, which defines a situation in which this difficulty can exist, is the "k-effective of the world" problem. That is, if one attempts to calculate the k_{eff} of the world using a Monte Carlo calculation, what k_{eff} would be computed assuming that there are several critical assemblies located around the world? The answer would likely be the k_{eff} of the world with no critical assemblies present. The cause of the erroneous result is the fact that the volume of fissile material in the world would be so large relative to the volume of fissile material in the critical assemblies that most commonly used forms of sampling would almost never "see" the critical assemblies. Hence, this would not reflect their existence in the computed k_{eff}.

A more commonly encountered example in which a user of Monte Carlo programs might observe this difficulty is illustrated by a 9 x 9 x 9 array of plutonium metal spheres with a radius of ~4 cm, spaced on 60 cm centers. The array is reflected on all sides by a thick-water reflector. The k_{eff} of this system is computed to be 0.93. If the sphere in the center unit of the array is replaced by a sphere of plutonium that is exactly critical as a bare unit and the calculation repeated in the standard fashion using the Monte Carlo method, the calculation will yield a k_{eff} of 0.93, reflecting the same difficulty encountered in the "world k_{eff}" problem.

The erroneous results for these types of problems are the result of the failure of the calculation to converge the source to the fundamental source mode. The difficulty can range from a problem which converges so slowly that the normal number of generations examined are insufficient to assure convergence to problems that perhaps will never converge.

The answer to the problem lies in being sure that source convergence is achieved. Most Monte Carlo programs start all neutrons initially with either a flat or a cosine distribution over the fissile material in the system. For the majority of problems, this is adequate and may be even exact. Unfortunately, the choice of a standard start procedure that is adequate for a system with a region of localized multiplication that is somewhat higher than the multiplication of the major portion of the volume of the system is difficult, if not impossible, to define. One difficulty, which should not be underestimated, is trying to determine if, and where, this situation exists. Because of this, it is not the intention of this paper to offer a solution to the general problem; but only to bring to the attention of the users of Monte Carlo programs the fact that the computed multiplication may be in error for such systems.

If the region of highest multiplication can be established, it appears to be adequate to ensure eventual source convergence to the fundamental mode by starting all neutrons in this region. If there are more than one such region, it may be necessary to run several cases varying the initial source in order to determine the initial conditions that will lead to a fundamental mode-source distribution.

The Monte Carlo method has opened up the path to very precise evaluations of the criticality safety of almost any situation likely to be encountered. Its use, however, should be tempered by the realization that unless the correct fission distribution is achieved, the results will most likely be nonconservative.

VIEW GRAPHS

You are a Nuclear Criticality Safety Expert,

Thou Shall Understand

1. The criticality Phenomenon and its Anomalies,
2. Transport and Monte Carlo Codes and Cross Sections,
3. Experimental Benchmark Data,
4. The Limitations of Both Codes and Cross Sections,
5. Nuclear Fuel Plant Products, Processes and Equipment,
6. Good Nuclear Criticality Safety Practice and Standards,
7. Nuclear Regulatory Commission Requirements, and
8. How to combine all the Above for a safe and economical business.

For Every Calculated result
(However Ridiculous)
There is a Logical Sounding Explanation

What is the k_{eff} of the World?

1. <1.0
2. =1.0
3. >1.0

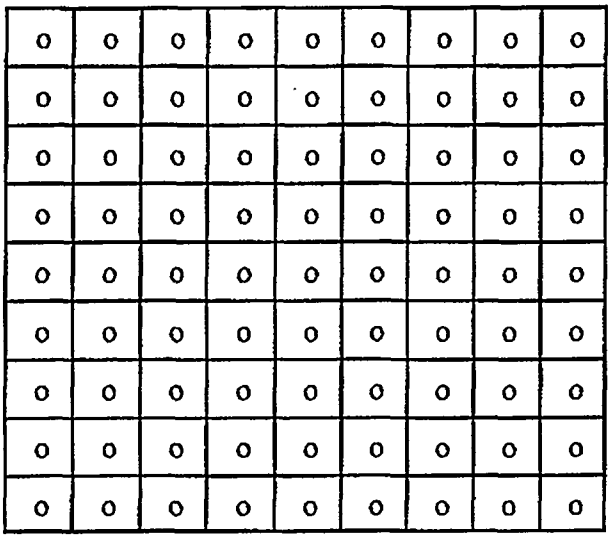

9 x 9 x 9 Array of Plutonium Spheres:
Radius of Sphere = 3.976 cm
C to C Spacing = 60.960 cm
Array Reflected on all Sides
with 30.0 cm Water
k_{eff} = 0.93

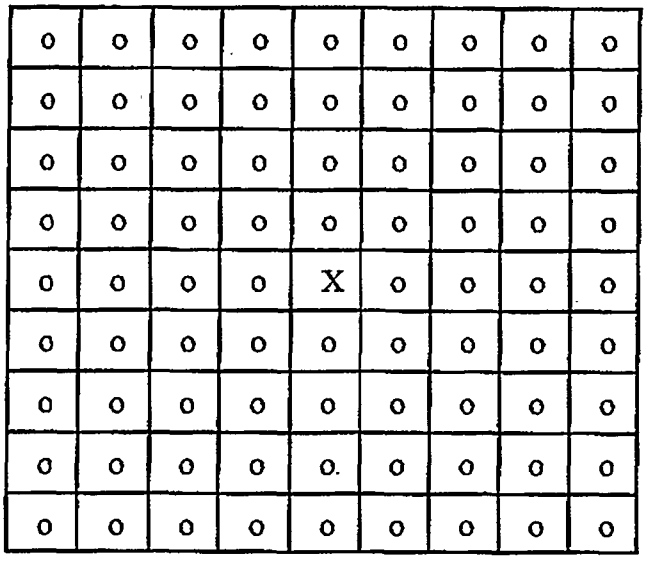

9 x 9 x 9 Array of Plutonium Spheres:
Radius of Sphere = 3.976 cm
C to C Spacing = 60.960 cm
Except Center unit Radius = 5.009 cm
Array Reflected on all Sides with
30.0 cm Water
k_{eff} = ?

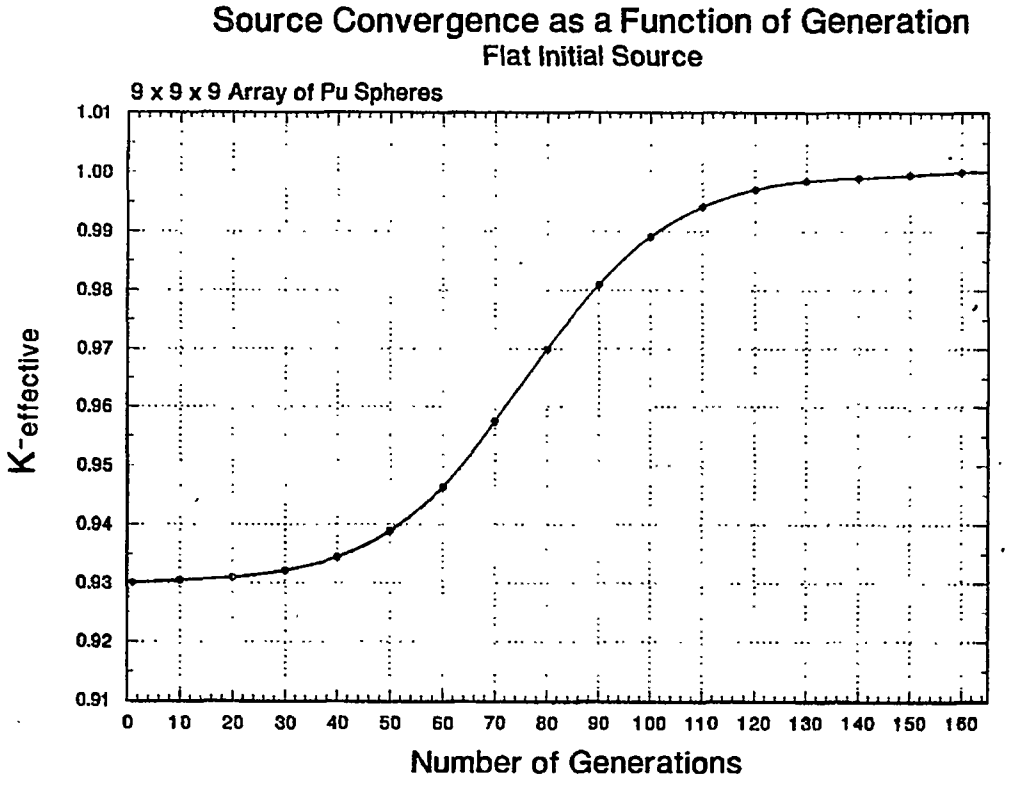
Source Convergence as a Function of Generation
Flat Initial Source
9 x 9 x 9 Array of Pu Spheres
K-effective
1.01
1.00
0.99
0.98
0.97
0.96
0.95
0.94
0.93
0.92
0.91
0 10 20 30 40 50 60 70 80 90 100 110 120 130 140 150 160
Number of Generations

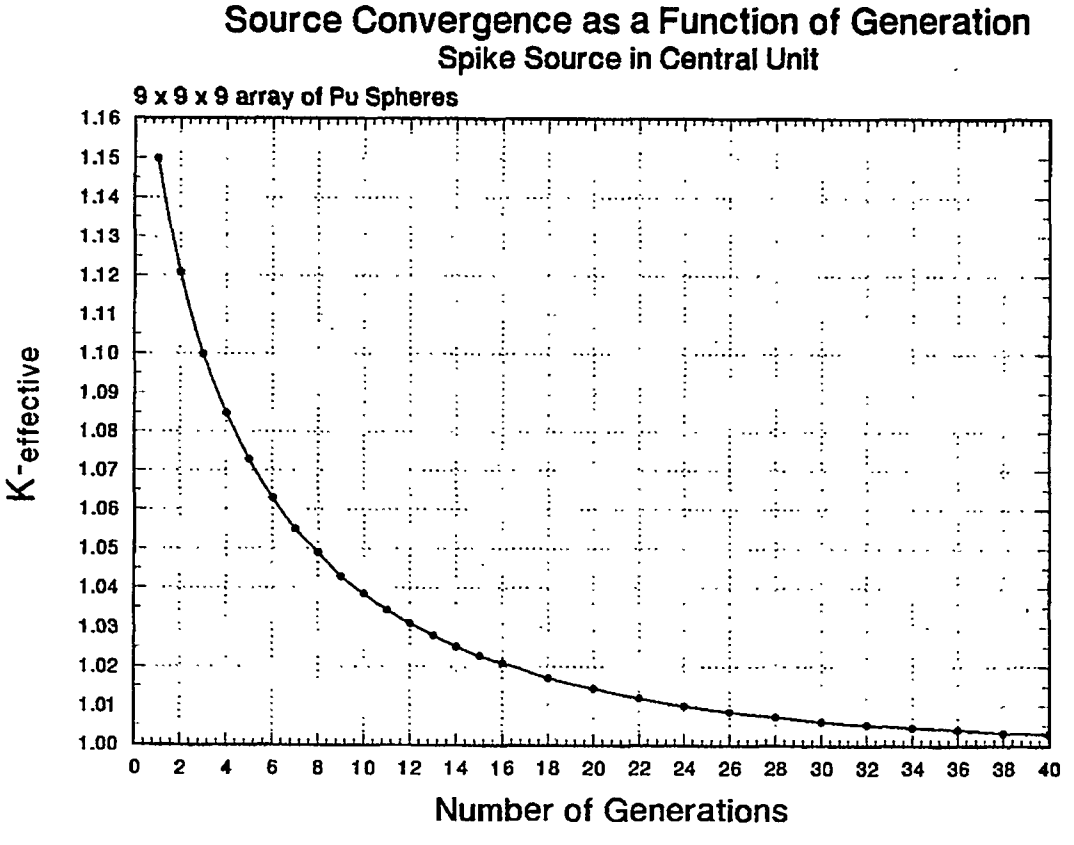
Source Convergence as a Function of Generation
Spike Source in Central Unit
9 x 9 x 9 array of Pu Spheres
K-effective
1.16
1.15
1.14
1.13
1.12
1.11
1.10
1.09
1.08
1.07
1.06
1.05
1.04
1.03
1.02
1.01
1.00
0 2 4 6 8 10 12 14 16 18 20 22 24 26 28 30 32 34 36 38 40
Number of Generations

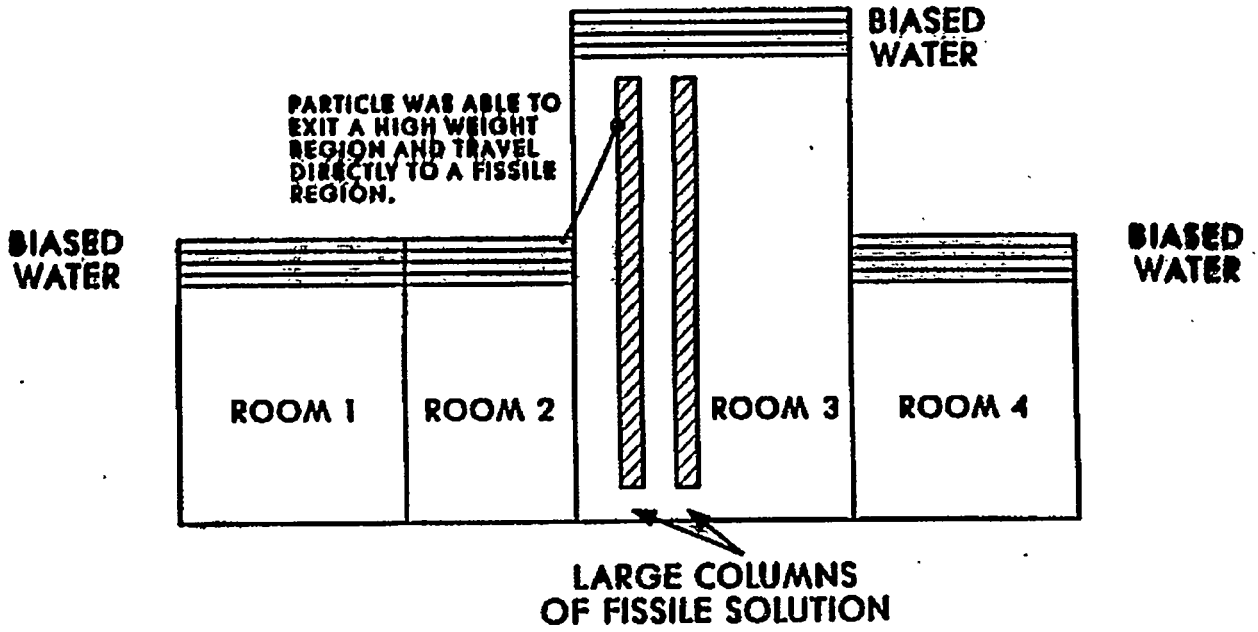
BIASED WATER
PARTICLE WAS ABLE TO EXIT A HIGH WEIGHT REGION AND TRAVEL DIRECTLY TO A FISSILE REGION.
BIASED WATER
BIASED WATER
ROOM 1
ROOM 2
ROOM 3
ROOM 4
LARGE COLUMNS OF FISSILE SOLUTION

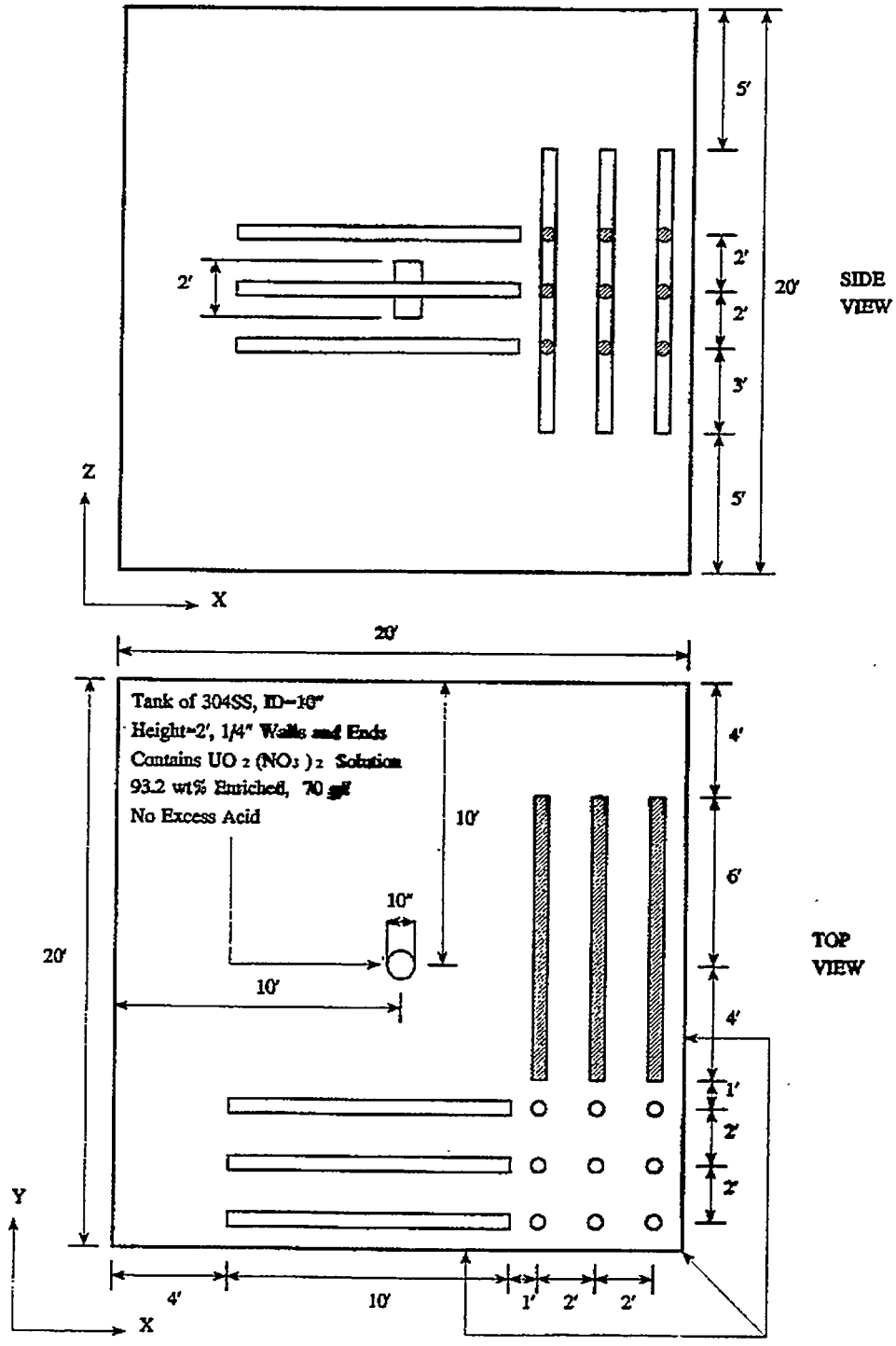

Use 12" Concrete Albedo for Walls

Three 3x3x1 Arrays of 6" ID Pipes, 10' Long, 2' CTC Spacing, 1/4" Walls of 304 SS, Contains $UO_2(NO_3)_2$ Solution 93.2 wt% Enr. 300 g/l. No Excess Acid

Clues to look for:

1. System physically large.

2. System contains fissile material with different geometrical configurations (including different dimensions of the same shape), or different physical properties, such as density, enrichment, etc., in different parts of the system.

3. Fissile material is separated by large distances or separated by isolating materials.

CONCLUSION

1. The Monte Carlo method can be used to model almost any situation,

2. The more complex a system, the more likely that source convergence can be a problem.

and,

3. If the source has not converged to the correct distribution, the computed k_{eff} will almost always be **too low**!

PITFALLS IN CRITICALITY SAFETY MONTE CARLO COMPUTATIONS: "THE k_{eff} OF THE WORLD"

Ely M. Gelbard

In work originally published in 1971,[1] Elliot Whitesides brought to our attention a problem still unsolved today. This was a problem he called "computing the keff of the world", a name which has survived for many years. The specific example which Whitesides discusses was a 9 x 9 x 9 array of plutonium spheres, surrounded by a water reflector. The computed keff of the array was .93. When the central sphere was replaced by a sphere which, when isolated, was exactly critical, the computed eigenvalue was still .93. It seems important to note that there are at least two potential sources of difficulty in such problems. One is an inadequate number of generations; the other is an inadequate number of starters per generation or, more precisely, inadequate sampling of physical detail within each generation. It is easy to see that these are really different types of difficulties. If sampling within each generation is inadequate increasing the number of generations won't help. And clearly increasing the amount of information gathered per generation won't help if the number of generations is inadequate. In a way the error due to undersampling within a generation is analogous to course-mesh errors in deterministic calculations, while inadequate source convergence acts similarly both in deterministic calculations and Monte Carlo.

It has been shown that the Monte Carol eigenvalue bias is given by the relations[2]

$$\Delta = -\frac{N}{2}\left(\sigma^2 - \sigma^2_{APP}\right) \qquad 1$$

where: Δ is the eigenvalue bias: σ^2 is the variance in the eigenvalue: σ^2_{APP} is the apparent variance in the eigenvalue computed as if eigenvalues in different generations were independent of each other: N is the number of generations. As the number of generations goes to infinity the variances decrease like 1/N, so that the bias eventually reaches an asymptote; it does not go to zero. It is pointed out in Ref. 3 that, if $N < 200$ and the relative standard deviations in eigenvalue is less than .25%, then $\Delta \leq \sigma$. But in criticality safety calculations both of these conditions may be violated.

Of course sampling per generation can always be improved simply by increasing the number of starters in each generation, but obviously this approach can be costly. Instead various devices may be used to improve sampling efficiency. In different ways each device uses knowledge of the importance of different regions in space and/or energy. In absorption-weighted tracking the details of the procedure determine which volumes of phase space will be emphasized. But other simple strategies may also be useful. Consider, as an example, the use of source biasing.

In the Whiteside 9 x 9 x 9 array the difficulty seems to be that few fission sites are created in any one of the spheres. Suppose we know the eigenvalue of each sphere in isolation. Probably one ought to know at least that much about any array before it is assembled. Given these eigenvalues, one could divide the whole configuration into zones and require a specified number of starters in each zone. Starting weights would be adjusted accordingly. For example in the 9 x 9 x 9 array one could surround the central sphere by a cube and place, let's say, a quarter of all starters in this cube. In the given case this method might suffice to give a reasonably good eigenvalue for the system. There could, however, still be important regions which remain undersampled. This might be true, for example, of spheres near the central sphere. But mapping of important zones could be considerably more detailed if necessary. It should be noted that in the interior of regular array it isn't necessary to sample the structure of the array in great detail, since neutrons traveling in one sphere are equivalent to neutrons in the other spheres. Only near irregularities is it necessary to sample details of the lattice structure.

Unfortunately this sort of source biasing can't be carried out at the beginning of each generation. Otherwise weight fluctuations would accumulate from one generation to another, increasing the variance in the eigenvalue. Source biasing could be repeated periodically, but infrequently.

In any slowly convergent Monte Carlo eigenvalue calculation there is still another problem. Probably most eigenvalue calculations give us what has been called above the "apparent" variance, computed as if eigenvalues in different generations were uncorrelated. In fact in weakly coupled systems successive eigenvalues are strongly positively correlated, and variances computed ignoring this correlation can be too small. The underestimation of variance is bothersome because it may give the user a false sense of security. Clearly the true statistical uncertainty is something we would like to know for its own sake. But the true standard deviation is useful also because of its connection with the eigenvalue bias. In fact, we see from Eq. (1) that, if we know the true eigenvalue variance we can compute the bias, and vice versa.

The true eigenvalue variance can often be roughly estimated by MacMillan's method,[4] but it still isn't clear just how reliable this method is. Probably a more reliable estimate can be obtained directly by replicating the eigenvalue calculation several times, using new starting random numbers for each replica. Of course this procedure increases running times but, on new parallel machines, or on parallelized networks, the cost of replicated Monte Carlos is not prohibitive. It probably isn't necessary to carry out such replications very frequently, but studies using replication would be useful, at this stage, to give us a better understanding of eigenvalue biases in difficult criticality safety problems. Such studies could also give us valuable information on the accuracy and reliability of MacMillan's method.

Finally, the replication process itself needs to be better understood. Certainly it gives an unbiased estimate of the eigenvalue variance, but it may still give a misleading estimate. One finds this situation, for example, in fixed source shielding calculations if rare events are crucially important. Suppose, in a criticality safety calculation, events in which fissions occur in one

relatively small portion of phase space are rare but crucially important. Then very infrequently one replica will give a very different eigenvalue from the great majority of others. In other words the estimated variance will be unbiased, but the distribution of estimates will be pathological. It would then be difficult to get a true variance by replication. In short we have a lot to learn about criticality safety Monte Carlo; but we now have the computing capacity and the theory to make a study of this sort of Monte Carlo application very fruitful.

REFERENCES

1. G. E. Whitesides (ORNL), A Difficulty in Computing the k-effective of the World.

2. R. J. Brissenden and A. R. Garlick, "Biases in the Estimations of K_{eff} and Its Errors by Monte Carlo Methods," Ann. Nucl. Energy, 13, 2, 63 (1986).

3. E. M. Gelbard and A. G. Gu, "Biases in Monte Carlo Eigenvalue Calculations," Nucl. Sci. and Eng., 117, 1-9 (1994).

4. MacMillan D. B. 91973). Monte Carlo Confidence Limits for Iterated-Source Calculations, Nucl. Sci. Eng. 50, 73.

EXPERIENCES WITH THE SUPERHISTORY POWERING ALGORITHM IN MONK

N. R. Smith

SUMMARY

For Monte Carlo algorithms aimed at solving criticality safety problems, the main distinguishing feature is the source specification and its convergence via a powering algorithm. Certain well-known problems of bias and instability can arise that need to be addressed. In the MONK software package the superhistory powering algorithm was developed in response to these problems and the method has been in general use for many years. This paper describes the superhistory powering algorithm and reviews experience of its usage since its development and subsequent implementation in the ANSWERS Software Service version of MONK.

1.0 INTRODUCTION

The standard analogue Monte Carlo neutron transport simulation comprises sampling source neutrons from a given distribution, tracking these samples throughout the system geometry and processing collisions with the nuclei of the system materials as and when they arise. During this process various quantities are scored which are then used to compute physical parameters of interest, such as neutron flux. Neutron samples are typically terminated when they cross the system geometry outer boundary or are parasitically absorbed as a result of a collision. In non-analogue Monte Carlo simulations various modified techniques can be implemented in order to increase the efficiency of the calculation, such as Russian Roulette/splitting or enhanced-survival collision processing.

For criticality applications, the main problem facing the Monte Carlo simulation in either the analogue or non-analogue form is the definition of the source distribution. The source distribution is not known exactly and in many cases it is difficult to identify a reasonable simple approximation. The Monte Carlo algorithm therefore takes the form of an iterative scheme whereby a guess of the source is made and regularly refined during the calculation itself. In order to acknowledge that the source is less than ideal it is common to disregard some of the early iterations whilst the source is changing most rapidly. However at some point in the calculation it must be assumed that the source is an adequate reflection of reality to enable the calculation proper to commence.

Certain well-known problems can arise during a criticality Monte Carlo simulation which may lead to biased results being produced. This is further compounded by the fact that the problems are difficult to spot in complicated situations without diligent investigation. Various techniques and hypotheses for resolving these problems have been investigated over the years

with varying degrees of success. This paper describes the superhistory powering technique that has been implemented in the Monte Carlo criticality software package MONK [1] and reviews experience of its usage.

2.0 SUPERHISTORY POWERING

2.1 Background

MONK is a Monte Carlo neutronics computer software package written to assist in the study of criticality safety problems. MONK originated from a code called GEM, which came out of the post-war nuclear weapons programme in the United Kingdom. The first appearance of MONK was about thirty years ago, and the main code user benefits have been retained to this day, although they have been considerably enhanced in the intervening years. These are:

- geometry modelling - the MONK geometry modelling package is the most easy-to use and flexible package in any generally available Monte Carlo particle transport code

- nuclear data/collision processing - the use by MONK of continuous energy modelling has significant benefits in terms of accuracy and ease-of-use when compared with multi-group methods

- user interface - MONK has an easy-to-use input syntax supported by wide-ranging validation data, user-oriented documentation and intelligible output syntax

MONK is widely used in both design environments and in support of regulatory license submissions and has been accepted by the USNRC following the submission of a Topical Report. MONK is distributed and actively supported in use by the ANSWERS Software Service of AEA Technology and development is performed within a collaboration between AEA and British Nuclear Fuels plc (BNFL).

The development of the MONK superhistory powering algorithm started in 1985 in response to the then topical problem of accurately analysing systems comprising loosely-coupled components [2] (i.e. systems comprising more than one fissile component where only limited interaction of the components occurs). The problem with such calculations had of course been noted much earlier (e.g. [3]) but the significant expansion of the reprocessing industry that was taking place in the UK in the 1980's, particularly the design and construction of the Thermal Oxide Reprocessing Plant (THORP) by BNFL brought the issue to renewed prominence.

Although the example presented in [2] was certainly extreme it was a good demonstration of the type of problems that could occur with criticality Monte Carlo simulations at that time, namely:

- for some interaction problems it was difficult (if not impossible) to obtain a reliable estimate of k-effective due to inadequate sampling arising from poor source convergence. Even when a good approximation to the neutron distribution was known, there were still potential problems caused by the finite size of each iteration and the procedure used to produce the source for the next iteration

- for some interaction problems, even where an apparently reliable estimate of k-effective was obtained, the estimate of the standard error was too small (which, as this is normally used to construct confidence limits on k-effective, is a potential safety issue)

The above problems led to a programme of work by Brissenden and Garlick [4], who proposed an effective solution in the form of a revised Monte Carlo source convergence algorithm which they christened 'superhistory powering'. A mathematical treatise on the new algorithm [5] led to the identification of the parameters that affect the source convergence and their significance when calculating k-effective and its standard error by conventional powering techniques. The bias on k-effective for such techniques was confirmed to be of order M^{-1}, where M is the number of neutrons in an iteration, whereas the the standard error estimator was shown to under-predict the true value by an quantity of order $(MN)^{-1}$, with N equal to the number of iterations. This under-prediction of the standard error resulted in differences between calculated and true values of up to a factor of two in extreme situations, although its magnitude was closely related to the geometry and material composition of the system. This work resulted in a version of the MONK software package which incorporated the new superhistory algorithm to overcome these problems (version MONK6A, distributed by the ANSWERS Software Service in 1987).

2.2 Conventional Powering Problems

The basic definition of k-effective is:

$$k = \frac{\text{rate of neutron production}}{\text{rate of neutron loss}}$$

where neutron production comprises neutrons born following fission events and neutron loss comprises neutrons absorbed or lost to the system by leakage.

$$\text{i.e.} \quad k = \frac{\upsilon \Sigma_f}{\Sigma_a + L}$$

where υ, Σ_f, Σ_a and L are all average values with respect to position, velocity and time of the neutron production from fission, the macroscopic fission and absorption cross-sections, and the leakage respectively.

Taking the time sequence as a single neutron generation, the definition of k-effective becomes:

$$k = \frac{\text{neutrons produced in one generation}}{\text{neutrons lost in the same generation}}$$

Therefore in an analogue Monte Carlo calculation we can calculate the value of k-effective for a large number of sample neutrons and then compute an average value. In its simplest implementation, this leads to an iterative calculation scheme where the neutrons produced as a result of fissions in one iteration form the basis of the source distribution for the next iteration; this is called powering of the source distribution. By taking appropriate measures it is possible in many situations for the calculation to converge to a stable and reasonable approximation of the true fission distribution, producing a converged estimate of k-effective.

The powering process is an attempt to simulate an indefinitely large sample of independent neutron histories in the steady-state condition. Due to the finite size of a calculation it is an approximation and it is therefore inevitably flawed.

The calculation requires:

- a reasonable initial source guess
- a powering algorithm to turn this into a good approximation of the steady-state source distribution as efficiently as possible (the settling process)
- a powering algorithm that maintains this good approximation of the steady-state source distribution for the duration of the calculation

Conventional or history powering is typically based on the following process (which is repeated for a number of iterations):

- select M neutrons from a given source distribution to form the starting points of the iteration
- track those neutrons to absorption or leakage (i.e. a single neutron generation)
- record those neutrons that terminate in fission collisions
- use an algorithm for selecting from the fission children produced in the current iteration to determine the source distribution to be sampled from for the next iteration

Brissenden and Garlick identified that conventional powering is not even-handed. For standard algorithms, iterations with below-average importance will tend to produce fewer children (and these will also tend to have below-average importance) and require above average duplication to make up the next M source neutrons. Conversely an iteration of above-average importance will tend to produce more children (of above-average importance) and these will require below-average duplication to form the next iteration source. The effect of this is that the source distribution is distorted by favouring the less important neutrons at the expense of the more important neutrons, thereby biasing the calculated value of k-effective. However for many

practical criticality applications this k-effective bias is likely to be small (or even negligible). Note that all supplementary scored quantities such as fluxes and reaction rates will be similarly affected.

Of more significance is the effect on the calculated standard errors, where Brissenden and Garlick demonstrated that the bias introduced can take a non-negligible negative value and hence impact on safety arguments which are based on confidence limits on calculated values of k-effective. This was further demonstrated in an analytical study performed about the same time [6]. The main cause of the under-estimation is the positive correlation that exists between iterations in conventional powering, whereas the derivation of the standard error assumes the sample histories in different iterations are independent. A further source of variation comes from the finite size of the neutron population sampled from the source distribution and in some situations this too can be significant.

2.3 Superhistory Powering Algorithm

The mathematical analysis of the standard fission source iteration process described above led to the development of the superhistory powering algorithm to significantly reduce the biases in the calculation of k-effective and its standard error. The superhistory algorithm requires the definition of the unit sample size to be changed.

Each iteration, instead of comprising single generation histories (from birth due to fission to termination by fission, capture or leakage), now comprises multi-generation superhistories, each of which starts from birth due to fission and terminates at L^{th} generation fission (or capture or leakage as before). A neutron superhistory is therefore the set of histories from a neutron and all its progeny through L fission generations (the default value of L is 10). Neutrons that undergo fission in the L^{th} generation are saved for use in determining the starting source for the next iteration. The first part of a superhistory is shown in Figure 1—note that all branches of the tree are followed as part of the superhistory up to the L^{th} generation.

In the normal course of events, for a sub-critical system, few superhistories will survive to the L^{th} generation; conversely for a super-critical system they will be too numerous. In order to stabilise the situation, the superhistory powering algorithm modifies the υ-value for fission throughout the system by dividing the actual value by the best current estimate of k-effective. This maintains the required approximation to equilibrium without in any way biasing the calculation. Obviously when scoring quantities used to compute k-effective this modification to the υ-value needs to be taken into account. As each iteration now comprises say ten generations rather than one (and as the algorithm is effectively simulating a critical system by the υ-value modification), each superhistory iteration is on average about ten times larger that a conventional iteration, and hence fewer iterations are required to achieve a particular statistical precision on k-effective. In addition fewer settling iterations are required before scoring commences.

Superhistory powering has the following attributes:

- Reduced k-effective bias because unimportant iterations are not favoured. Each iteration contains a long sequence of fission generations to establish a good approximation to the steady-state
- Each iteration is effectively an independent trial - hence there is a much reduced standard error bias
- The noise introduced by sampling the preceding iteration progeny is greatly reduced hence for a given sample size the standard error on k-effective is reduced
- Loosely-coupled systems are treated properly - this a major problem with conventional powering because unreactive components, being also relatively unimportant, are favoured at expense of reactive components. Superhistory powering naturally concentrates on the most reactive parts of the system

Superhistory powering will solve the inherent problems associated with history powering processes provided:

- a reasonable initial source distribution is specified which does not preclude the sampling of all fissile material zones present in the system
- sufficient superhistories per iteration are employed to adequately represent the steady state fission distribution
- sufficient total superhistories are scored (i.e. sufficient iterations are performed) to enable adequate sampling from the steady-state fission distribution to be performed

However in very complex cases, a poor initial source distribution coupled with inadequate calculation control parameters can still result in inadequate sampling (albeit on a smaller scale) and this may be difficult to identify. To address this issue, further development of MONK is planned aimed at diagnosing when unsuitable control parameters are employed by performing in-code settling and sampling checks. For the time being however such checks need to be performed by analysing the full range of scored parameters and performing comparison calculations.

The first generally-available version of MONK containing the superhistory powering algorithm was released by the ANSWERS Software Service of AEA Technology in 1987. Essentially the same algorithm is included in the current release of the software package MONK7A. The rest of this paper will describe experience with the superhistory powering algorithm within the MONK computer software package.

3.0 SUPERHISTORY POWERING IN USE

Superhistory powering has been the default mode of calculation in MONK for several years and during that time a very large number of calculations have been performed, including both in-service application usage and benchmarking exercises. Subject to the above guidelines concerning recommended calculation control parameters, the performance of the software package has been reliable and consistent, with credible standard error estimates being produced whenever comparison calculations have been performed. The first section below examines a typical interaction problem and demonstrates the ability of the superhistory algorithm to deal with such situations - this problem has similar characteristics to those of the interaction problem that initiated the original superhistory algorithm development. The second section below analyses the MONK standard error estimation by performing a set of repeated calculations for a number of applications of interest - this is recognition that the standard error bias is the most significant bias that superhistory powering was designed to alleviate.

3.1 Interaction Problems

In order to investigate the benefits arising from superhistory powering for the solution of interaction problems, a simple demonstration case has been set up. The model comprises four cylinders containing UO_2/graphite/water located in the corners of a concrete walled room, with a sphere of highly-enriched uranium located in the centre of the room. A plan view of the model is shown in Figure 2.

This simple case mirrors the main properties of the classic interaction problem, with more than one area of fissile material of differing multiplications (in this case we have four equivalent areas and one different) with little interaction between the low and high multiplication areas. In this case very few neutrons emerging from any of the cylinders (of height 100cm) will enter the sphere (of radius 9cm). In addition once neutrons enter the sphere, those that escape will almost certainly not return as they will either enter the cylinders, either directly or via reflection at the concrete walls, or be lost to the system by absorptions in the concrete or leakage.

Two preliminary calculations were performed to determine the value of k-effective for the isolated components: firstly, with just the four cylinders in the corners of the concrete room, and secondly, with just the metal sphere in the centre of the concrete room. The results for these cases were 0.8682 and 1.0376 respectively. It is expected that the multiplication for the whole system (cylinders and sphere) will be close to (and slightly greater than) that for just the sphere due to the limited interaction.

A series of MONK calculations was performed, both using superhistory powering and conventional powering (achieved by setting the superhistory parameter L equal to one). Three different sets of control parameters were considered and for each, six different starting source descriptions were employed. The cases are summarised in Table 1 with the MONK results shown

in Table 2. Note that the results show interim results when the calculated standard deviation on k-effective is 0.0050, 0.0040, 0.0030, 0.0020 and 0.0010 (the final precision obtained). The convergence for each case is also shown in Figures 3, 4 and 5.

The results show that:

- for all cases, convergence of the source occurred more rapidly and reliably with superhistory powering than with conventional powering
- the continuing convergence of some of the conventional powering results makes the calculated standard errors unbelievable
- conventional powering with only 100 neutrons per iteration produces significantly biased values of k-effective for this situation. Even for 1000 neutrons per iteration there are significant differences between the values of k-effective for the different starting sources.
- the effects of a poor starting source choice are more pronounced for conventional powering, confirming the claim that superhistory powering naturally concentrates on the most reactive parts of the system. For superhistory powering the spread of the results for the different source configurations is smaller at each step.

It is concluded that the MONK superhistory powering algorithm can successfully solve interaction problems that are beyond the range of conventional powering algorithms.

3.2 Standard Error Estimation

It was noted above that the most significant bias that the superhistory powering algorithm was designed to overcome was that in the calculation of the standard error on k-effective. In order to investigate the extent to which this has been successful, a number of repeat calculations have been performed to enable an observed external estimate of the standard error to be obtained from the distribution of calculated k-effective values. This can then be compared with the internal estimate of the standard error computed by MONK.

Although such analysis was performed when superhistory powering was first introduced [6], computer hardware limitations of the time meant that only a relatively simple case could be considered. With the availability of plentiful cheap computing it is now possible to look at a range of situations more typical of MONK applications.

The study has comprised six different MONK models, each being calculated one hundred times, with each calculation employing a different starting random number generator seed. These calculations were run to achieve a requested standard deviation (between 0.0010 and 0.0030 depending on the length of the calculation) and this value was then compared with that obtained from the observed variation in calculated values of k-effective.

The six situations considered are shown in Table 3 with the results obtained for the sets of one hundred calculations shown in Table 4.

These results show that the standard error computed by MONK is a good estimate of the true standard error derived from the variation in k-effective for repeat calculations, with the difference between mean calculated and observed values lying within two standard deviations for all six cases, and within one standard deviation for five of them.

The distribution of calculated results for each case has been assessed by performing χ^2 goodness-of-fit tests for each set of results. The hypothesis is that the calculated results follow a normal distribution. The goodness-of-fit test was performed by observing the number of calculated results within each of ten equi-probable bins from a standardised normal distribution and comparing with the expected value of 10 (=100 values/10 bins). The χ^2 values for the six cases are 7.4, 6.9, 3.0, 5.8, 2.8 and 6.6 compared with a 5% significance level value of 14.1, confirming the normal hypothesis in each case at this level of significance. Plots of the distribution of observed k-effective values for the ten equi-probable normal distribution bins are given in Figure 6.

It is therefore concluded that the MONK superhistory powering algorithm produces effectively unbiased estimates of the standard deviation on k-effective for practical criticality applications.

4.0 CONCLUSIONS

This paper has reviewed the development and subsequent usage of the superhistory powering algorithm in the Monte Carlo criticality software package MONK. Superhistory powering has the following attributes:

- Reduced k-effective bias because unimportant iterations are not favoured. Each iteration contains a long sequence of fission generations to establish a good approximation to the steady-state
- Each iteration is effectively an independent trial - hence there is a much reduced standard error bias
- The noise introduced by sampling the preceding iteration progeny is greatly reduced hence for a given sample size the standard error on k-effective is reduced
- Loosely-coupled systems are treated properly - this a major problem with conventional powering because unreactive components, being also relatively unimportant, are favoured at expense of reactive components. Superhistory powering naturally concentrates on the most reactive parts of the system

Calculations have been performed which have demonstrated these features in practical criticality safety applications. The superhistory powering algorithm in MONK has been in use within the nuclear industry for several years and has enabled the MONK software package to be used with confidence to solve many complex criticality problems beyond the range of conventional powering algorithms.

REFERENCES

1. Smith N R and Morrell G A, "An Introduction to MONK7", *International Conference on Nuclear Criticality Safety ICNC'95* (Albuquerque, 1995).

2. Prescott A, "Criticality Interaction Problems Associated with Monte Carlo Computer Codes", *Topical Meeting on Criticality Safety in the Storage of Fissile Material (Jackson,* 1985).

3. Whitesides G E, "A Difficulty in Computing k-effective of the World", *8th International Conference on Radiation Shielding* (Arlington, 1994).

4. Brissenden R J and Smith N R, "Further Studies of the Prescott Interaction Problem using Superstage Powering in MONK6.4", *Topical Meeting on Criticality Safety in the Storage of Fissile Material (Jackson,* 1985).

5. Brissenden R J and Garlick A R, "Biases in the Estimation of K-eff and its Error by Monte Carlo Methods", *Annals of Nuclear Energy,* **13 No. 2** (1986).

6. Wakeford R, Clemson P D, Barratt S and Skilling K, "A Statistical Analysis of Results from Monte Carlo Codes", *International Seminar on Nuclear Criticality Safety ISCS'87* (Tokyo, 1987).

Table 1. Summary of Interaction Calculations

Case	Description
1	Conventional powering with 100 neutron histories per iteration and 20 settling iterations
2	Conventional powering with 1000 neutron histories per iteration and 20 settling iterations
3	Superhistory powering with 1000 neutron superhistories per iteration and 2 settling iterations (L=10)
Source	**Description**
A	Uniform source distributed over the whole inside of the concrete room
B	Uniform source distributed within the four cylinders
C	Uniform source distributed within the four cylinders and the sphere
D	Uniform source distributed within the sphere
E	Uniform source distributed within the concrete walls of the room
F	Uniform source distributed optimally[1] within the four cylinders and the sphere

[1] Optimal distribution of source between cylinders and sphere (based on calculated fission distribution from other superhistory cases) - this is approximately 40% of source particles in the sphere and 15% in each of the cylinders. Note that within each of the fissile zones the selection of source points is uniform.

Table 2. Results of Interaction Calculations

Case	k-effective ($\sigma = 0.0050$)	k-effective ($\sigma = 0.0040$)	k-effective ($\sigma = 0.0030$)	k-effective ($\sigma = 0.0020$)	k-effective ($\sigma = 0.0010$)
1A	0.9195	0.9563	0.9783	1.0070	1.0241
1B	1.0447	1.0341	1.0272	1.0178	1.0069
1C	0.9913	0.9964	1.0123	1.0235	1.0203
1D	1.0097	1.0238	1.0228	1.0189	1.0190
1E	1.0058	0.9719	1.0000	1.0184	1.0152
1F	1.0278	1.0165	1.0263	1.0101	1.0180
2A	0.9760	0.9951	1.0143	1.0295	1.0361
2B	0.9610	0.9732	0.9970	1.0225	1.0343
2C	1.0276	1.0282	1.0322	1.0396	1.0438
2D	1.0520	1.0529	1.0446	1.0434	1.0423
2E	0.9570	0.9738	1.0019	1.0269	1.0342
2F	1.0272	1.0289	1.0305	1.0311	1.0343
3A	1.0373	1.0343	1.0411	1.0428	1.0385
3B	1.0316	1.0366	1.0391	1.0452	1.0421
3C	1.0266	1.0304	1.0342	1.0370	1.0373
3D	1.0345	1.0426	1.0454	1.0416	1.0407
3E	1.0420	1.0448	1.0456	1.0421	1.0428
3F	1.0332	1.0387	1.0411	1.0435	1.0416

Table 3. Summary of Standard Error Comparison Calculations

Case A	Single sphere of high-enriched uranium metal
Case B	An array (3x3x3) of Plexiglas cylinders of high-enriched uranyl nitrate with no interstitial moderation
Case C	Typical PWR fuel storage rack containing 20x3 locations with 3% enriched fuel stored on a chequer-board configuration (fully water-flooded)
Case D	AGR fuel transport flask (shipping cask) containing an array of 5x3 fuel elements
Case E	Pulsed column with hafnium sieve plates containing plutonium nitrate solution - concrete-reflected
Case F	Geometrically safe storage tank ('harp tank') containing plutonium nitrate solution - concrete reflected

Table 4. Results of Standard Error Comparison Calculations

Case	Mean MONK k-effective	Mean MONK Standard Deviation	Observed Standard Deviation	Difference[1]
A	1.00147 ± 0.00011	0.00100 ± 0.00003	0.00112 ± 0.00008	1.4
B	0.99836 ± 0.00020	0.00200 ± 0.00003	0.00197 ± 0.00014	0.2
C	0.87742 ± 0.00032	0.00300 ± 0.00003	0.00317 ± 0.00022	0.8
D	0.80866 ± 0.00032	0.00300 ± 0.00003	0.00319 ± 0.00023	0.8
E	0.90567 ± 0.00020	0.00200 ± 0.00003	0.00200 ± 0.00014	0.0
F	0.62663 ± 0.00020	0.00200 ± 0.00003	0.00201 ± 0.00014	0.1

[1] $\text{Difference} = \dfrac{\left|\text{Mean MONK Standard Deviation} - \text{Observed Standard Deviation}\right|}{\sigma_{\text{DIFFERENCE}}}$

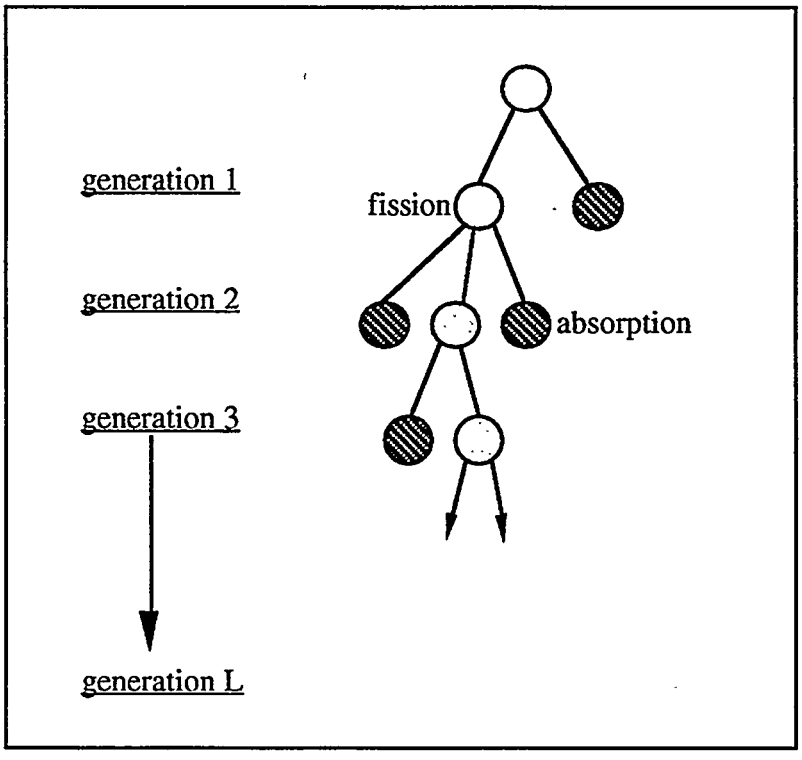

Figure 1. Part of a typical Superhistory

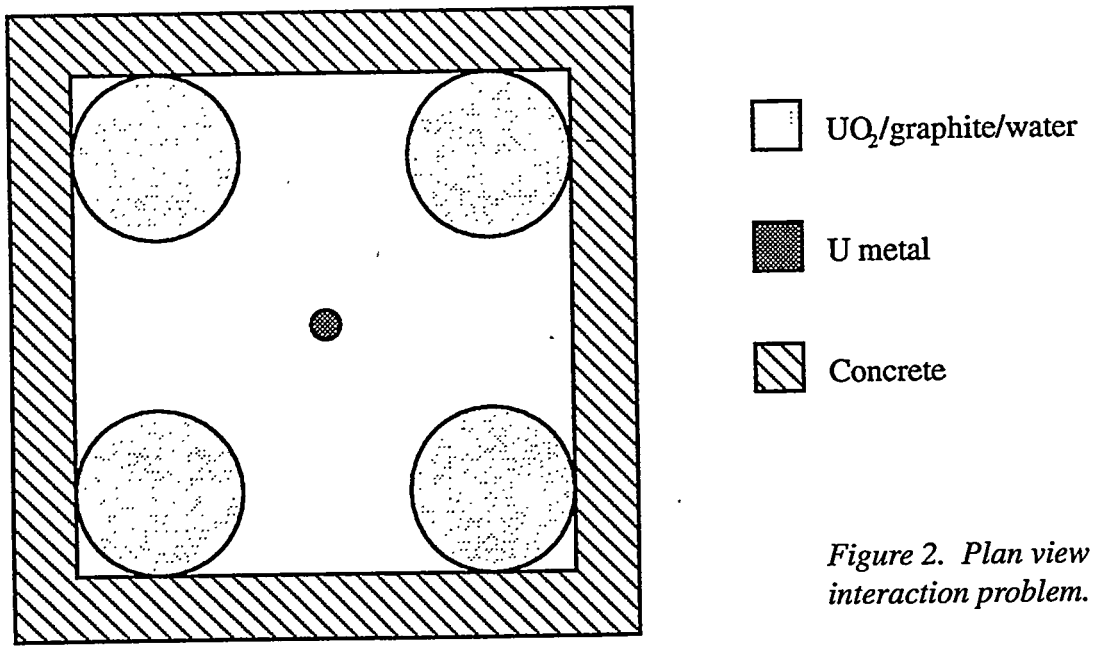

Figure 2. Plan view of interaction problem.

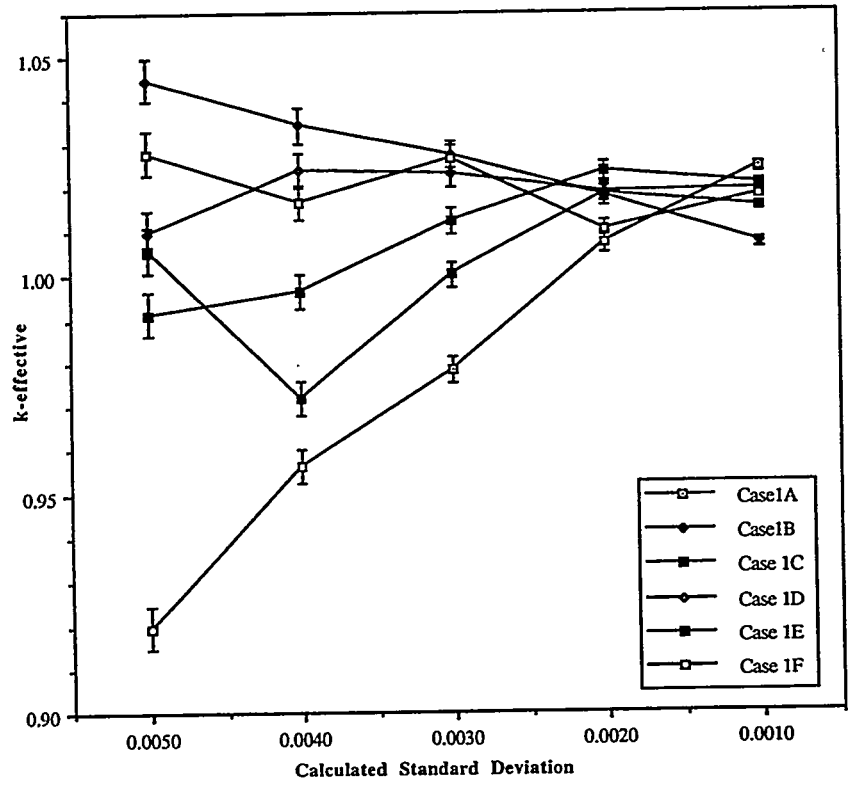

Figure 3. Convergence plot for Interaction Case 1
Conventional Powering(100 neutron histories per iteration and 20 settling iterations)

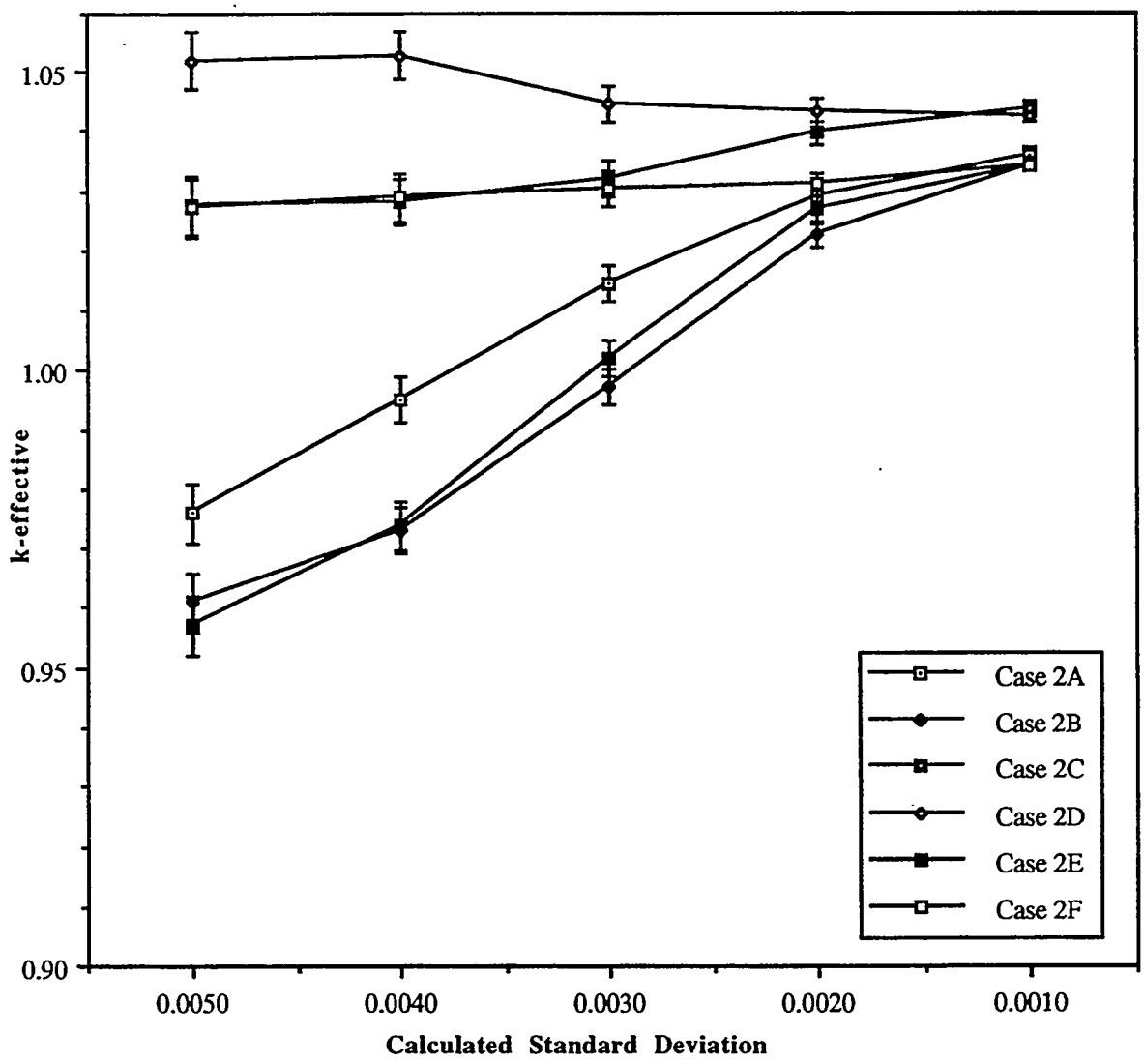

Figure 4. Convergence plot for Interaction Case 2
Conventional Powering(1000 neutron histories per iteration and 20 settling iterations)

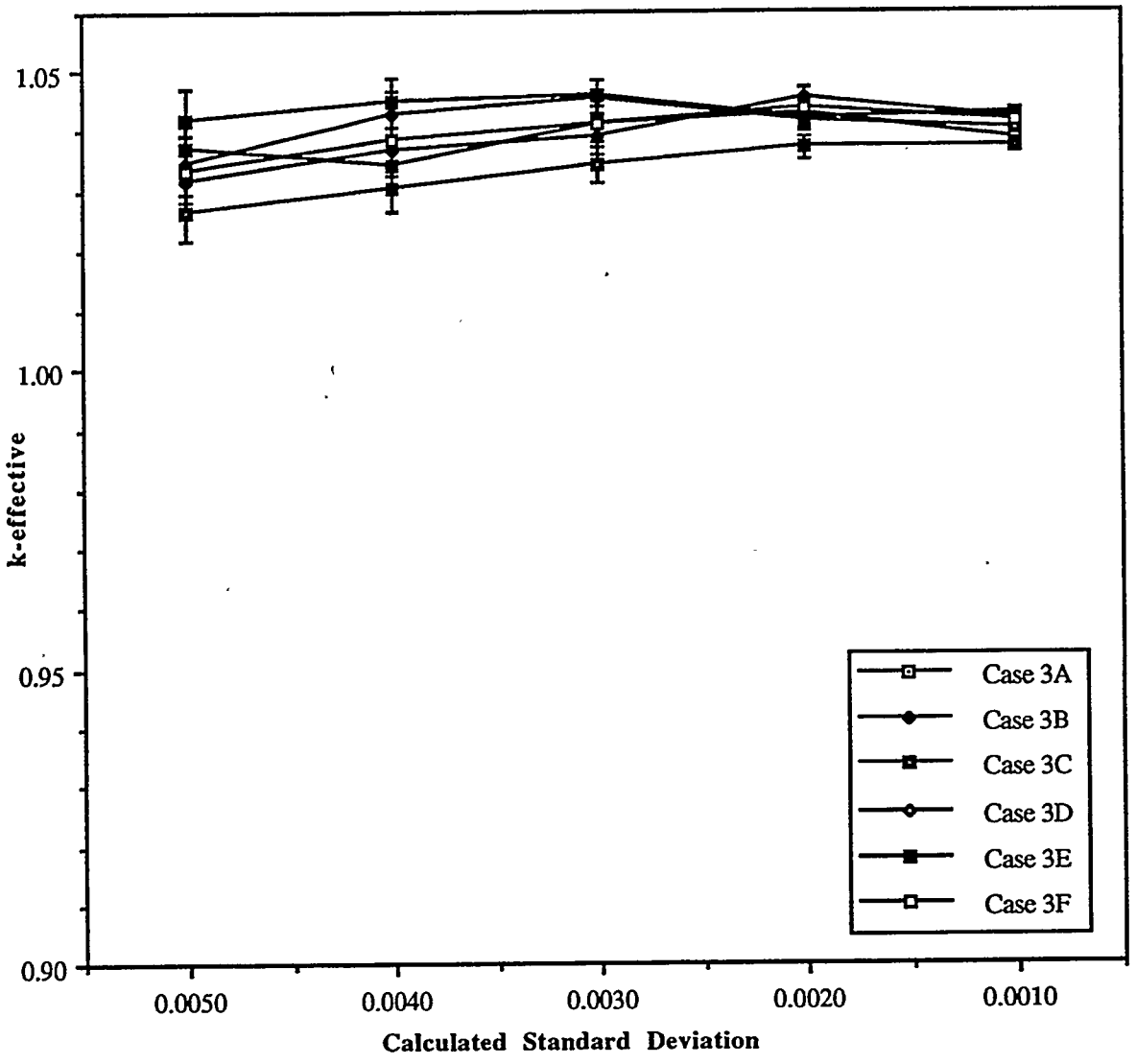

Figure 5. Convergence plot for Interaction Case 3
Superhistory Powering (1000 neutron superhistories per iteration and 2 settling iterations)

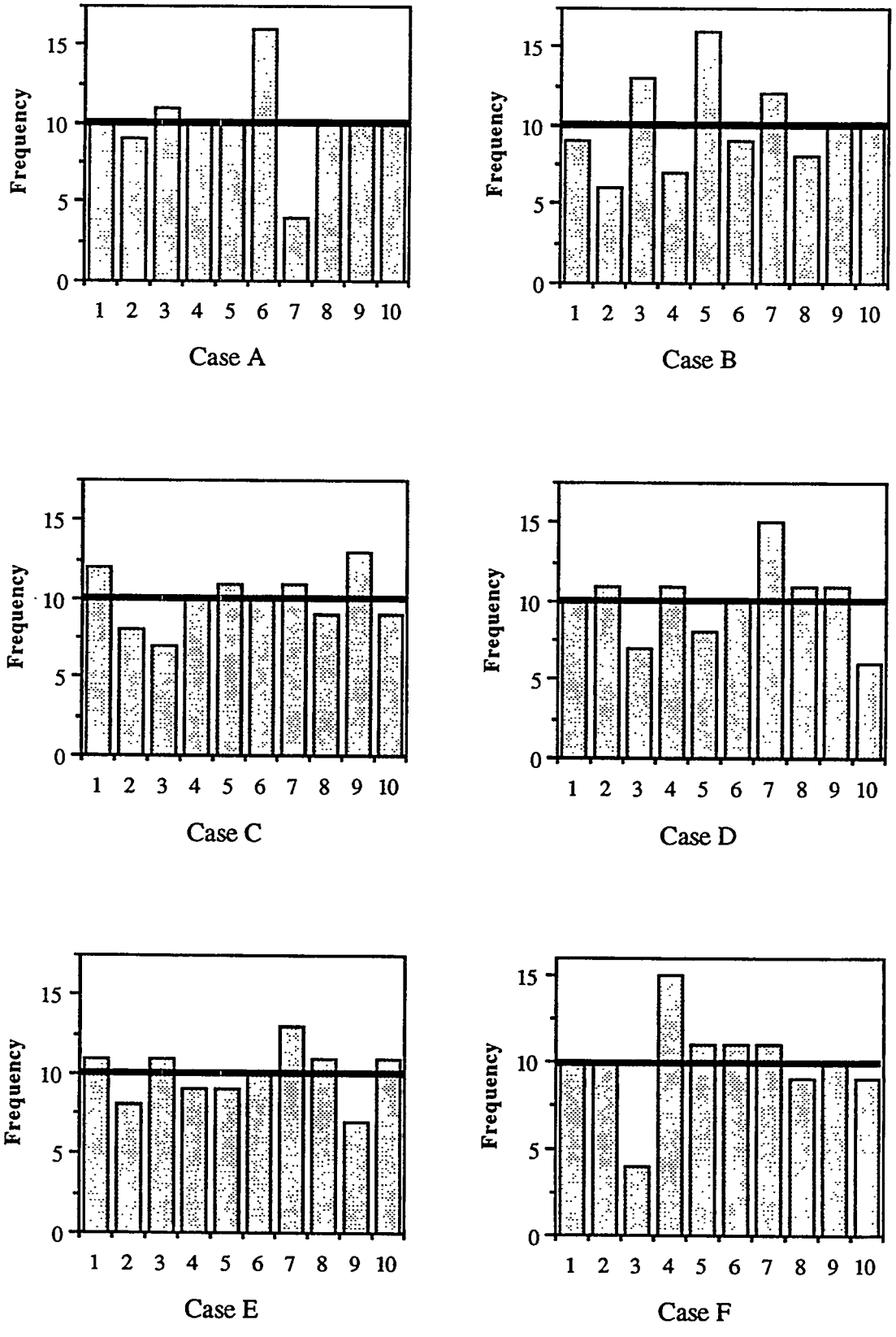

Figure 6. Goodness-of-fit results

WEDNESDAY, MAY 17, 1995

SESSION II
MONTE CARLO VULNERABILITIES OF EXECUTION AND INTERPRETATION

ASSURANCES ASSOCIATED WITH MONTE CARLO CODE RESULTS

D. F. Hollenbach and L. M. Petrie
Oak Ridge National Laboratory

All Monte Carlo computer codes have an uncertainty associated with the final result. This uncertainty (or standard deviation) is due to the sampling method inherent within the Monte Carlo technique. The basic assumptions required for the final result and uncertainty to be valid are (1) the random numbers used are truly random, (2) there is no correlation between histories, (3) the number of histories used is sufficient to represent the problem, and (4) the entire problem is adequately sampled. The first two assumptions are an integral part of the computer code and the user has minimal control over them. The last two assumptions are strongly dependent on how a problem is setup and the number of histories processed. These are items the user has direct control over. This paper examines six aspects of the KENO Monte Carlo code that affect the above mentioned four assumptions.

For a random number generator to work properly, it must have a viable algorithm and a starting seed that will produce long strings of random numbers ($>10^{15}$ numbers) prior to repeating itself. Most random number generators in use today are based on the linear congruential method. Different machines use different random number generations. In the workstation version of KENO, the random number generator combines three independent linear congruential method streams to create a series of random numbers that have a flat distribution. This set of random numbers is used to generate random numbers for other types of distributions. For certain computers and random number generators the initial seeds have been tested to ensure they produce a long string prior to repeating. If a different sequence of random numbers is desired, for example to run the same problem again, it may be desirable to use one of the random numbers previously generated as the initial random number. This has the effect of simply starting a different position in the same string of random numbers. If an initial random number is chosen at random, for some random number generators, it is possible the random number series will either not be sufficiently random or rapidly start repeating itself.

In Monte Carlo codes the uncertainty associated with the final results can be reduced by increasing the number of histories processed. The total number of histories processed is a product of the number of histories per generation and the number of generations run. KENO defaults to 300 histories per generation and 103 generations. This is sufficient to produce good results for a small relatively simple problem. A balance between histories and generations is needed to produce good results. Too few generations and the source distribution may not converge, too few histories per generation and the problem volume may not be completely sampled. Either of these conditions will degrade the quality of the final result and associated standard deviation. The standard deviation generally decreases inversely with respect to the square root of the number histories processed. It is possible to reduce the standard deviation as low as desired by processing more histories. However beyond a certain point the standard deviation calculated is not

representative of the true uncertainty of the final result. This can be especially critical in sensitivity studies where small differences become important.

Machine precision can also have a significant effect on a problem. Single precision computer codes will not properly process problems with geometry differences of 10^7 or greater in the same coordinate system. On most computers a single precision real number has seven significant figures. If two numbers that differ by greater than 10^7 are added together the larger number remains unchanged. One needs to also be aware that if two numbers that differ by only 10^5 are added together the smaller number contains only 2 significant figures regardless of the number of figures it may actually have. Although KENO-V.a does its processing in double precision the geometry data is stored in single precision.

Biasing (or weighing) is used to decrease the CPU time needed to process a problem. Biasing is primarily used on the reflector material surrounding a given fissile assembly or group of fissile assemblies. The most efficient biasing scheme is to weight a histories by a function inversely proportional to its importance at that position. KENO has biasing data for Concrete, Paraffin, Water, and Graphite based on distances from fissile source. The biasing data contains from six to twenty regions of a specified thickness that go from the lowest biased region next to a fissile region to the highest biased region furthest from the fissile region. If the biasing regions are set up so that upon exiting a high bias region a particle can enter a low bias region or a fissile region without passing through the intermediate bias regions, a large increase in the variance of the results is possible. In KENO, a discontinuity or step change in the standard deviation in the k_{eff} vs. generation plot would be an indication of this type of problem.

For the final result to have any value the source distribution must be converged. For a source to converge the number of histories per generation must be large enough to represent the system. Given a sufficiently large initial source distribution, a minimum of three and possibly many more generations are usually required before a source will converge to its steady state result. In some problems the source may never converge but instead fluctuate between volumes of high reactivity. A good example of this is a spent fuel shipping cask with high burnup, low reactivity and enrichment, in the center and low burnup, high reactivity and enrichment at both ends of the fuel assemblies. This problem requires many times the histories per generation to produce a converged source than is required by the same problem with either a constant or cosine distribution enrichment throughout the fuel assemblies. A good method for ensuring the entire problem is properly sampled is to examine the flux densities and fission densities. If a unit containing a large amount of fissile material relative to the other units in the problem has a low flux or fission density, that unit is probably not being properly sampled. This problem may be eliminated by either increasing the number of neutrons per history or explicitly starting histories in that particular unit.

Source convergence can be sped up by specifying an initial source that closely resembles the converged source. In addition to a uniform distribution throughout all fissile material, KENO allows the initial source to be started as a cosine distribution over a specified volume, in

specified units or positions in an array, or at specified positions in the global unit. If a reasonable initial source is not provided the system may never converge.

As is apparent from the above discussion simply accepting a result without verifying its quality is a dangerous practice. Simply because a code successfully produces a result does not mean the result is valid. A good understanding of the problem and the methods used to solve the problem are essential to producing accurate results. Monte Carlo computer codes should never be used as a "black box."

MCNP ANALYSES OF CRITICALITY CALCULATION RESULTS

R. A. Forster and T. E. Booth
Los Alamos National Laboratory

1. INTRODUCTION

Careful assessment of the results of a calculation by the code itself can reduce mistakes in the problem setup and execution. MCNP has over four hundred error messages that inform the user of FATAL or WARNING errors that have been discovered during the processing of just the input file. MCNP4A performs a self assessment of the calculated results to aid the user in determining the quality of the Monte Carlo results.

MCNP4A contains new, built-in sensitivity analyses of the MCNP Monte Carlo calculation that provide the user with simple WARNING messages for both criticality and fixed source calculations. The goal of the new analyses is to provide the MCNP criticality practitioner with enough information in the output to assess the validity of the k_{eff} calculation and any associated tallies. The results of these checks are presented in the k_{eff} results summary, several k_{eff} tables and graphs, and tally tables and graphs. Plots of k_{eff} at the workstation are also available as the problem is running or in a postprocessing mode to assess problem performance and results.

2. k_{eff} RESULTS SUMMARY

The MCNP k_{eff} results summary of the problem execution begins with the numbers of inactive and active cycles and histories requested and run. The next two pieces of information address how acceptable the Monte Carlo solution appears to be. The first check is to determine if all cells with fissionable material had fission source points on any cycle. This serves as a geometry sampling check. If so, a line is printed to acknowledge that fact that all cells were sampled. Otherwise, a WARNING message is printed in the output and at the terminal to inform the user which fissionable cells had no tracks entering, and/or no collisions, and/or no fission source points.

Another check involves the behavior of the average k_{eff} versus active cycle numbers. It is highly unlikely that the average k_{eff} would increase or decrease monotonically during the last ten active cycles for a problem with a properly converged spatial fission source. A WARNING message is issued if there is a monotonic trend during the last ten average k_{eff} values. This message could indicate incomplete spatial convergence of the fission source.

Information is then provided about the apparent normality of the active cycle k_{eff} values for each of three MCNP k_{eff} estimators: collision, absorption, and track length. The normality of each

of the three sets of active k_{eff} cycle data is checked at the 95 and 99 percent confidence levels. A printed line for each of the three k_{eff} estimators indicates the level of passage. WARNING messages are printed for k_{eff} cycle sets that do not appear normal at the 99% confidence level. Any k_{eff} data that does not pass at the 99 percent confidence level should be considered as not normally distributed. Perhaps this is a statistical occurrence, or perhaps more k_{eff} cycles should be skipped for improved convergence of the spatial fission source. The calculation should be examined further; e.g., by examining the behavior of the solution as function of the number of inactive cycles.

A box is then printed that contains the final estimated average k_{eff}, standard deviation, and three different confidence intervals. These averages are a statistical combination of the three k_{eff} estimators. If all three estimators appear nonnormal at the 99% confidence level, the final boxed k_{eff} confidence intervals are NOT printed. A WARNING message is printed in its place. (The final confidence intervals are available elsewhere in the output if the user insists on using them. Normality checks and confidence intervals for different numbers of inactive k_{eff} cycles are available in the k_{eff}-by-cycles-skipped table.) The final box is also NOT printed if fewer than thirty active k_{eff} cycles have been used in the calculation. Fewer than thirty cycles is not recommended because the quality of the spatial convergence of the fission source cannot be adequately addressed.

A conservative (toward large k_{eff} values) average k_{eff} confidence interval is also estimated by assuming that the largest cycle k_{eff} value for each of the three estimators occurs on the next cycle. This conservative average k_{eff} confidence interval can be used for extra conservatism for a correct calculation.

3. BATCHED k_{eff} RESULTS

A table of batched (using more than one cycle) k_{eff}s using more than one active cycle for each k_{eff} is now available. This table is useful in determining the impact of cycle-to-cycle correlations in the spatial fission source distributions on the estimated standard deviation. The table includes the k_{eff} results that would be found if the k_{eff}s were taken in batch sizes greater than one. This table is included so that the user can evaluate the impact of different batch sizes on the combined k_{eff} estimator and the estimated standard deviation. This information is a built-in sensitivity study of the k_{eff} confidence intervals as a function of batch size.

The average of the three individual k_{eff} estimators are the same for all batch sizes, but the estimated statistical standard deviations and the combined k_{eff} confidence intervals are not. Batch sizes greater than one may reflect a better estimate of the true deviation because the k_{eff}s are assumed to be independent from cycle to cycle when the statistical uncertainties are calculated. (They are not independent because of fission source correlations from cycle to cycle.) The larger batches will have less correlation between the batches than the correlation between the individual k_{eff} cycles with a batch size of one. The user can now assess the impact on different batch sizes on the k_{eff} confidence interval.

4. k_{eff} RESULTS BY CYCLE

This table lists the neutron histories, individual, cumulative average, and cumulative combined k_{eff}s by cycle. The table is a relisting of the cycle-dependent prints (with deviations instead of relative errors) in a more convenient form. The figure of merit, which is an indicator of problem efficiency and stability, is also included as a convergence rate check for k_{eff}. The largest and smallest active values of k_{eff} are printed for each estimator to indicate the spread of values sampled so far in the calculation.

5. PRINTED PLOT OF THE COMBINED k_{eff} BY CYCLE

This is the most important k_{eff} plot for the user. A trend in k_{eff} relative to the final value and the estimated standard deviation can be quickly determined visually. The estimated one standard deviation confidence intervals that are printed for each line are useful for helping to spot meaningful trends in the behavior of the average k_{eff}.

6. k_{eff} RESULTS BY CYCLES SKIPPED

This table tells the user what the values of the various k_{eff} estimators would have been for a different number of inactive cycles without having to rerun the problem. This information is another built-in sensitivity study of the k_{eff} confidence intervals as a function of the number of k_{eff} cycles skipped. The normality for each of the three sets of k_{eff} data are calculated and printed for each number of active cycles. The active cycle number where the minimum standard deviation of the combined k_{eff} occurred is printed. If this cycle is an inactive cycle, the number of cycles skipped was probably adequate. If the number of inactive cycles is significantly less than this cycle, it may indicate that not enough cycles were skipped.

The first and second active halves of a valid k_{eff} calculation should have nominally the same k_{eff} and estimated standard deviation of the average value of k_{eff}. MCNP calculates and prints the combined k_{eff} and the statistical uncertainty for the first half and second active halves of the problem. This comparison is a built-in sensitivity analysis of the two active halves of the calculation. WARNING messages are printed in the output and at the terminal if the 99 percent confidence intervals do not overlay or the estimated standard deviations do not appear to be statistically the same. Either or both might indicate that the normal spatial mode was not achieved during the early part of or even all of a calculation.

7. PRINTED PLOT OF THE COMBINED k_{eff} BY CYCLES SKIPPED

This printed plot shows the combined k_{eff} confidence interval by cycle skipped. This plot can be used to visually assess how many cycles should have been skipped. An "*" on the plot

vertical axes indicates how many active cycles were used in the original calculation. The number of cycles that should have been skipped can be estimated from this plot, the location of the minimum estimated variance of k_{eff} as a function of the number of cycles skipped, and the stabilization of the average k_{eff} printed plot.

8. GRAPHICAL k_{eff} OUTPUT

MCNP has the capability to plot the individual and average k_{eff}s and their one standard deviation confidence intervals, as well as the average k_{eff} estimator, during a calculation or by postprocessing. These plots provide additional insights into the behavior of k_{eff} during the calculation.

9. NEW STATISTICAL CHECKS FOR MONTE CARLO TALLIES

Two new statistical diagnostics for tallies have been developed and included into MCNP: 1) the relative variance of the variance; and 2) the empirical history score probability density function $f(x)$. Statistical studies have shown that these two quantities are excellent indicators for false convergence of difficult Monte Carlo tallies. These and other quantities have been incorporated into ten statistical checks involving the estimated mean, relative error, relative variance of the variance, figure of merit, and the logarithmic "slope" of the largest $f(x)$ values. These ten checks for one tally bin of each MCNP tally are made and the user is given a "yes" or "no" for satisfying the test criteria. The empirical $f(x)$ values are printed in the output and can be plotted for detailed examination by the user. The track length estimator of k_{eff} can be done easily as a separate tally to apply these new techniques to assess k_{eff} convergence. The MCNP user now has much more information about the statistical quality of a tally result than just the value of the estimated relative error and its behavior as a function of the number of histories.

10. SUMMARY OF MCNP CRITICALITY WARNING MESSAGES

MCNP provides the following WARNING messages based on analyses of the results of a criticality calculation:

1) no sampling of cells with fissionable material;

2) the average k_{eff} has a monotonic trend during the last ten active cycles;

3) k_{eff} sets that do not appear normal at the 99% confidence level;

4) all three k_{eff} sets do not appear normal at the 99% confidence level and the final boxed k_{eff} is not printed;

5) fewer than thirty active k_{eff} were run and the final boxed k_{eff} is not printed;

6) the k_{eff} confidence intervals for the first and second active halves of the problem do not overlap at the 99% confidence level; and

7) the estimated standard deviations for the first and second halves of the problem do not appear to be the same.

The appearance of one or more of these WARNING messages is reason for additional scrutiny of the calculation. The calculation may be continued for any number of additional active cycles desired.

11. EXPERIENCES WITH THE NEW CAPABILITIES

The new self assessment checks in MCNP have made an impact on the criticality user community. One non-LANL user commented that the cell sampling check showed a cell that had not been sampled. The reason was that an object had been mistakenly placed far out of position and no neutron histories ever reached it. The object location was corrected and the calculation proceeded normally. The normality checks of the k_{eff} sets have the capability to find problems with a poor (too small) number of inactive k_{eff} cycles. Deliberately not skipping enough cycles has resulted in all three k_{eff} data sets not appearing to be normally distributed at the 99% percent confidence level.

We have run the k_{eff}-of-the-world array problem with 729 4.7 cm radius spheres containing Jezebel plutonium (0.037047 atoms/b-cm Pu-239, 0.001751 Pu-240, 0.000117 Pu-241, and 0.001375 Ga), spaced at 60 cm surrounded by a thick water reflector. The 4.7 cm radius is much smaller than the 6.385 cm radius of Jezebel required for criticality. The calculation uses a uniform volume source in the array for the initial spatial distribution, 1000 neutrons per cycle, skipping 20 cycles, and running a total of 120 cycles. The value of 1000 neutrons per cycle was used because this is probably a lower limit for most criticality calculations today with the availability of fast PCs and workstations. Sampling of the array is poor on a per-object basis because there are only about 1.4 histories per object. The fact that the objects are identical makes this calculation tenable with only 1000 neutrons per cycle. The 99% k_{eff} confidence interval for this system is 0.920 to 0.932. There were no WARNING messages, and all three k_{eff} data sets appeared normally distributed at the 95% confidence level. The first and second active half 99% confidence intervals were 0.919 to 0.937 and 0.916 to 0.932. All aspects of the calculations were well behaved.

Figure 1 shows a MCNP 2-D plot of the water-reflected array geometry with Jezebel at the center instead of the 4.7 cm radius sphere. Inserting Jezebel with a radius of about 6.385 cm in the center of the array changed the behavior of the problem drastically, but not the final confidence interval. The final 99% k_{eff} confidence interval result was 0.942 to 0.958, which is far from the correct critical value. Two WARNING messages were produced: 1) the k_{eff} results were monotonically increasing over the last ten active k_{eff} cycles; and 2) the first and second half k_{eff} confidence intervals appeared to be different at the 99% confidence level (the first half was 0.922

to 0.940 and the second half was 0.960 to 0.978). The MCNP plot of the average k_{eff} versus cycle number CLEARLY showed the increasing trend, as is shown in Fig. 2. This trend is caused by more and more fission source points being created in Jezebel as additional k_{eff} cycles are run because the Jezebel array element is so much more reactive than the other elements. The well-behaved array problem without Jezebel (labeled "no jez") is shown for comparison in Fig. 2. The three k_{eff} sets appeared normal at the 99% level, but not 95%. This result is not necessarily a strong indicator of nonnormal behavior, but could indicate a problem. The figure of merit decreased by 30% during the last twenty active cycles, showing that statistical error in k_{eff} was not decreasing as the inverse of the square root of the number of histories during the last portion of the active calculation. One of the ten statistical checks failed on the separate tally of the track length k_{eff}: the mean was monotonically increasing during the last active half of the problem. The quality of this solution is CLEARLY unacceptable and more calculations need to be done.

Continuing the problem to 500 k_{eff} active cycles (520 total cycles) supplies the correct result in the k_{eff}-by-cycles-skipped table, but not as the boxed final answer, which is 0.986 to 0.994 at the 99% confidence level. This problem produced one WARNING message: the first and second half k_{eff} confidence intervals appeared to be different at the 99% confidence level (the first half was 0.973 to 0.985 and the second half was 0.997 to 1.005). This message should be interpreted as NOT being able to accept the final boxed k_{eff} result because the confidence intervals are so far apart. The minimum estimated standard deviation in the k_{eff}-by-cycles-skipped table occurs with 108 inactive cycles and 412 active cycles, producing a 99% confidence interval of 0.996 to 1.003. Examination of the two printed k_{eff} plots confirms the quality of the result based on the behavior of k_{eff} by both the average and by cycles skipped as shown in the MCNP plots in Figs. 3 and 4.

If the problem were run for only thirty active cycles and 1000 neutrons per generation, there would be no WARNING message clue to the difficulties. The only clue is that thirty cycles and about one neutron per object per k_{eff} cycle is simply not enough to adequately calculate the proper spatial source distribution for such a complex, heterogeneous configuration. Using 5000 neutrons per cycle produces the WARNING that the first and second half k_{eff} confidence intervals appeared to be different at the 99% confidence level (0.946 to 0.964 for the first half and 0.990 to 1.001 for the second half). Figure 5 is an MCNP plot that shows the expected faster rate of convergence for 5000 histories per cycle compared with 1000 histories per cycle because there is more sampling of the Jezebel element during each k_{eff} cycle.

12. SUMMARY

The above statistical and geometry sampling checks, built-in sensitivity analyses, WARNING messages, and yes/no indicators provide the MCNP user with more information to assess that a problem has been calculated properly. The MCNP4A documentation including the MCNP4A Manual (LA-12625-M) and the new MCNP Criticality Primer (LA-12827-M) have been updated to describe these new features. If a criticality calculation appears to have an unsatisfactory spatial

source convergence based on the k_{eff} normality checks or fewer than thirty active k_{eff} cycles, the final boxed k_{eff} confidence intervals will not be printed. These WARNING messages have caught real user errors and are effective for the k_{eff}-of-the-world problem as long as at least 100 active cycles are run.

Although these statistical and geometry sampling checks of the calculation results reduce the likelihood of a user accepting a poorly executed MCNP calculation, it would be foolish to assume that these checks, by themselves, can prevent all erroneous Monte Carlo criticality estimates. These checks are important tools to aid the criticality expert in evaluating MCNP results. They are NOT intended as a substitute for criticality expertise and judgment.

MCNP is a Trademark of the Regents of the University of California, Los Alamos National Laboratory.

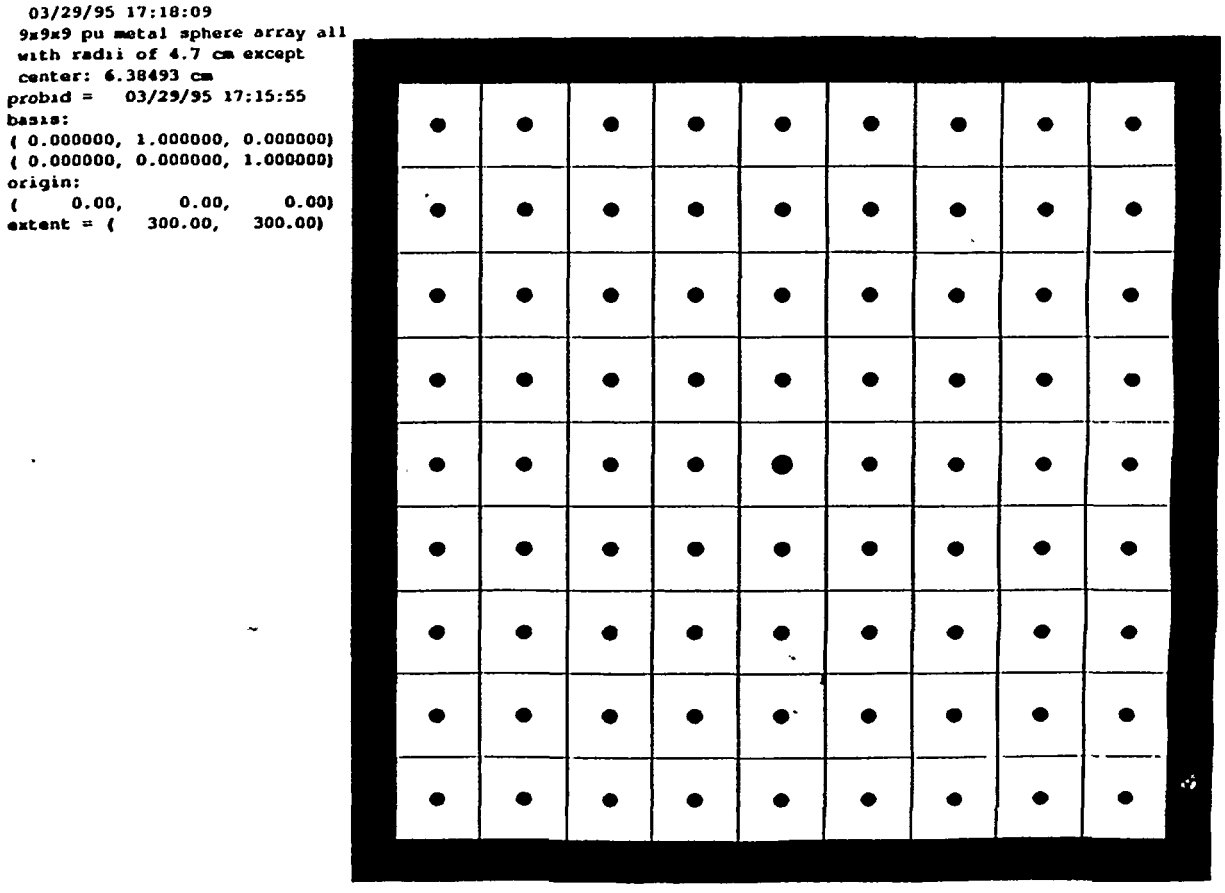

Fig. 1. MCNP plot of a cross section of the water-reflected array problem with Jezebel in the center.

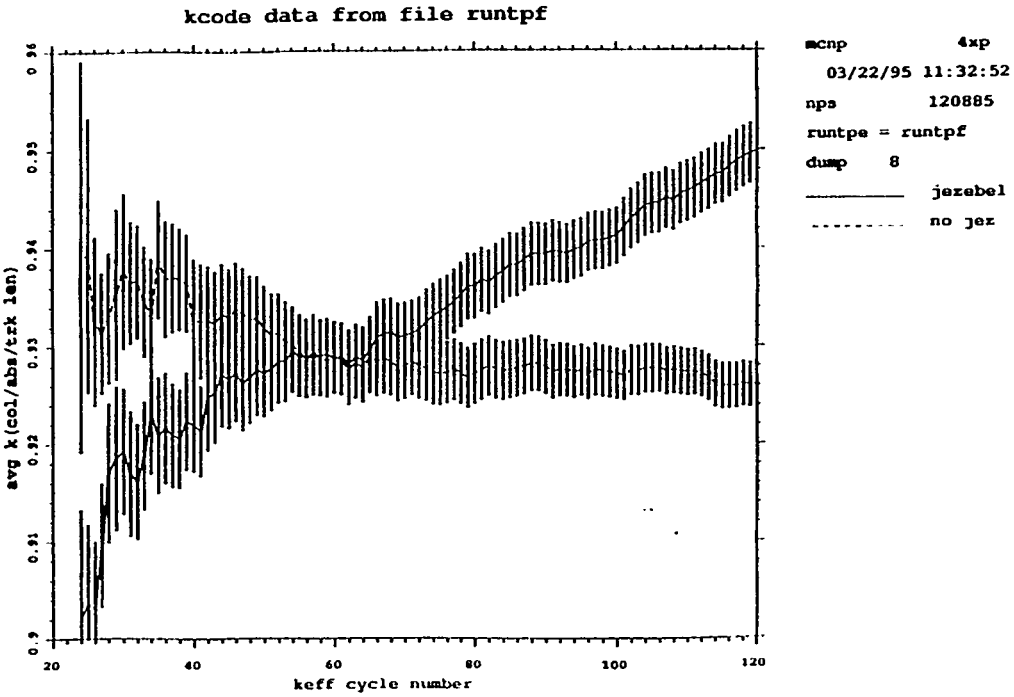

Fig. 2. One standard deviation confidence interval for the average keff of the array with and without Jezebel for 120 cycles.

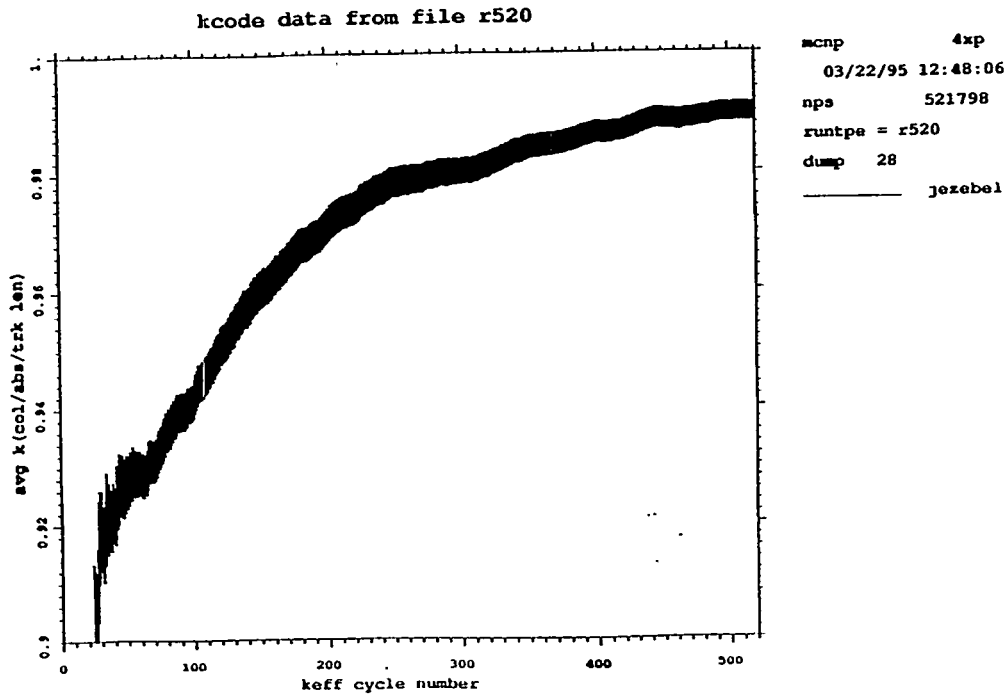

Fig 3. One standard deviation confidence interval for the average keff of the array with Jezebel for 520 cycles.

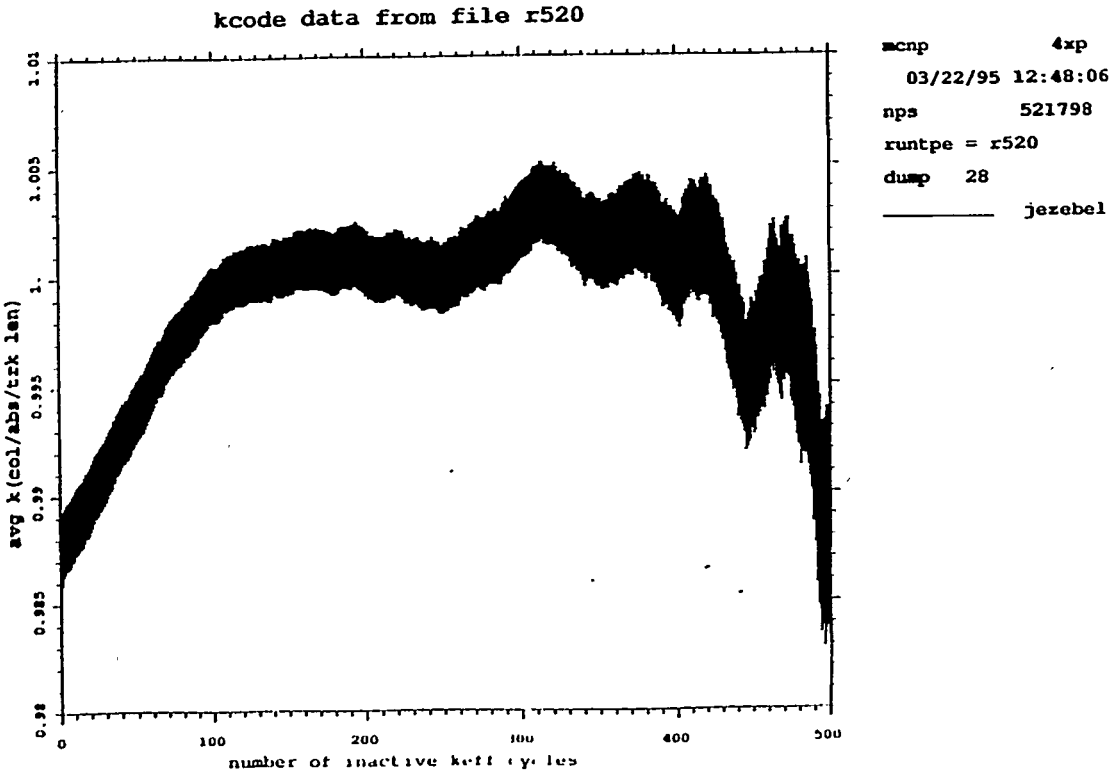

Fig 4. One standard deviation confidence interval for the average keff of the array with Jezebel as a function of the number of cycles skipped (inactive cycles).

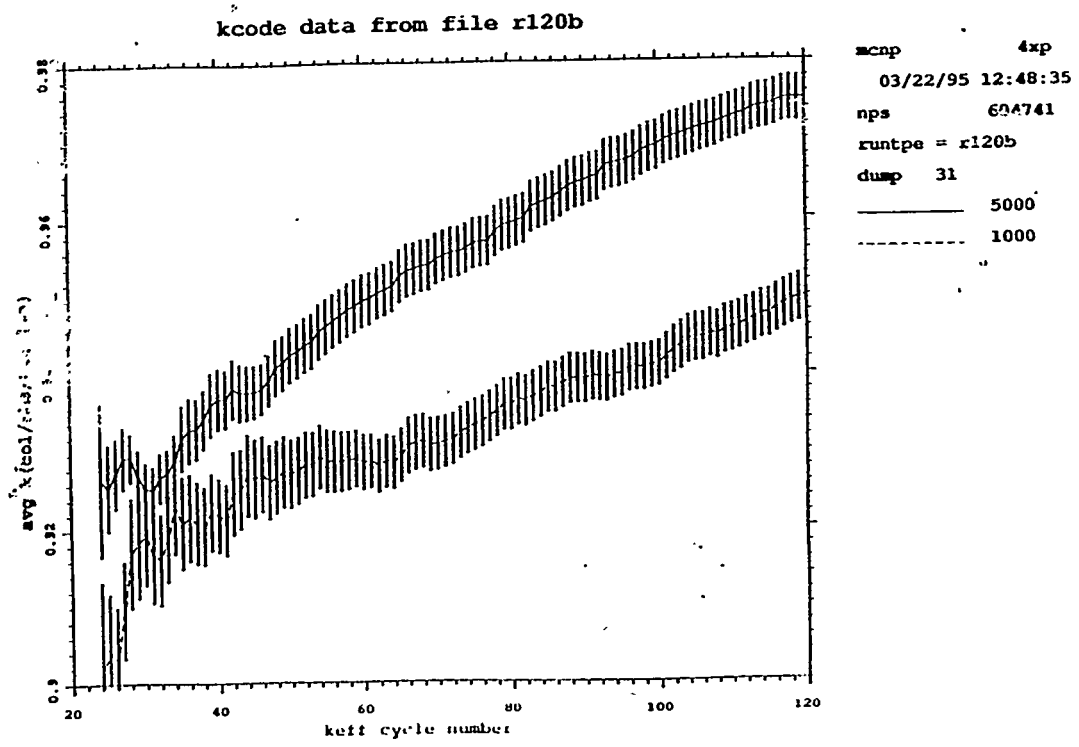

Fig 5. One standard deviation confidence interval for the average keff of the array with Jezebel for 5000 and 1000 neutrons per cycle for 120 cycles.

ESTIMATION AND INTERPRETATION OF k_{eff} CONFIDENCE INTERVALS IN MCNP

Todd J. Urbatsch
University of Michigan

R. Arthur Forster, Richard E. Prael, and Richard J. Beckman
Los Alamos National Laboratory

INTRODUCTION

In criticality calculations, MCNP has three types of individual k_{eff} estimators: collision, absorption, and track length.[1] At each cycle, or computational fission generation, MCNP produces a k_{eff} estimate of each type. The final k_{eff} estimator of each type is the average of several cycle k_{eff} estimates. MCNP's best estimator is a combination,[2] in least squares fashion, of all three estimators, that takes into account variances and covariances between the individual estimators. This work examines the theory and behavior of the three-combined estimator and compares it with other estimators. It is emphasized that the final result from an MCNP criticality calculation is not a point estimate of k_{eff}, but rather a confidence interval.

THREE-COMBINED k_{eff} ESTIMATOR

The three-combined k_{eff} estimator is appealing because it uses all the available information. It is essentially the least squares solution of a multivariate linear regression of the cycle k_{eff} estimates of one estimator type on those of the other two types and is based mainly on a paper by M. Halperin.[4] The three combined k_{eff} estimator, $\hat{u}$ and its variance, $\sigma_{\hat{u}}^2$, each in matrix and reduced form[2] are as follows:

$$\hat{u} = z_1 - \mathbf{S}_{z12}\,\mathbf{S}_{z22}^{-1}\bar{\mathbf{d}} = \frac{\sum_{\ell=1}^{3} f_\ell \bar{x}_\ell}{\sum_{\ell=1}^{3} f_\ell} \quad ,$$

and

$$\sigma_{\hat{u}}^2 = \left(\Sigma_{z11} - \Sigma_{z12}\,\Sigma_{z22}^{-1}\,\Sigma_{z21}\right)\left(\frac{1}{n} + \bar{\mathbf{d}}'\,\mathbf{S}_{z22}^{-1}\,\bar{\mathbf{d}}\right) = \frac{S_1}{gn}\left(1 + n\left(\frac{S_2 - 2S_3}{(n-1)^2 g}\right)\right) \quad ,$$

where $\bar{\mathbf{d}} = (z_2 \;\; z_3)'$; z_i are the transformations of the individual average k_{eff} estimators, $\bar{x}_\ell$: $z_1 = \bar{x}_1$, $z_2 = \bar{x}_2 - \bar{x}_1$, and $z_3 = \bar{x}_3 - \bar{x}_1$; n is the number of k_{eff} cycles used; $\mathbf{S}$ contains the sums

of squares of deviations about the means; Σ is the estimated covariance matrix, where the subscripts indicate a transformation and partitioning;[4]

$$f_l = \hat{\sigma}^2_{jj}\left(\hat{\sigma}^2_{kk} - \hat{\sigma}^2_{ik}\right) - \hat{\sigma}^2_{kk}\hat{\sigma}^2_{ij} + \hat{\sigma}^2_{jk}\left(\hat{\sigma}^2_{ij} + \hat{\sigma}^2_{ik} - \hat{\sigma}^2_{jk}\right) \quad ,$$

where l indicates a particular partial permutation of i, j, and k and the $\hat{\sigma}$ are the variances and covariances; g is the sum of all three f_l's; and S_i are sums of products of the $\bar{\chi}$'s and $\hat{\sigma}$'s.[2]

The Gauss-Markov Theorem states that, when the variance-covariance matrix is known, the least squares solution of the linear regression parameters is unbiased and has minimum variance; it is the best possible. Here, the variance-covariance matrix is not known and must be estimated from the data. The three-combined k_{eff} estimator uses the estimated variance-covariance matrix and is therefore almost optimal. Statistical studies show that this almost optimal estimator is very good.[2]

CONFIDENCE INTERVALS

A confidence interval is a range of values that is expected to contain the true value with some specified confidence. In the cases studied here, confidence intervals are constructed by including some multiple of the estimated standard deviation (square root of the variance) above and below the average value. For this combined estimator,[4] the multiplier is the Student's t-percentile and depends on the desired confidence level and the degrees of freedom available in the estimation of the standard deviation. To increase the probability that a k_{eff} confidence interval contains the true k_{eff}, the interval must be made larger; to decrease the size of a given confidence interval, more histories need to be run.

Understanding confidence intervals is especially important in criticality safety. To present a 68% confidence interval implies that there is a 32% chance that the interval does not include the true value. The 68% confidence intervals for the three-combined estimator are shown in Figure 1 for each of one hundred independent MCNP runs[3] for a U-233/light water system. The horizontal lines demark the 68% confidence interval for the average over all 100 runs, which is the best estimate of the true value. Of the one-hundred 68% confidence intervals, seventy cross the mean and thirty do not. The 99% confidence intervals (not shown) all cross the mean. Since the confidence intervals include the true mean the expected number of times, the coverage rates in this example are good.

Overall, the three-combined *keff* estimator performs better than the simple average and the individual estimator with the smallest variance.[2] In multiple independent MCNP runs, for several different systems, the correctness of the three-combined estimator, its variance, and its confidence interval coverage rates was verified.

AN EXAMPLE OF THE BEHAVIOR OF THE THREE-COMBINED ESTIMATOR

One property of the three-combined estimator is that, for highly positively correlated estimators, it may lie outside the range of the three individual estimators. This is correct, as shown in a statistical study, where the expected value of each of three highly correlated estimators is unity. Figure 2 shows that, of 100 samples, 64 have estimator ranges that do not include unity. Of those, 55 have three-combined estimators that lie outside the individual estimator range and closer to the expected value.

CONCLUSION

The three-combined k_{eff} estimator has been derived and verified, both theoretically and empirically (for the cases studied), to be the best available estimator in MCNP. It has been shown to be superior to other estimators such as the simple average and the individual estimator with the smallest variance. The three-combined k_{eff} estimator should be presented as a confidence interval, which has been shown to have the correct coverage rates for several realistic problems.

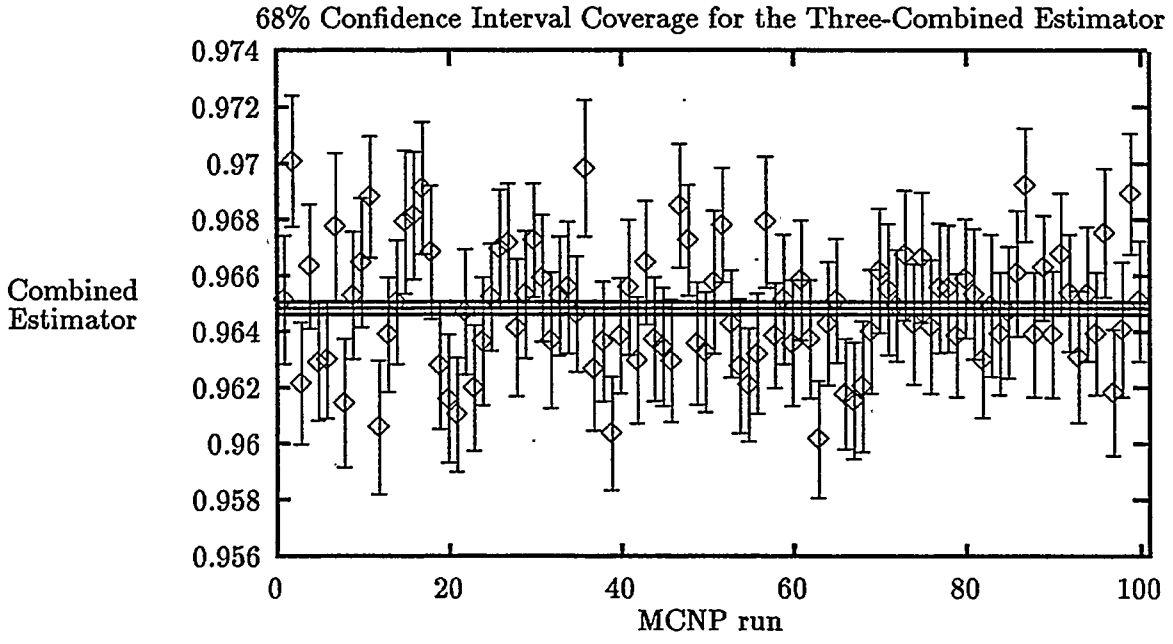

Figure 1: The 68% confidence intervals from 100 independent runs (vertical lines) shown with the 68% confidence interval of the overall mean (horizontal lines).

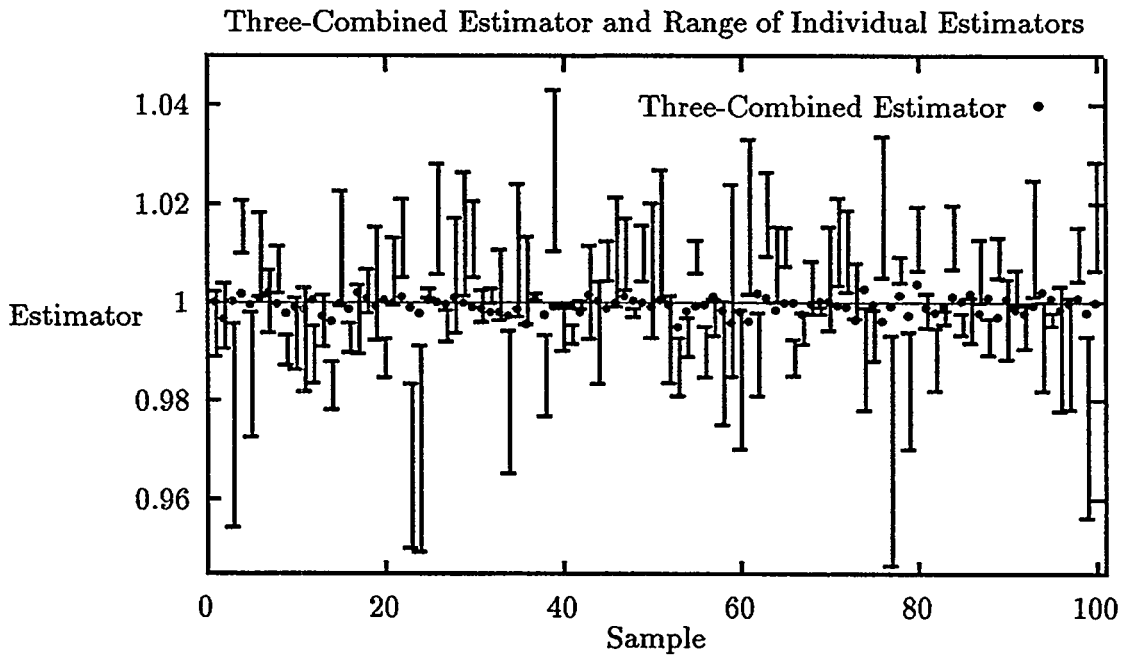

Figure 2: The range of three individual estimators, connected by vertical lines, and the three-combined estimator for 100 samples.

REFERENCES

1. Briesmeister, J.F., Ed.; "MCNP-A General Monte Carlo Code for Neutron and Photon Transport," LA-7396-M, Rev. 2, Los Alamos National Laboratory (1986).

2. Urbatsch, T.J.; Forster, R.A.; Prael, R.E.; Beckman, R.J.; "Estimation and Interpretation of k_{eff} Confidence Intervals in MCNP," LA-12658, Los Alamos National Laboratory, to be published.

3. Halperin, Max, "Almost Linearly-Optimum Combination of Unbiased Estimates," *American Statistical Association Journal,* March 1961.

4. Rombough, C.T., private communication to R.A. Forster, July 8, 1993.

A REVIEW OF THE STATISTICS USED IN MONTE CARLO CODES

Stuart G. Vessard
Los Alamos National Laboratory

1.0 INTRODUCTION

Using Monte Carlo codes requires understanding of statistical terms such as standard deviation, standard deviation of the estimated mean, and confidence interval. The standard deviation is the spread in the samples ($x_1, x_2, x_3, \ldots, x_N$) that the result is based on and is usually denoted as $\sigma(x)$, see Section 1.3 for a definition of $\sigma(x)$. For the above defined samples ($x_1, x_2, x_3, \ldots, x_N$), the estimated mean is denoted as $\hat{x}$ and is equal to $\frac{1}{N}\sum_{i=1}^{N} x_i$. The standard deviation of the estimated mean is the standard deviation of the samples divided by the square root of the number of samples $\frac{\sigma(x)}{\sqrt{N}}$, and shall be denoted throughout the rest of this paper as $\sigma(\hat{x})$. In Monte Carlo analyses, the samples ($x_1, x_2, x_3, \ldots, x_N$) to be analyzed are the active cycles of k_{eff} (i.e., $k_{eff(1)}, k_{eff(2)}, k_{eff(3)}, \ldots k_{eff(N)}$). The standard deviation of the estimated mean is the standard deviation of the samples (active k_{eff} cycles) divided by the square root of the number of active cycles used in the analysis. The confidence interval is the result of multiplying the standard deviation of the estimated mean by a constant that is based on the number of degrees of freedom for the problem. This constant is a table look up but is based on the number of degrees of freedom for the problem, and the desired level of confidence. Values for this constant can be obtained from various math handbooks. For a large number of active cycles (e.g., ≥100) this constant is approximately equal to 1 for a 68% confidence interval, approximately equal to 2 for a 95% confidence interval, and approximately equal to 3 for a 99.7% confidence interval. The standard deviation of the samples (active k_{eff} cycles) remains fairly constant for a problem, regardless of the number of cycles executed. However, both the standard deviation of the estimated mean and the confidence interval decrease proportionally as $\frac{1}{\sqrt{N}}$, where N is the number of samples (active k_{eff} cycles).

The fact that we can define a standard deviation of the samples, $\sigma(x)$, a standard deviation of the estimated mean, $\sigma(\hat{x})$, and therefore a confidence interval is based on the premise of the Central Limit Theorem. This theorem states

$$\lim_{N\to\infty} \Pr\left[E(x) + \alpha\frac{\sigma(x)}{\sqrt{N}} < \hat{x} < E(x) + \beta\frac{\sigma(x)}{\sqrt{N}}\right] = \frac{1}{\sqrt{2\pi}}\int_{\alpha}^{\beta} e^{-t^2/2}dt$$

where α and β can be arbitrary values, Pr[Z] means the probability of Z, and E(x) is the true expected mean for the population x.

The significance of this theorem is that for large N, and independent identically distributed random variables (x_i) with finite means and standard deviations, the distribution of $\hat{x}$'s, approaches a normal distribution, as defined by the right hand side of the equation. This normal distribution of $\hat{x}$'s will have a true mean value, E(x), and the population will have a standard deviation for the estimated mean of $\sigma(\hat{x})$. Based on this we can state that

$\hat{x} - \sigma(\hat{x}) < E(x) < \hat{x} + \sigma(\hat{x})$, ~ 68.3% of the time;

$\hat{x} - 2\sigma(\hat{x}) < E(x) < \hat{x} + 2\sigma(\hat{x})$, ~95.4% of the time; and

$\hat{x} - 3\sigma(\hat{x}) < E(x) < \hat{x} + 3\sigma(\hat{x})$, ~99.7% of the time.

The first equation represents a 68% confidence interval, the second equation represents a 95% confidence interval, and the third equation represents what we will call a 99% confidence interval as defined by the standard tables for the normal distribution function. Note that the above equations are for an infinite number of samples.

As a practical example of understanding confidence intervals, the following table lists the results of running 50 MCNP runs where the only difference between runs is the starting seed. The individual results listed in Table 1.1 would be the $\hat{x}$'s, i.e., the estimated means, now these 50 $\hat{x}$'s will be normally distributed (see Table 1.1 and Figure 1.1), and the true mean E(x) is expected to fall within the respective confidence intervals as defined above.

Figure 1.1 shows the 68% Confidence Interval (CI) (0.001867) and the 95% CI (0.003734) for the 50 MCNP k_{eff}'s presented in Table 1.1. We can expect (1- CI)% of our results to fall outside the defined CI. Additionally, we can see the randomness of the individual MCNP problems, i.e., the results look like a handful of sand thrown on Figure 1.1. Again, this emphasizes the need to report and evaluate Monte Carlo results as confidence intervals and not discrete values, and emphasizes how Monte Carlo results are not precise. Finally, are our samples statistically distributed? If we look at the 95% confidence interval, we should expect (1- 0.95) x 50 = 2.5 samples to fall outside the 95% confidence interval. Looking at Figure 1.1 there are 2 samples that fall outside the 95% CI. Likewise, we should expect (1- 0.68) x 50 = 16 samples outside our 68% CI, and looking at Figure 1.1 there are 16 samples that fall outside the 68% CI. Thus we can state that our samples appear normally distributed.

Even with an understanding of the statistical terms, the results for a Monte Carlo code can be misused. This happens when Monte Carlo results are applied outside a chosen confidence interval associated with the results. To illustrate how Monte Carlo results can be used outside the confidence interval for the results, the following examples are provided.

Table 1.1: k_{eff}s for 50 MCNP Runs

file #N	k_{eff}[a]	file #N	k_{eff}[a]	file #N	k_{eff}[a]	file #N	k_{eff}[a]
1	0.99185	14	0.99092	27	0.99399	40	0.98832
2	0.99195	15	0.99190	28	0.99356	41	0.99310
3	0.99053	16	0.99159	29	0.99325	42	0.99372
4	0.99288	17	0.99155	30	0.99031	43	0.99384
5	0.99225	18	0.99312	31	0.99213	44	0.99175
6	0.99307	19	0.99058	32	0.99026	45	0.99532
7	0.99012	20	0.99213	33	0.99140	46	0.99470
8	0.99200	21	0.99637	34	0.99596	47	0.99437
9	0.99123	22	0.99139	35	0.99200	48	0.99702
10	0.99416	23	0 99308	36	0.99165	49	0.99407
11	0.99499	24	0.99459	37	0.99345	50	0.99105
12	0.99478	25	0 99528	38	0.99119		
13	0.99272	26	0.98904	39	0.99113		

a. Estimated Standard Deviation (ESD) for each problems is approximately 0.002

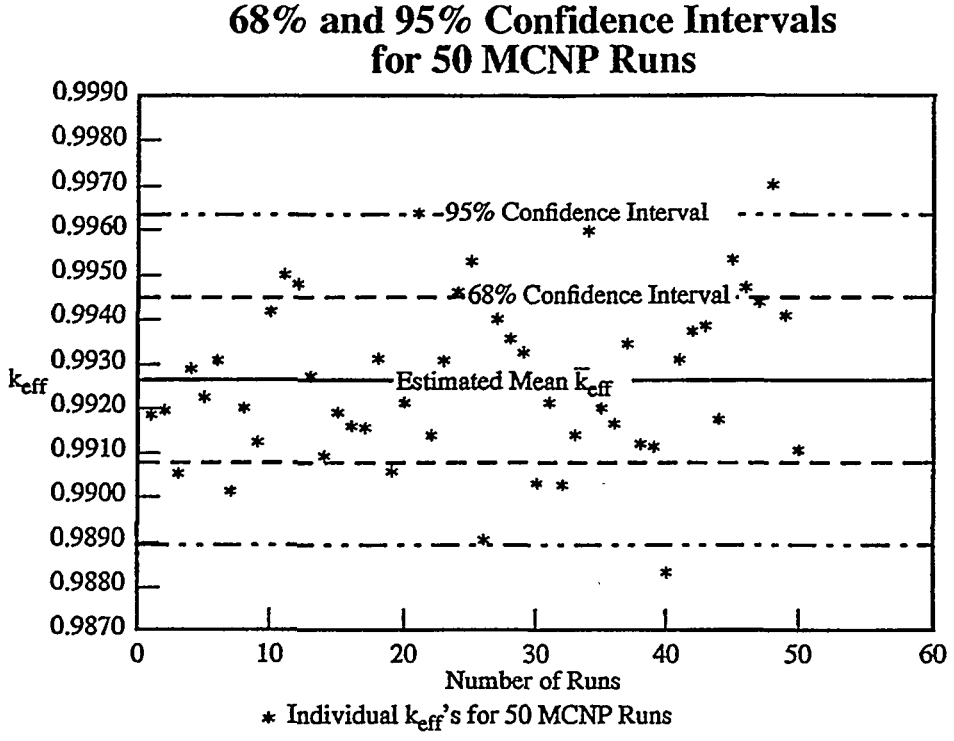

Figure 1.1
68% and 95%
Confidence Intervals
for 50 MCNP Runs.

1.1 Illustrations on the Misuse of Monte Carlo Results

During preliminary studies of a small research reactor, we attempted to evaluate the reactivity effect of different units in an access port of the reactor. Our reference evaluation was of the reactor with all the access ports normally loaded with their respective reflectors and shields.

The following cases were modeled using MCNP with 100 active cycles per Case and 10,000 particles per cycle.

- Case 1: Reference Case.
- Case 2: Removal of one unit from access port.
- Case 3: Removal of two units from one access port.

For all three cases, k_{eff} was calculated. Since each unit had positive reactivity, the removal of any one unit should yield a lower k_{eff} than that of the reference case. This is exactly what the MCNP calculations indicate as shown in Table 1.2.

Table 1.2: AGN-201M Reactor MCNP Results for Three Cases

Case	k_{eff}	Estimated Standard Deviation
1	1.01947	0.0012
2	1.01891	0.0012
3	1.01767	0.0011

Without doing an in-depth evaluation of the results, at first glance it appears that MCNP is providing reasonable results, i.e., the more units removed from the port, the lower the value of k_{eff}. However, we then modeled each of the above two units as the sum of three parts, i.e., additional geometry planes were used to define the units.

Based on this model we evaluated the following cases with MCNP with 100 active cycles per Case and 10,000 particles per cycle.

- Case 4: Reference case with 3 part units. This should be the same as Case 1.
- Case 5: Removal of two, 3-part units. This should be the same as Case 3.

Table 1.3 lists the results for these two cases.

Table 1.3: AGN-201M Reactor MCNP Results for Two Cases

Case	k_{eff}	Estimated Standard Deviation
4	1.01682	0.0010
5	1.01767	0.0011

Now the results appear suspicious. Although Case 4 is the same configuration as Case 1, but with more geometry planes, the values of k_{eff} are different. The interesting thing is that if we only had Table 1.3 to evaluate the trend for k_{eff}, and if we ignored the estimated standard deviations associated with the results, then we would find the results disconcerting because the removal of positive reactivity units resulted in an increase of reactivity. So, what is the problem with our MCNP analysis? The problem is not with the analysis but rather with using the results from a Monte Carlo code outside, in this instance, the 95% confidence interval associated with the results.

If we were doing a straightforward k_{eff} calculation, rather than a system perturbation, then an Estimated Standard Deviation on the estimated mean (which from now on will be called ESD) of 0.001 on keff would be considered more than sufficient by most users. However, when we calculate Δk_{eff}'s of 0.002 or less, then an ESD of 0.001 on k_{eff} is not sufficient. If we look at a 2 sigma confidence interval for the above results, i.e., a 95% confidence interval, then the uncertainty at the 95% confidence level is approximately equal to 0.002. Now if we plot each of the obtained k_{eff}'s with their 95% confidence intervals (error bars) (Figure 1.2), we see that all the intervals (Case 1 through Case 5) overlap, i.e., the statistics for these problems were not sufficiently converged for us to state that a real difference exists for the results based on a 95% confidence interval. This is a good example of using the results of a Monte Carlo code outside the confines of the chosen confidence interval of 95%. Additionally, this points out the fact that we must look at k_{eff}'s and Δk_{eff}'s as confidence intervals and not discrete values, i.e., the results must include the error bars to give a meaningful analysis.

With this illustration of misapplication, what are some of the statistical parameters we need to understand to correctly evaluate the results of a Monte Carlo code like MCNP?

1.2 Expectation Values

If we let x represent a random variable, for example, some property of a Monte Carlo history, then the expectation value for x is defined as

$$E(x) = \int_{-\infty}^{\infty} x f(x)\, dx \qquad 1.1$$

where f(x) is the probability density function for selecting x. If we were to repeat a Monte Carlo calculation infinitely many times, then E(x) is the mean value of x that we would expect to achieve. In other words, we can state that the true mean value $\bar{x}$ for a probability density function f(x) is equal to the expectation value E(x)

$$E(x) = \bar{x} = \int_{-\infty}^{\infty} x f(x)\, dx \qquad 1.2$$

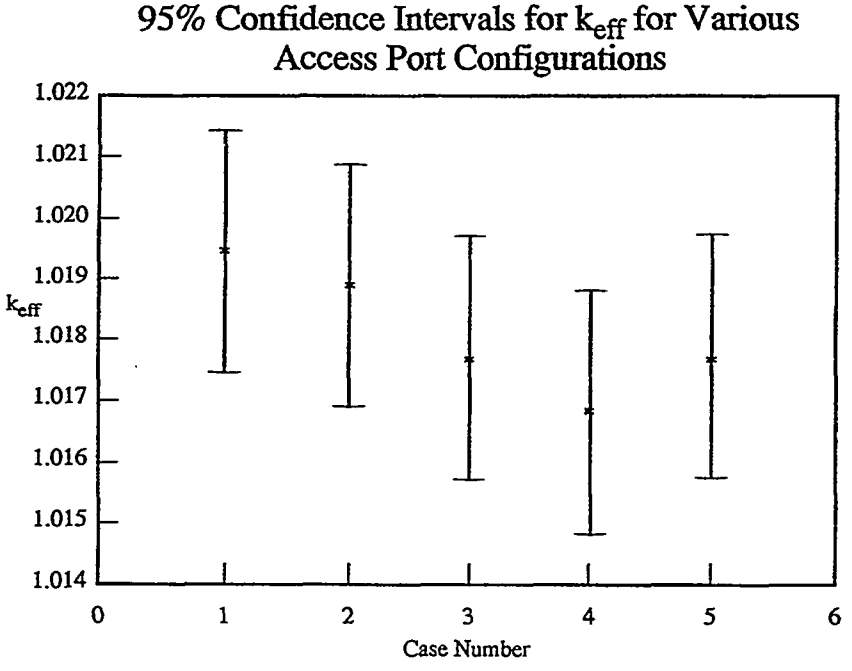

Figure 1.2 95% CIs for k_{eff} for Various Access Port Configurations

1.3 Estimated Mean and Variance

Since we do not have the time to run an infinite number of Monte Carlo calculations, then how can we estimate the mean value? Based on the Central Limit Theorem, we can state that for large N and identically distributed independent random variables, x_i, with finite means and variances, the distribution of x's approaches a normal distribution. Therefore, for a group of samples (x_1, x_2,, x_3, x_4, . . ., x_N) the estimated mean is defined as

$$\hat{x} = \frac{1}{N} \sum_{n=1}^{N} x_n \qquad 1.3$$

For large N our estimated mean, $\hat{x}$, approaches the true mean $\bar{x}$. Furthermore, the uncertainty of $\hat{x}$ decreases with increasing number of samples (N), and in most cases it does so proportionally to $\frac{1}{\sqrt{N}}$.

The variance for the above samples (x_i's) is

$$\sigma^2(x) = \frac{1}{N-1}\sum_{n=1}^{N}\left(x_n - \hat{x}\right)^2 \qquad 1.4$$

This can also be written as

$$\sigma^2(x) = \frac{N}{N-1}\left[\frac{1}{N}\sum_{n=1}^{N} x_n^2 - \hat{x}^2\right] \qquad 1.5$$

where for large values of N the $\frac{N}{N-1}$ term is typically set equal to one.

The estimated standard deviation for the above samples (x_i's) is the square root of the variance, and is denoted by $\sigma(x)$. For large N, the estimated standard deviation for the samples (x_i's) is a constant, and does not depend on the number of samples executed as long as the number of samples is large.

The estimated standard deviation of the estimated mean ($\hat{x}$) is $\sigma(\hat{x})$, and is equal to

$$\sigma(\hat{x}) = \frac{\sigma(x)}{\sqrt{N}} \qquad 1.6$$

where N is the number of samples. Unlike $\sigma(x)$, $\sigma(\hat{x})$ is dependent on the number of samples; to reduce $\sigma(\hat{x})$ by a factor of 10 would require a factor of 100 increase in the number of samples, which translates to an increase in computer time of 100.

1.4 Computing the Difference Between Two Estimated Mean Values

How should we compute the differences of estimated mean values, that is, the difference between estimated k_{eff}'s. To do this we need to define what the statistical uncertainty is for the difference. This will allow us to state the difference as a confidence interval.

Given two normal distributions ($a_1, a_2, a_3, \ldots, a_N$) and ($b_1, b_2, b_3, \ldots, b_N$) each with estimated mean values of $\hat{a}$ and $\hat{b}$ respectively, and the estimated standard deviations for the N samples of a and b being $\sigma(a)$ and $\sigma(b)$ respectively, then the standard deviation associated with $\hat{a} - \hat{b}$ is

$$\sigma(a-b)\,\sigma_\Delta = \sqrt{\sigma^2(a) + \sigma^2(b) - 2 \times \mathrm{cov}(a,b)} \qquad 1.7$$

Again, $\sigma(a)$ and $\sigma(b)$ are the estimated standard deviation of the samples a and b and not the standard deviation of the estimated mean. The term cov(a, b) is the covariance for the two

populations a and b. The covariance [cov(a, b)] for two populations (a_1, a_2, a_3, a_4, . . ., a_N) and (b_1, b_2, b_3, b_4, . . ., b_N) is defined as

$$\mathrm{cov}(a, b) = \frac{1}{N-1}\left[\sum_{n=1}^{N} a_n b_n - \frac{1}{N}\left(\sum_{n=1}^{N} a_n \sum_{n=1}^{N} b_n\right)\right] \qquad 1.8$$

$$= \frac{\sum_{n=1}^{N} a_n b_n - N\hat{a}\hat{b}}{N-1}$$

From Equation 1.8 we see that we can only calculate a covariance for $N > 1$, which is the same for calculating the standard deviation. But one what? It turns out that we can calculate the covariance and the standard deviation on any set of values that we can define as a sample. Each sample could exist, for example, of a number of Monte Carlo runs where in each run the only difference is the starting pseudorandom number. As an example, we can evaluate a given problem by running a number of Monte Carlo runs, then we can make a desired change and run another set of Monte Carlo runs, and from these two sets of runs we can evaluate an estimated mean, standard deviation for the samples, the standard deviation of the estimated mean, and the covariance. From these the correlation for the above sample, with a covariance of cov(a, b) and standard deviations for the samples $\sigma(a)$, $\sigma(b)$, is defined as

$$\mathrm{cor}(a, b) = \frac{\mathrm{cov}(a, b)}{\sigma(a)\,\sigma(b)} \qquad \{(-1, 1)\} \qquad 1.9$$

Two samples are considered uncorrelated, i.e., independent, if cor (a, b) $\cong$ 0; however, the closer to either extreme, i.e., -1 or 1 the correlation becomes, the more strongly correlated (positive or negative) are the two samples. Typically, correlations that lie in the range of $-0.5 <$ cor(a, b) < 0.5 are considered uncorrelated to slightly correlated. This is important because for uncorrelated (which most problems are) to slightly correlated populations, Equation 1.7 reduces to the usual form

$$\sigma(a - b) = \sigma_\Delta = \sqrt{\sigma^2(a) + \sigma^2(b)} \qquad 1.10$$

The answers we obtain with MCNP and other Monte Carlo codes are estimated mean values ($\bar{k}_{eff}$) commonly denoted as k_{eff}, and Estimated Standard Deviations on the estimated mean (ESD). Given this, how can we compute the ESD for the difference between two $\bar{k}_{eff}$'s, each with an ESD? From our earlier discussions we can state

$$\mathrm{ESD}(a) = \sigma(\hat{a}) = \frac{\sigma(a)}{\sqrt{N}} \qquad 1.11$$

With this equation, and with N being the same for both problems, we can substitute into Equation 1.10 for $\sigma(a)$ and likewise for $\sigma(b)$ and we obtain

$$\sigma(a-b) = ESD(a-b) = \sigma_{\Delta} = \sqrt{ESD^2(a) + ESD^2(b)} \qquad 1.12$$

Again, this assumes that the population N is the same for both problems.

From the above we can now approximate the confidence interval for the difference of two estimated mean values, i.e., we can calculate the confidence interval for Δk_{eff} For two estimated mean values, i.e., k_{eff} (a) and k_{eff} (b), with ESD(a) and ESD(b), and for a large number of active cycles per Monte Carlo run (i.e., no. active samples ≥100) the confidence intervals may be defined as

Δk_{eff} - ESD(a - b) < μ < Δk_{eff} + ESD(a - b), ~68.3% of the time;

Δk_{eff} - 2ESD(a - b) < μ < Δk_{eff} + 2ESD(a - b), ~95.4% of the time; and

Δk_{eff} - 3ESD(a - b) < μ < Δk_{eff} + 3ESD(a - b), ~99.7% of the time.

Given the foregoing discussion, it is clear that ESD(a - b) = σ_{Δ} must be smaller than Δk_{eff} in order to be able to state that a change in k_{eff} has been observed. As an example, the reference case cited in Section 1.1 has a k_{eff} = 1.0025. If two units are removed from an access port, this will result in a Δk_{eff} = 0.0023. The associated ESD(a-b) for this Δk_{eff} is $(0.0012^2 + 0.0011^2)^{0.5} = 0.0016$. Therefore, we can state, with 68% confidence, that the removal of two units of reflector results in a change in k_{eff}. However, for the same problem, two times ESD(a-b) is 2 x 0.0016 = 0.0032. Therefore, we can state, with 95% confidence, that the removal of two units of reflector **does not** allow us to state that a change in k_{eff} has occurred, i.e., two times ESD(a-b) is greater than Δk_{eff}. This illustrates that as we increase our level of confidence, i.e., we go from a 68% to a 95% to a 99+% confidence interval, then the magnitude of the Δk_{eff} we can evaluate with confidence also increases.

Based on the above example how small must σ_{Δ} or ESD(a-b) be to allow us to state with some certainty that the removal of the units results in a change in k_{eff}? To do this, we must choose the level of uncertainty we desire for the computational results. The higher the confidence interval is, the longer the time required to perform the evaluations. However, time is not the only factor to consider. The bottom line is, to what level of confidence do we want to be able to state our conclusions? Using a 95% confidence interval as our basis and with σ_{Δ} defined per Equation 1.10 and Equation 1.12, because ESD(a -b) = σ_{Δ}, we can define our upper acceptable bounds for σ_{Δ} using the following equation:

$$\sigma_{\Delta} \leq \frac{\Delta k_{eff}}{X} \qquad 1.13$$

In the above equation, X is the number of σ's, e.g., for a 95% confidence interval X = 2. Therefore, for the above analysis with a $\Delta k_{eff} = 0.0023$ and a 95% confidence interval, then $\sigma_{\Delta} \leq 0.0023/2 \leq 0.0012$. From this, the upper limit for a 95% uncertainty can be determined if we assume that ESD(a) ≅ ESD(b). From Equation 1.12

$$0.0012 = \sqrt{2ESD^2(a)}$$

$$ESD(a) = 0.00085 = ESD(b)$$

The above gives us an upper bound on the ESD(a) and ESD(b) we need in order to report a Δk_{eff} at a 95% confidence interval. Of course the smaller our values of ESD(a) and ESD(b), i.e., the better we do at converging our Monte Carlo results, then the higher our confidence (the smaller the confidence interval) becomes in stating that our Monte Carlo model predicts a change in k_{eff}. However, we need to be careful by distinguishing between the ability to predict the sign of a change, and predicting the magnitude of the change that has occurred. This is based on the fact that the results of Monte Carlo codes are confidence intervals. Therefore, the difference of the results of two Monte Carlo runs is a confidence interval. In other words, the magnitude of the change will have an associated confidence interval, and we must state at what level our confidence intervals are reported, that is, are they 68%, 95% or 99% confidence intervals.

In general, reports typically list k_{eff}'s and/or Δk_{eff}'s along with an upper bound on the estimated standard deviation of the estimated mean (ESD) for all evaluations. This leads to Monte Carlo results being viewed and reported as discrete values as opposed to confidence intervals. Again we point out the above to heighten the awareness of all users of Monte Carlo codes to the fact that Monte Carlo codes do not provide precise answers. Instead the answers obtained from Monte Carlo codes are in the form of a confidence interval.

ACCELERATION OF MONTE CARLO CRITICALITY CALCULATIONS

Todd Urbatsch and Edward W. Larsen
University of Michigan

1 INTRODUCTION

The Monte Carlo method is enjoying increasing popularity in nuclear criticality calculations. However, for some systems, the computer time necessary for convergence is enormous, often impractically so. Systems that have difficulty converging are those with high dominance ratios. Typical systems with high dominance ratios are large thermal nuclear reactors and arrays of isolated barrels of nuclear waste—any system with poor neutron communication between its distant regions.

We describe a method that accelerates the convergence of the slowly converging components of the fission source. Since our method unfortunately enhances high order fluctuations in the fission source, it requires filtering out the statistical noise. Nevertheless, in the one-dimensional, monoenergetic problems presented, the method produces speedups of about 5.0, depending upon physical and computational parameters.

2 SOURCE CONVERGENCE ACCELERATION

2.1 Derivation

The integral transport equation for the fission source $f(x)$, is

$$f(x) = \frac{1}{k}\mathbf{L}f(x) \ , \tag{1}$$

Where $\mathbf{L}$ is an integral operator acting only on the spatial variable. The Monte Carlo source iteration method is represented by introducing iteration indices to Equation 1,

$$f^{(i+\frac{1}{2})} = \frac{1}{k^{(i)}}\mathbf{L}f^{(i)} \ , \tag{2}$$

$$f^{(i+1)} = f^{(i+\frac{1}{2})} \ , \tag{3}$$

We desire the exact additive correction, $g^{(l+1)}$, to the most recent source iteration fission source, $f(l+\frac{1}{2})$, that results in the exact fission source. Using Equations 1 and 2, we formulate $g^{(l+1)}$ as follows:

$$g^{(\ell+1)} \equiv f - f^{(\ell+\frac{1}{2})} = \frac{1}{k}\mathbf{L}f - f^{(\ell+\frac{1}{2})} \quad , \tag{4}$$

$$= \frac{1}{k}\mathbf{L}(f - f^{(\ell+\frac{1}{2})}) + \frac{1}{k}\mathbf{L}f^{(\ell+\frac{1}{2})} - f^{(\ell+\frac{1}{2})}. \tag{5}$$

Collecting the $g^{(l+1)}$ terms on the left and rearranging the right hand side, we obtain

$$(\mathbf{I} - \frac{1}{k}\mathbf{L})g^{(\ell+1)} = \frac{1}{k}\mathbf{L}f^{(\ell+\frac{1}{2})} - f^{(\ell+\frac{1}{2})} = (\frac{1}{k}\mathbf{L} - \mathbf{I})f^{(\ell+\frac{1}{2})} \tag{6}$$

$$= (\frac{1}{k}\mathbf{L} - \mathbf{I})\frac{1}{k^{(\ell)}}\mathbf{L}f^{(\ell)} = \frac{1}{k^{(\ell)}}\mathbf{L}\left(\frac{1}{k}\mathbf{L}f^{(\ell)} - f^{(\ell)}\right) \tag{7}$$

$$= \mathbf{L}\left(\frac{1}{k}f^{(\ell+\frac{1}{2})} - \frac{1}{k^{(\ell)}}f^{(\ell)}\right) \quad . \tag{8}$$

This is an exact equation for $g^{(l+1)}$, the exact additive correction to the most recent fission source estimate, $f^{(l+\frac{1}{2})}$. However, this equation is too complex to solve exactly. Therefore, we shall approximate it.

To do this, we must approximate the analytic quantities in Equation 8. The quantities $f^{(l)}$, $f^{(l+\frac{1}{2})}$, and $g^{(l+1)}$ are collections of Monte Carlo particles. We convert them to vectors by discretizing the system, summing the fission source particles in each spatial cell, and normalizing. The fission matrix, $\hat{\mathbf{L}}$, whose $(i,j)th$ element is the probability that a neutron born in cell j produces a subsequent source neutron in cell i, is based to this mesh. $\hat{\mathbf{L}}$ is estimated from the Monte Carlo data during the calculation. The fission matrix has dominant eigenvalue $\hat{k}$ and eigenvector $\hat{f}$. Substituting these approximations, Equation 8 becomes

$$(\mathbf{I} - \frac{1}{\hat{k}}\hat{\mathbf{L}})\hat{g}^{(\ell+1)} = \hat{\mathbf{L}}\left(\frac{1}{k^{(\ell+1)}}\hat{f}^{(\ell+\frac{1}{2})} - \frac{1}{k^{(\ell)}}\hat{f}^{(\ell)}\right), \tag{9}$$

where $\hat{g}^{(l+1)} = \hat{f}^{(l+1)} - \hat{f}^{(l+\frac{1}{2})}$. Equation 9 does not automatically have a solution. Utilizing the Fredholm-Alternative Theorem[1], we obtain a solvability condition by taking the inner product of both sides of Equation 9 with the adjoint eigenvector, $\hat{f}^*$. The latter is obtained from the adjoint fission matrix. The left hand side is zero,

$$\left(\hat{f}^*, (\mathbf{I} - \frac{1}{\hat{k}}\hat{\mathbf{L}})(\hat{f}^{(\ell+1)} - \hat{f}^{(\ell+\frac{1}{2})})\right) = \left((\mathbf{I} - \frac{1}{\hat{k}}\hat{\mathbf{L}}^*)\hat{f}^*, (\hat{f}^{(\ell+1)} - \hat{f}^{(\ell+\frac{1}{2})})\right) = 0, \tag{10}$$

giving us the solvability condition,

$$k^{(\ell+1)} = k^{(\ell)}\frac{\left(\hat{f}^*, \hat{\mathbf{L}}\hat{f}^{(\ell+\frac{1}{2})}\right)}{\left(\hat{f}^*, \hat{\mathbf{L}}\hat{f}^{(\ell)}\right)} = k^{(\ell)}\frac{\left(\hat{\mathbf{L}}^*\hat{f}^*, \hat{f}^{(\ell+\frac{1}{2})}\right)}{\left(\hat{\mathbf{L}}^*\hat{f}^*, \hat{f}^{(\ell)}\right)} = k^{(\ell)}\frac{\left(\hat{f}^*, \hat{f}^{(\ell+\frac{1}{2})}\right)}{\left(\hat{f}^*, \hat{f}^{(\ell)}\right)}. \tag{11}$$

Using the value of $k^{(l+1)}$ from Equation 11 in Equation 9, we solve for $\hat{g}^{(l+1)}$, the additive correction. The value of the additive correction is not unique, since any multiple of the fission matrix eigenvector, $\hat{f}$, added to it is also a solution of Equation 9. Therefore, we make $\hat{g}^{(l+1)}$ unique by requiring it to be orthogonal to the adjoint fission matrix eigenvector.

The additive correction $\hat{g}^{(l+1)}$ is used to update, or accelerate, the most recent fission source. The correction is scaled by a factor β, $0 < \beta < 1$, to enhance stability. The method with $\beta = 0$ is source iteration with no acceleration, and with $\beta = 1$ is full acceleration. The additive correction is converted to a multiplicative correction by the following approximation,

$$f^{(\ell+1)} = f^{(\ell+\frac{1}{2})} + \beta\hat{g}^{(\ell+1)} \approx f^{(\ell+\frac{1}{2})}\left(1 + \beta\frac{\hat{g}^{(\ell+1)}}{\hat{f}^{(\ell+\frac{1}{2})}}\right). \tag{12}$$

Based on the departure of the multiplicative correction from unity, the fission source particles are either killed, cloned, or left untouched.

The steps for the accelerated source iteration are summarized as follows:

1. Perform a transport cycle, Equation 2.
2. Calculate the eigenstate of the fission matrix and adjoint fission matrix,

$$\hat{f} = \frac{1}{\hat{k}}\mathbf{L}\hat{f} \quad , \quad \hat{f}^* = \frac{1}{\hat{k}}\hat{\mathbf{L}}^*\hat{f}^*. \tag{13}$$

3. Calculate $k^{(l+1)}$, the solvability condition from Equation 11.
4. Calculate the fission source correction using Equation 9.
5. Apply the correction using Equation 12, and return to step 1 for another cycle.

2.2 Fourier Analysis Tool

To gauge the convergence of the fission source, we extract the individual Fourier mode parameters of the fission source by an experimental Fourier analysis. This involves taking the inner product of the fission source with trigonometric functions of various frequencies. For a one-dimensional slab of width X, M cells of width Δx, and a fission source f, the Fourier parameter for the n^{th} mode is

$$F(n\pi) = \frac{1}{X}\sum_{m=1}^{M} f_m sin\frac{n\pi(m-\frac{1}{2})}{M}\,\Delta x \approx \frac{1}{X}\int_0^X f(x) sin\frac{n\pi x}{X} dx, \tag{14}$$

where n = 1,2,...,M. Unlike the usual Fourier analysis for an infinite medium, the boundary effects here keep the modes from being entirely independent.

2.3 Filtering the Statistical Noise

Our proposed acceleration method is applicable to both deterministic and Monte Carlo criticality calculations. The scaling factor β in Equation 12 damps out the correction for all frequency modes, λ. Implementing the acceleration in a Monte Carlo calculation may also require filtering the statistical noise, which we assume has high frequency. The filter, whose strength depends on a parameter α^2, selectively smooths the high frequency fluctuations in a function ρ, producing the function γ,

$$-\alpha^2\frac{d^2}{dx^2}\gamma(x) + \gamma(x) = \rho(x). \tag{15}$$

An assumed form of ρ shows how γ has damped high frequencies,

$$\rho(x) = e^{i\lambda x} \;\rightarrow\; \gamma(x) = \frac{\rho(x)}{1+(\alpha\lambda)^2}. \tag{16}$$

The smoothing operation defined by Equation 15 is applied to $\hat{f}^{\left(l+\frac{1}{2}\right)}$ and $\hat{f}^{(l)}$ on the right side of Equation 9. Note that to do this, we must impose a spatial grid and discretize Equation 15.

3 RESULTS AND DISCUSSION

We apply the acceleration method to two one-dimensional, monoenergetic problems. The first is a 60-mean free path homogeneous slab with a dominance ratio of approximately 0.991. Figure 1 shows the convergence of the first and second Fourier modes for both the unaccelerated and accelerated cases. Convergence is depicted when the Fourier modes level off. For this symmetric system, the second Fourier mode has expected value zero. The unaccelerated case takes approximately 110 cycles to converge, and the accelerated case takes about 20 cycles. Comparing the computer times at those cycles gives a speedup of 5.0.

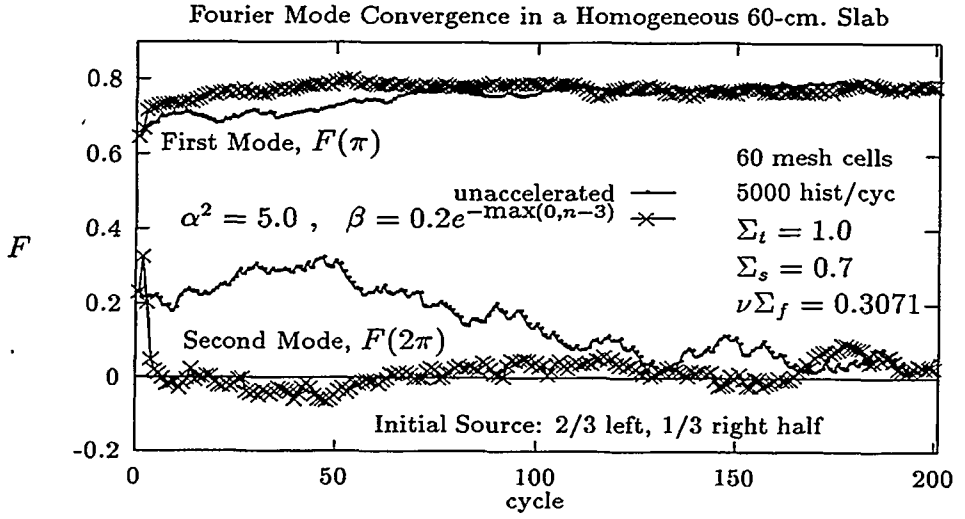

Figure 1: Convergence of the first and second Fourier modes for unaccelerated Monte Carlo and filtered and dampened accelerated Monte Carlo in a homogeneous slab.

The second problem simulates Whitesides' "k_{eff} of the world" problem[2]. It consists of a uniform lattice of alternating 1 cm portions of absorber and 2 cm portions of fuel. There are 19 fuel components and the middle component is hotter than the rest. Figure 2 shows that unaccelerated Monte Carlo converges on the hot component in about 35 cycles, whereas the accelerated Monte Carlo takes about 6 cycles. The computational time a speedup is about 4.8.

Compared to the second problem, the acceleration in the first problem is more sensitive to the damping and filtering parameters, β and α^2. The difference occurs because of the different particle densities in the important fissionable volumes. The "k_{eff} of the world" simulation, upon convergence, has a very large particle density in the hot component and a low particle density elsewhere, and appears almost deterministic. (In a deterministic calculation, filtering is not required and, unless it is severely heterogeneous, neither is damping.) The large homogeneous system has more statistical noise, so the filtering becomes very important. The filter may not smooth the fission source optimally, and the noise that the filter does not remove must be damped out. Therefore, the parameters of α^2 and β are not independent. We are working to develop guidelines for determining these parameters based upon the physical properties of the system and the computational parameters of the calculation.

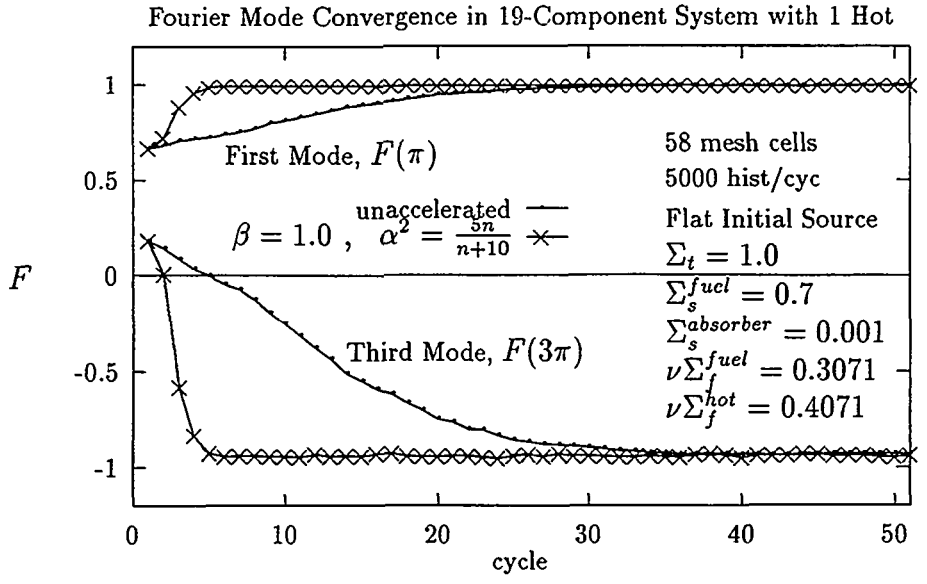

Figure 2: Convergence of the first and second Fourier modes for unaccelerated Monte Carlo and filtered and accelerated Monte Carlo in a "k_{eff} of the world" simulation.

Our proposed acceleration method is designed to reduce the number of inactive cycles, those required to converge the fission source. It works best when the initial assumed fission source is far from the true fission source. Our method is also good for systems with high dominance ratios. These are systems for which unaccelerated Monte Carlo would require many inactive cycles to converge the source. Criticality code users may not allow the number of cycles necessary to converge the fission source for these types of problems, so even a modest speedup of 5.0 is very beneficial in obtaining accurate solutions. The method cannot, however, overcome some inherent deficiencies in Monte Carlo criticality calculations. For instance, if all the components in the "k_{eff} of the world" problem were equally hot and nearly independent, Monte Carlo would not achieve the correct fission source due to statistical noise.

References

1. Kreyszig, Erwin, Introductory Functional Analysis with Applications, John Wiley & Sons, New York (1978).

2. Whitesides, G. E., "A Difficulty in Computing the k-effective of the World," *Trans. Am. Nucl. Soc.*, **14**, 680 (1971).

WEDNESDAY, MAY 17, 1995

SESSION III
MONTE CARLO VULNERABILITIES OF REPRESENTATION

NUCLEAR DATA FOR CRITICALITY SAFETY - CURRENT ISSUES

L. C. Leal
W. C. Jordan
R. Q. Wright

INTRODUCTION

Traditionally nuclear data evaluations have been performed in support of the analysis and design of thermal and fast reactors. In general, the neutron spectra characteristic of the thermal and fast systems used for data testing are predominantly in the low- and high-energy range with a relatively small influence from the intermediate-energy range. In the area of nuclear criticality safety, nuclear systems arising from applications involving fissionable materials outside reactors can lead to situations very different to those most commonly found in reactor analysis and design. These systems are not limited to thermal or fast and may have significant influence from the intermediate energy range. The extension of the range of applicability of the nuclear data evaluation beyond thermal and fast systems is therefore needed to cover problems found in nuclear criticality safety.

Before criticality safety calculations are performed, the bias and uncertainties of the codes and cross sections that are used must be determined. The most common sources of uncertainties, in general, are the calculational methodologies and the uncertainties related to the nuclear data, such as the microscopic cross sections, entering into the calculational procedure. The aim here is to focus on the evaluated nuclear data pertaining to applications in nuclear criticality safety.

Current Issues

In the winter of 1993, an article[1] in the Criticality Safety quarterly pointed out differences in the calculated infinite multiplication factor (k_{eff}) of calculations performed with the SCALE code system[2] and the MCNP code.[3] The systems considered in the calculations were fictitious mixtures made of metal mixed with ^{235}U, namely, Al/^{235}U, Fe/^{235}U, and Zr/^{235}U. Since the MCNP calculational methodology is based on the continuum energy approach, an assumption was made that the MCNP results were correct. In absence of experimental data for these metal/^{235}U systems, to understand the cause of the discrepancies between the results, it was decided to calculate the k_{eff} of the metal/^{235}U systems using a variety of computer codes and cross section libraries. It turned out that the k_{eff} results of these calculations were not in agreement with MCNP. Since several sources of uncertainties contribute to the overall uncertainty in the integral results, the lack of agreement among the different calculational methodologies led us to investigate the methods and data used in the calculations. Firstly, a detailed examination of the MCNP results suggested that the pointwise cross section data of its library used in the calculations were not adequate for the systems under consideration. Particularly, it was found out that the aluminum cross sections in the ENDF library were given as averaged smooth cross

sections which cannot be energy self-shielded even though aluminum has resonance structure. It is well known that resonance parameters representations are needed to properly account for resonance self-shielding effects. The neutron spectrum characterizing the Al/^{235}U system studied was in the intermediate energy range where the resonance self-shielding effects on the aluminum cross sections play an important role, and, therefore, strongly indicate the pointwise cross section representation ENDF/B is inadequate. In a separate study, a criticality safety assessment of the fuel cycle facility[4] at Argonne National Laboratory, Idaho Falls, also indicates a similar problem related to the pointwise cross section representation. In this study, it was verified that the cross section representation of chlorine (Cl), a material with resonance structure, is not represented with resonance parameters, but rather with averaged smooth cross sections.

These issues highlight areas where there appears to be a deficiency in the ENDF evaluations, specifically data for materials used in criticality safety which have no resonance representation.

Nuclear Data Needs for Criticality Safety Analyses

Nuclear systems commonly found in criticality safety applications encompass a wide range of fissionable, moderator, and absorber materials. The characteristic neutron spectrum of these systems span a wide range from thermal to fast. Of particular interest for many current applications are systems with a neutron spectrum which peaks in the intermediate range. In general, the intermediate energy range is between 3 eV and 3 keV. A system is considered an intermediate system when the energy corresponding to the average lethargy of the neutron causing fission (AEF) falls in this range. This energy range, from the viewpoint of differential data, is extremely important since resonance effects in the cross sections are dominant. The status of nuclear data for the majority of isotope of interest to criticality safety applications in the basic nuclear data files has to be examined. As an example, Table 1 lists eight materials of interest in criticality safety identified as having questionable ENDF/B-VI evaluations.

Table 1. Isotopes for which measurements and evalutaion are needed.

Isotope	Cross Section Representation	
	Last Evaluation	Resonance Data
^{20}Ca	Aug71	No[a]
^{27}Al	Dec73	No
^{17}Cl	Feb67	No[a]
^{19}K	Feb67	No[a]
^{31}P	Oct77	No
^{14}Si	Feb74	No[a]
^{12}Mg	Feb78	No[a]
^{233}U	Dec78	Yes

[a]Isotopic Evaluations Needed.

There are a variety of isotopes that can be added to the list in Table 1. One specific need is to improve the ^{235}U capture-to-fission ratio (alpha). Existing ^{235}U evaluations do not reproduce the measured alpha value and consequently impacts criticality safety analyses of highly enriched intermediate spectrum systems.

From the point of view of integral data, there is a need for high quality critical experiments with intermediate energy spectra (3 eV to 3 keV) to validate methods and data. An assessment of existing experimental data relevant to criticality safety applications has to be performed. Table 2 shows four experiments of interest for data assessment for criticality safety applications.

Table 2. Critical Experiments with Intermediate Energy Spectra.

Critical Experiments	Description
HISS(HUG)	Homogeneous Uranium-Graphite
HISS(HPG)	Homogeneous Plutonium-Graphite
UH_3-UR	High Enriched Uranium with Low Enriched Uranium Reflector
PCTR	Low Enriched UO_3/H_2O with a Range of H/U

Concluding Remarks

The issues mentioned above indicate a need for new data and evaluations. To satisfy specific needs for criticality safety applications, closer collaboration between the nuclear criticality safety community and the Cross Section Evaluation Working Group (CSEWG) must be established. In this framework, a broader set of CSEWG benchmark testing should be developed to help extend the energy range of cross section validation. Detailed evaluations of many isotopes with resonance in the intermediate energy range are clearly needed.

References

1. Palmer, B., "keff for Certain Metals Mixed with ^{235}U," Criticality Safety Quarterly, Sponsored by DOE DO-62, Winter 1993.

2. "SCALE: A Modular Code System for Performing Standardized Computer Analysis for Licensing Evaluation," NUREG/CR-0200, Rev. 4 (ORNL/NUREG/CSD-2R4), Vols. I, II, and III. Available from Radiation Shielding Information Center at Oak Ridge National Laboratory as CCC-545.

3. Briesmeister, J. F., Editor, "MCNP: A General Monte Carlo Code for Neutron and Photon Transport, Version 3A," Los Alamos National Laboratory, report LA-7396-M, Rev. 2 (1986).

4. Lell, R. M., et al, "Criticality Safety Evaluation of the Fuel Cycle Facility Electrorefiner," 1993 Topical Meeting on Physics and Methods in Criticality Safety, September 19-23, 1993, Nashville, Tennessee.

MULTIGROUP CROSS-SECTION REPRESENTATION

R. M. Westfall
L. C. Leal
Oak Ridge National Laboratory

This paper presents a discussion of the approximations inherent in representing the energy variation of neutron cross sections and their associated secondary neutron energy and angular dependences with multigroup values averaged over a grid of energy boundaries. The increasingly popular alternative is to perform stochastic sampling on these parameters in continuous-energy, direct-physics-analog Monte Carlo models. The presentation concludes with a summary of the relative advantages and disadvantages of the two approaches.

Of primary interest in criticality safety analyses is the fissile-system effective-multiplication factor. This can be defined as the ratio of the number of fission neutrons produced in successive generations. The effective multiplication factor is determined through solution of the stationary form of the neutron transport equation, which involves the calculation of the neutron flux as a function of space, energy and angle. The geometric complexity of fissile systems, particularly under upset conditions, has made the Monte Carlo approach the preferred method for treating the spatial variation as a continuous variable. The national consensus standard governing these analyses is ANSI/ANS 8.1, "Nuclear Criticality Safety in Operations with Fissionable Material Outside Reactors." Paragraph 4.3.5 of ANSI/ANS 8.1 states that "Nuclear properties such as cross sections should be consistent with experimental measurements of these properties." Towards this end, the criticality methods community in the United States utilizes the Evaluated Nuclear Data Files (ENDF/B) in developing energy-pointwise and multigroup cross-section libraries. In either approach, the objective is to produce cross sections which accurately represent the differential parametric variation in terms of reaction type magnitude and secondary energy and angular distributions.

The basic assumption in multigrouping is that an approximate energy variation of the neutron flux can be utilized to average the pointwise data into fine group values. Furthermore, it is assumed that the residual energy dependence in the fine group values is adequate for treating this aspect of the neutron reaction types and kinematics on a problem-dependent basis. These assumptions and their implications are discussed.

Generally, the initial weighting spectrum used in obtaining the fine group values is a combination of a fission neutron spectrum in the high energy range coupled to a slowing-down (1/E or 1/{E*Sigma Total}) spectrum in the intermediate energy range, which, in turn, is coupled to a thermal Maxwellian calculated at some temperature representative of a broad class of problems. This practice has worked well for very fast systems and for highly thermalized systems, such as fast and thermal reactors. For uranium-235, the number of neutrons produced per neutron absorption is 2.3 at 1 MeV, 1.9 between 1 and 100 keV, and 2.1 at thermal.

Therefore, even though the relative cross-section magnitudes favor the design of reactors with fast or thermal spectra, neutron production in the slowing-down or intermediate energy range is sufficient to sustain criticality.

Ideally, the fine group energy boundaries are chosen such that threshold reactions and important high-energy structure, for example, the "iron window" at 24 keV, are well represented. The multigroup transfer matrix, expanded as a function of scattering order, represents the secondary energy and angular distributions. Also in the intermediate energy range, provision must be made for self-shielding and the temperature dependence of the unresolved and resolved resonances. These functions are performed with levels of technical detail and rigor varying from narrow resonance approximations and two region models to pointwise slowing-down calculations with multizone transport solutions. Similarly, many problems require a fine-group transport solution over the thermal scattering kernels, with proper attention paid to upscatter convergence as well as the kernels temperature and angular dependence. Most software systems have provision for treating these phenomena with rigorous, fine-group transport solutions in one-dimensional, multizone geometries. Additional provision is made for broad-group collapsing and spatial averaging of constants to be used in multidimensional analyses.

The principal advantage of the continuous-energy, Monte Carlo approach is its replication of the single neutron collision kinematics, with some qualification on its ability to exactly treat unresolved resonances and thermal upscatter in a single neutron sense. The associated disadvantage is the requirement to simulate a great many neutron histories to assure adequate sampling and source convergence. The issue of adequately treating space-angle coupling in loosely-coupled fissile systems has been recognized and discussed. In the energy domain, the difficulty of treating intermediate spectrum systems and fast-thermal coupling could be equally important.

The principal advantage of the multigroup approach is that, at some acceptable level of technical rigor, there is an assurance that all of the important phenomena and neutron kinematics have been treated. Furthermore, in addition to Monte Carlo solutions, the multigroup constants can be applied in deterministic methods which give universal solutions for the neutron flux distributions. As well as forcing systematic coupling, these closed-form solutions provide capabilities for obtaining reaction rates and for performing sensitivity analyses based on adjoint methods. The disadvantage of the multigroup approach is the requirement for careful and knowledgeable preparation of constants through a many-step procedure in which mistakes can be made or wrong decisions taken.

It is evident that the continuous-energy and multigroup approaches are complimentary and that both methodologies should be nurtured and utilized.

UTILIZATION OF VIM MONTE CARLO CALCULATIONS FOR FAST REACTOR EXPERIMENTAL DATA ANALYSIS

P. J. Collins and S. E. Aumeier
Argonne National Laboratory

Calculations with the VIM Monte Carlo code have been vital in the analysis of experimental measurements for fast reactors at Argonne National Laboratory over the past 20 years. The full use of the data has been achieved by generalized least squares fitting of the results with a data sensitivity/adjustment method in the GMADJ code.[1,2] This has enabled correlation of different measurements both in the same assembly and between different assemblies at ZPPR and also between critical assemblies at other facilities. The VIM code has been vital in obtaining calculated results with uncertainties that are lower than those of the measurements which, using the GMADJ code, enables the identification of inconsistencies in measurements and points to possible systematic errors. This review describes some of the areas where VIM has proved essential, with emphasis on criticality results.

Heterogeneity

The early assemblies at ZPPR were devoted to confirming the calculated physics parameters of the Clinch River Breeder Reactor (CRBR). A fast reactor benchmark with the same inner core composition of plutonium/uranium oxide with sodium and steel was provided by ZPR-6 assembly 7 in Illinois. Great importance was placed on confirmation of the calculated breeding ratio and its uncertainty in the initial design and to this end the ratio of capture in ^{238}U to fission in ^{239}Pu (C8/F9) was measured in hundreds of cell locations throughout the reactor. The VIM code had been used to validate the heterogeneity calculations at ANL with the MC²/SDX codes. The VIM code was also used to check experimental techniques for obtaining the cell average reaction rates from foil measurements. All results showed a persistent over calculation of C8/F9 and indicated the need for an independent test of the experimental measurements. This was provided by the UK measurements in ZEBRA-8 which covered a range of spectra in zero-leakage test zones.

The connection between reaction rates in the spectra of the essentially infinite media and those in CRBR was provided by a data sensitivity/adjustment procedure.[3] This method had, in addition, the advantage of using measurements of k_∞ or k_{eff} as well as those of reaction rates. The k-values are measured to high accuracy (tenths of a percent) compared with the accuracy in the reaction rate measurements (several percent).

The ZEBRA-8 zero-leakage cells were designed for fast reactor data testing in Pu/U/Na/steel compositions. Two had spectra harder than that of an LMFBR while ZEBRA-8D was similar to

*Work supported by the U.S. Department of Energy, Reactor Systems, Development and Technology, under Contract W-31-109-Eng-38.

ZPR-6/7. ZEBRA-8A had a much softer spectrum than ZEBRA-8C. The ZEBRA cells were very simple in construction which resulted in heterogeneity which was much larger than in ZPPR assemblies or ZPR-6/7. In ZEBRA-8A the calculated heterogeneity correction to k_∞ was 7% while the corrections for ZEBRA-8C and ZEBRA-8D were 6% and 3%, respectively. These compare with Δk (het) in ZPR-6/7 of about 1.3% and fall outside the range of validation.

Consequently, results for ZEBRA were obtained with the VIM Monte Carlo code. The VIM calculations were followed until statistical uncertainties were obtained which were lower than uncertainties in the measurements. A comparison of deterministic and VIM results using ENDF/B-5.2 data is given in Table 1.

Table 1. Comparison of Deterministic and VIM Calculation

Core/Reaction	Deterministic	VIM (α,%)	Heterogeneity %
Jezebel			
k_{eff}	0.9984	0.9983 (0.09)	—
F25/F25	0.2031	0.2060 (0.07)	—
F49/F25	1.4116	1.4132 (0.61)	—
Zebra-8A			
k_∞	0.9888	0.9780 (0.20)	7.3
F28/F25	0.0127	0.0135 (0.60)	23.1
C28/F49	0.1290	0.1267 (0.60)	16
F49/F25	1.2410	1.2334 (0.60)	5.5
Zebra-86			
k_∞	0.9544	09.640 (0.20)	6.3
F28/F25	0.0108	0.0114 (0.60)	20.4
C28/F49	0.1309	0.1304 (0.50)	16
F25/49	1.0849	1.0447 (0.50)	1.5
Zebra-8C			
k_∞	0.9681	0.9742 (0.20)	3.4
F28/F25	0.0184	0.0187 (0.50)	16.9
C28/F49	0.1304	0.1297 (0.50)	11
F25/F49	1.0218	1.0141 (0.50)	3.2

The results from the least-squares fit with GMADJ, using values and statistical uncertainties from VIM, are given in Table 2.[1] The fitted results are in excellent agreement with experiment. This would not be true, apart from the homogeneous Jezebel, if deterministic results were used rather than the VIM results.

Benchmark Cores

The LANL benchmark cores provide fundamental data testing for fast reactors in all versions of ENDF/B data. These are simple homogeneous spheres, either bare or uranium reflected, which allow for calculations to be readily performed using high order S_nP_n methods.

Initial data fitting with the GMADJ code showed inconsistencies in fitting the uranium reflected Flattop-Pu and Flattop-25 whereas the bare spheres Jezebel and Godiva were completely consistent with other data. The problem was traced to anisotropy in inelastic scattering in the uranium reflector. This inelastic anisotropy was not treated in the MC²/SDX data processing system at ANL (although it was treated in NJOY). The VIM code was used to treat this anisotropy and values of k_{eff} with statistical uncertainties of 0.1% were obtained, which were comparable to uncertainties in experiment (Table 3).

Table 2. Results of Least Squares Fitting for Zebra and k_{eff} Values

	σ(E,M)[a]	σ(c)[b]	C/E-1	Adjusted/E-1	σ(A)[c]
Jezebel	0.2	1.8	-0.17	-0.26	0.23
Zebra-8A	0.7	2.0	-1.4	-0.98	0.71
Zebra-8C	0.5	1.9	-2.2	-0.51	0.52
Zebra-8D	0.5	2.6	0.1	0.61	0.52
ZPR-6/7	0.3	1.6	-0.8	-0.1	0.32

[a]Combined uncertainty of experiment and calculation
[b]Uncertainity due to ENDF/B-5.2 data
[c]Uncertainty after GMADJ fit

A further problem in the GMADJ fit was found with Jezebel-Pu, a variant of Jezebel with a higher ^{240}Pu content. Inclusion of Jezebel-Pu in the least-squares fit resulted in an unacceptably large value of chi-square per degree of freedom. To quote reference 1: "It was concluded that the k_{eff} values of the two Jemina's, Jezebel-Pu, and Flattop-Pu are inconsistent with the rest of the data base and among themselves." Later, in ENDF-B-6 data testing, it was found that the benchmark specifications for Jezebel-Pu had an error in the core radius. Correction for this resulted in consistency between calculated and experimental results for Jezebel-Pu.

Space-reactor Cores

The fast space reactor cores are small and characterized by a high leakage fraction and complicated geometry. For SP-100, MCNP Monte Carlo was used as the basic calculation method.[4] Experiments for SP-100 were done in ZPPR-20 and analyzed, with much labor, by the same method. During this program, the automated construction of VIM models[5] for the experimental loading database was achieved. This provided basic confirmation of the MCNP results and confirmation of the delicate corrections for removal of part of the delayed-neutron source in the reactivity calibration. Following the measurements, the high accuracy of the Monte Carlo calculation enabled an analysis of the source of discrepancies to be made, although the discrepancies were conservative for the design. Important results achieved were: (a) Explanation of the overprediction in criticality by 1% Δk whereas the highly-enriched uranium benchmark Godiva was well predicted, (b) Explanation of the underprediction of control rod worths by 10%

due to too low $^{10}B(n,\alpha)$ cross sections in the hard spectrum range. This latter analysis was confirmed by the re-evaluation of the boron standards data in ENDF/B-6.[6]

Table 3. VIM Calculations of k_{eff} for Benchmark Cores

				GMADJ Fit[c]	
	Deterministic[a]	VIM[a]	σ(%)[b]	Discrepancy (%) (A/E-1)	Uncertainties (%)
Jezebel	0.9984	0.9983	0.09	-0.26	0.23
Flattop-Pu	1.0124	1.0071	0.11	0.37	0.17
Godiva	0.9976	0.9971	0.08	0.10	0.14
Flattop 25	1.0106	1.0036	0.10	-0.10	0.14
Jezebel-Pu	0.9925	——	0.20[e]	-0.30	0.29
Jezebel-Pu[d]	1.0000	0.9998	0.09	-0.20	0.22

[a] All results used ENDF/B-5.2 data.
[b] Statistical uncertainty from VIM. Experimental uncertainties are about 0.1%.
[c] The GMADJ fit used VIM results when available.
[d] Corrected radius.
[e] Estimated uncertainty from TWODANT.

Fuel Criticality in the IFR

For the Pu/U/Zr metal fueled IFR, it was necessary to validate criticality calculations for the fuel casting crucible. No experimental data existed for fuel of this type although benchmarks existed for Pu (Jezebel) and enriched U (Godiva). Hence, a series of criticality measurements was made in ZPPR-21.[7] These covered six assemblies ranging from an all-Pu loading in ZPPR-21A and, by progressively varying the Pu/U content, to an all ^{235}U loading in ZPPR-2lF. In contrast to the simple-geometry/simple composition assemblies, these used the plate structure of ZPPR assemblies but advantage was taken of the automated set-up of the VIM model from the reactor loading database.[5] The cores had a graphite reflector and a lithium hydride room return shield. The reflector thickness was varied to bring each core close to critical, as monitored by period measurements. Experimental uncertainties were between 0.1% and 0.2% while VIM calculations were run for 500,000 histories to give a statistical uncertainly of 0.1%.

An important part of the ZPPR-21 analysis was its use in GMADJ to validate the experiments against results from a number of independent experiments. Data sensitivity was necessary to treat the full range cores; hard-spectrum benchmarks, space reactors, metal-fueled cores and oxide-fueled cores. These results are shown in Table 4.

Table 4. Consistency between k_{eff} of ZPPR-21 and other LMR Cores

Assembly	Measurement and Calculation Uncertainty[f] (%)	Error in Fitted Parameter (%)	Standard Deviation of Fit (%)
[a]Jezebel	0.20	-0.26	0.23
[b]ZPPR-21A	0.16	0.02	0.19
[b]ZPPR-21B	0.17	-0.07	0.22
[b]ZPPR-21C	0.19	-0.03	0.21
[b]ZPPR-21D	0.20	0.09	0.22
[b]ZPPR-21E	0.21	0.01	0.25
[b]ZPPR-21F	0.23	-0.15	0.26
[a]Godiva	0.20	0.08	0.14
[c]Big10	0.20	0.12	0.32
[d]ZPPR-15A	0.20	0.25	0.30
[c]ZPR-6/6A	0.20	-0.15	0.32
[d]ZPPR-15D	0.20	0.09	0.30
[c]ZPR-6/7	0.20	-0.10	0.32

[a]Bare spheres of Pu and U.
[b]Pu/U/Zr mixtures varying from all Pu to all U.
[c]LANL benchmark of 10%-enriched uranium.
[d]Metal fuel cores of U/Zr and Pu/Zr.
[e]Oxide fuel cores of U and Pu.
[f]Exclusive of data uncertainties.

The fit to these data is excellent and confirms the accuracy of the ZPPR-21 experiments to better than 0.2%. Finally, the VIM code was used to produce corrections to a simple RZ homogenous model with high accuracy (0.14%). This model enabled the ZPPR-21 data to be used easily with other criticality codes such as KENO.

Summary

With present super computers or workstations, it is feasible to perform calculations of half a million histories with the VIM continuous-energy Monte Carlo code and achieve statistical uncertainties which are lower than experimental uncertainty estimates. This enables statistical analysis of the experimental measurements with data sensitivity codes. This, in turn, enables testing of the consistency of a measurement against a range of independent measurements, identification of discrepancies (which points to systematic errors), and can show where further investigation is required before accepting the measurement as a 'benchmark' data point.

The use of the automated construction of VIM Monte Carlo models from the experimental database greatly enhances the usefulness of VIM and eliminates the possibility of human error. The high accuracy achievable with VIM enables cylindrical benchmarks with simple composition to be constructed from complex loadings and for these to be used with other criticality codes.

Acknowledgment

Much of the work on the GMADJ code, its nuclear data covariance file and testing of integral data was achieved in cooperation with W. P. Poenitz.

References

1. W. P. Poenitz and P. J. Collins, "Utilization of Experimental Integral Data for the Adjustment and Uncertainty Evaluation of Reactor Design Quantities," Proc. NEACRP Specialists' Meeting, Jackson, WY (1988).

2. P. J. Collins, et al., "A Data Base for the Adjustment and Uncertainty Evaluation of Reactor Design Quantities," Proc. NEACRP Specialists' Meeting, Jackson, WY (1988).

3. P. J. Collins and M. J. Lineberry, "The Use of Cross Section Sensitivities in the Analysis of Fast Reactor Integral Parameters," Proc. Seminar on Theory and Application of Sensitivity and Uncertainty Analysis, Oakridge, TN (1978).

4. P. J. Collins, S. E. Aumeier, and G. L. Grasseschi, "Evaluation of Integral Measurements for the SP-100 Space Reactor," Proc. ANS Topical Meeting on Advances in Reactor Physics, Charleston, SC (1992).

5. R. W. Schaefer, R. D. McKnight, and P. J. Collins, "Lessons Learned from Applying VIM to Fast Reactor Critical Experiments," Proc. Embedded Topical Meeting on Misapplications and Limitations of Monte Carlo Methods Directed Toward Criticality Safety Analysis, San Diego, CA (1995).

6. W. P. Poenitz and A. D. Carlson, "The Data Base of the Standards and Related Cross Sections After ENDF 1 8-VI," Int. Symposium on Nuclear Data Evaluation Methodology, BNL, Upton, NY, 75-87 (1993).

7. D. N. Olson, P. J. Collins, and S. G. Carpenter, "Experiments for IFR Fuel Criticality in ZPPR-21," Proc. International Conference on Nuclear Criticality Safety, Oxford, UK (1991).

TESTING OF THE ENDF/B-VI NEUTRON DATA LIBRARY ENDF60 FOR USE WITH MCNP™

S. C. Frankle and R. E. MacFarlane
Los Alamos National Laboratory

ABSTRACT

The continuous-energy neutron data library ENDF60, for use with the Monte Carlo N-Particle radiation transport code MCNP4A,[1] was released in the fall of 1994. It is comprised of 124 nuclide data files based on the ENDF/B-VI evaluations through Release 2. Forty-eight percent of these materials are new or modified evaluations, while the balance are translations from ENDF/B-V. The new evaluations include most of the important materials for criticality safety calculations, and include significant enhancements such as more isotopic evaluations, better resonance-range representations, and the new correlated energy-angle distributions for emitted particles. As part of the overall quality assurance testing of the ENDF60 library, calculations for well known benchmark assemblies were performed. The results of these calculations help the user to know how the combination of ENDF60 and MCNP4A will perform for real problems.

INTRODUCTION

Accurate calculations of radiation transport and neutron multiplication in systems with complex composition and geometry are common in the criticality safety field. As computer power, user sophistication, and regulatory oversight have advanced, more of these calculations are made using physically detailed methods, such as the Monte Carlo N-Particle transport code MCNP. Highly capable codes like MCNP also require up-to-date nuclear data, such as those contained in the latest version of the US standard Evaluated Nuclear Data Files, ENDF/B-VI.[2] For the criticality safety expert, it is the combination of the transport code and data library that must be proven, and the purpose of this paper is to present results to help in making this judgment.

ENDF/B-VI (B-VI) was first released in 1990. The original release was followed by minor updates in Release 1 in 1991, and by a number of significant improvements in Release 2 in 1993. Fifty-two percent of the evaluations used for the ENDF60 library are translations from ENDF/B-V. The remaining forty-eight percent are new or modified evaluations, which have sometimes changed significantly. Among these changes are a greatly increased use of isotopic evaluations (especially for important structural materials like Fe, Cr, Ni, and Cu), much more sophisticated and extensive resonance-parameter evaluations (such as ^{235}U and ^{238}U), and energy-angle correlated distributions for emitted particles. Fission yield and radioactive decay data have also

been hugely expanded. The bulk of B-VI and its many new features have somewhat delayed its usage in the applications community.

The ENDF-format evaluations were processed using the NJOY Nuclear Data Processing System[3] to produce data libraries in the ACE (A Compact ENDF) format used by MCNP. During the period 1989 to 1993, NJOY was gradually updated to handle most of the new features of B-VI. In addition, there was a cooperative effort between the NJOY and MCNP teams to enable MCNP and the ACE format to support these new features. Some of the new features include the addition of three new scattering laws (which also involved new data formats, processing methods, transport physics, and a next-event estimator and point detector sampling scheme). These three laws are the Kalbach-87 energy-angle formalism (ENDF File 6 LAW=1, LANG=2; MCNP law 44), correlated angle-energy distributions (ENDF File 6 LAW=7; MCNP law 67), and the phase-space law (ENDF File 6 LAW=6; MCNP law 66). Extensive tests were carried out to ensure that the new scattering laws were properly implemented in MCNP4A and that both transport and next-event estimator solutions agreed. A more detailed discussion of these laws can be found in reference 4.

This work culminated in the processing of the materials for the ENDF60 library using NJOY in late 1993, the testing of the library with MCNP4A during the summer of 1994, and the release of the ENDF60 library in the fall of 1994 to the Radiation Shielding Information Center at Oak Ridge National Laboratory.

ENDF60 DATA TESTING

A number of new quality assurance tests for the ENDF60 library were implemented by the Nuclear Theory and Applications group (T-2) and the Radiation Transport group (X-6). At the lowest level, these included trials to make sure that the files could be printed, plotted, converted to other forms, and staged into MCNP correctly. Key materials were examined by eye and new features were validated by comparison to hand calculations. Many of these low level tests have now been incorporated into the ACER module of the NJOY code to help other users to be able to generate reliable data libraries. Additionally, integral tests were performed by comparing the ENDF60 library with previously available data libraries for a set of infinite-medium and photon production simulations.[5,6]

These kinds of checks are useful for finding errors in the codes and data sets, but most users are more interested in how the combination of the transport code and the data library will perform for their applications. For this reason, the ENDF60 data library was also compared with experimental benchmarks using the Lawrence Livermore Pulsed Sphere experiments and a set of four iron benchmark experiments.[7,8] Additionally, results from the ENDF60 and the ENDF/B-V (B-V) data libraries were compared for a set of nine benchmark critical assemblies that have been used in the past for testing MCNP and for a set of twenty-five benchmark problems for the KENO code.[9,10] Some of the previous MCNP benchmarks had been simplified, and some of the

KENO problems are repeats of one another or fictitious (such as an infinite cylinder). Because of these limitations, these results were useful for seeing how the codes and libraries have changed, but were not necessarily useful for ensuring the accuracy of the computational system. With these caveats, Tables 1 and 2 show the results from both sets of criticality benchmarks using the existing B-V based library and the new ENDF60 library.[4] The column labeled "Recommended" in Table 1 shows the results when the ^{239}Pu in a plutonium assembly is replaced by the recommended evaluation, which was generated for ENDF/B-V.2 and formed the base for the B-VI evaluation.

PERFORMANCE TESTING

For real performance testing, it is important to have a realistic model for the critical assembly. We have revised four of the MCNP models for the assemblies in LA-12212 and defined eight new benchmarks using the specifications from the Cross Section Evaluation Working Group (CSEWG) data testing manual.[11] The remaining five critical assemblies in LA-12212 are still under review. The material specifications for the 3x3 array of Pu fuel rods is known to be correct and the improved B-VI results are thought to be accurate.[9,17] No review of the KENO tests cases has been performed. In the current test suite, there are now four bare critical assemblies; Godiva (CSEWG-F5)[9,11-13] is a bare sphere of highly enriched uranium, Jezebel (CSEWG-F1)[9,11-13] is a bare sphere of enriched ^{239}Pu, Jezebel-Pu is a bare sphere of 20% ^{240}Pu plutonium (CSEWG-F21)[9,11-13], and Jezebel-23 (CSEWG-F19)[11,12] is a bare sphere of ^{233}U. There are four natural uranium reflected assemblies; Flattop-25 (CSEWG-F22)[11-13] has a core of enriched uranium, Flattop-Pu (CSEWG-F23)[11-13] has a core of Pu-239, Flattop-23 (CSEWG-F24)[11-13] has a core of U-233, and Bigten (CSEWG-F20)[11] is a larger assembly with a 10% U-235 core. Additionally, there is also a natural thorium reflected ^{239}Pu sphere benchmark, Thor (CSEWG-F25).[11,12] There are three thermal benchmarks; ORNL-1 (CSEWG-T1)[11] a large sphere of uranyl nitrate solution, L-7 (proposed CSEWG)[15] a water-reflected sphere of uranyl fluoride solution, and a water-reflected uranium sphere[9,14].

The results for these assemblies are given in Table 3 for both the ENDF/B-V and ENDF/B-VI libraries. The entries for Godiva, Jezebel, Jezebel-Pu, and the water reflected uranium sphere can be compared to the corresponding entries in Table 2 to see the effects of the revised models. The results for Godiva have decreased and increased for the B-V and B-VI based libraries respectively, with the B-VI library giving a value for k_{eff} closer to 1.0. The results for the plutonium spheres of the Jezebel assemblies have decreased, coming closer to a value of 1.0 for both libraries. The results for the water-reflected uranium sphere remain relatively unchanged for both libraries. Overall, the results for the bare uranium and plutonium spheres are quite good with the B-VI based library ENDF60.

The ^{233}U evaluation was translated from B-V to B-VI, however photon production was added after the MCNP B-V based library was processed. For these benchmarks, the addition of photon production to the evaluation should not affect the results. The primary changes between MCNP

Table 1. Critical Assembly Benchmarks

	Recommended	ENDF/B-V	ENDF/B-VI
Godiva 93.71% Enriched Bare Sphere	*	1.0001 ± 0.0010	0.9952 ± 0.0011
Jezebel - 95.5% Enriched ^{239}Pu	0.9986 ± 0.0021	1.0151 ± 0.0022	1.0023 ± 0.0022
Jezebel - 80% Enriched ^{239}Pu	1.0080 ± 0.0012	1.0160 ± 0.0012	1.0097 ± 0.0012
Uranium Cylinder 10.9% Enriched ^{235}U	*	1.0010 ± 0.0006	0.9998 ± 0.0005
Uranium Cylinder 14.11% Enriched ^{235}U	*	1.0009 ± 0.0006	0.9972 ± 0.0005
Graphite-Tamped Uranium Sphere	*	0.9869 ± 0.0010	0.9810 ± 0.0010
Water-Reflected Uranium Sphere	*	0.9967 ± 0.0019	0.9961 ± 0.0019
Three Cylinders of Uranium Solution	*	1.0016 ± 0.0013	0.9961 ± 0.0014
3x3 Array of Pu Fuel Rods	1.0008 ± 0.0017	1.0076 ± 0.0017	0.9992 ± 0.0015

libraries for ^{233}U are due to improvements in the processing code NJOY. The results in Table 3 indicate that both libraries give similar results for Jezebel-23 and Flattop-23.

All of the natural uranium reflected assemblies give moderately high results for k_{eff} for both B-V and B-VI. This has been a long-standing feature of CSEWG calculations for these assemblies, and it suggests that some work needs to be done on the transport cross section for ^{238}U. The thorium reflected assembly, Thor, has improved somewhat from B-V to B-VI, however the result is still quite high for B-VI. This has also been a long-standing feature of the CSEWG benchmark, and may indicate a need for a new evaluation of thorium.

The performance of ENDF60 for thermal systems is somewhat more complicated. The results for the water-reflected sphere of uranium were discussed above and remain relatively unchanged. The three cylinders of uranium solution[16] from Table 1 is known to have material specification problems that have not been corrected, and cannot be used to judge the accuracy of ENDF60 at this time. The results from ORNL-1 show a significant decrease, while the results from L-7 remain relatively unchanged. It is difficult to separate out the contribution to the change in k_{eff} as H, O, C, and F are also all new evaluations. Simulations performed using the B-V evaluation for

Table 2. KENO Benchmarks

	ENDF/B-V	ENDF/B-VI
Keno 1	0.9999 ± 0.0009	0.9936 ± 0.0009
Keno 2	0.9999 ± 0.0009	0.9936 ± 0.0009
Keno 3	0.9993 ± 0.0011	1.0002 ± 0.0011
Keno 4	1.0008 ± 0.0028	0.9998 ± 0.0026
Keno 5	1.0004 ± 0.0028	1.0044 ± 0.0029
Keno 6	0.7461 ± 0.0007	0.7426 ± 0.0007
Keno 7	1.0002 ± 0.0008	0.9954 ± 0.0008
Keno 8	0.9404 ± 0.0008	0.9381 ± 0.0007
Keno 9	2.2910 ± 0.0010	2.2597 ± 0.0009
Keno 10	0.9999 ± 0.0009	0.9936 ± 0.0009
Keno 11	0.9999 ± 0.0009	0.9936 ± 0.0009
Keno 12	0.9987 ± 0.0012	0.9994 ± 0.0013
Keno 13	0.9949 ± 0.0008	0.9914 ± 0.0008
Keno 14	0.9985 ± 0.0008	0.9969 ± 0.0008
Keno 15	1.0016 ± 0.0010	1.0003 ± 0.0011
Keno 16	0.9907 ± 0.0009	0.9924 ± 0.0009
Keno 17	1.0029 ± 0.0014	0.9986 ± 0.0015
Keno 18	1.0280 ± 0.0013	1.0308 ± 0.0013
Keno 19	0.9987 ± 0.0012	0.9994 ± 0.0013
Keno 20	0.9971 ± 0.0013	0.9981 ± 0.0015
Keno 21	0.9951 ± 0.0008	0.9929 ± 0.0009
Keno 22	0.9978 ± 0.0008	0.9955 ± 0.0008
Keno 23	0.9999 ± 0.0009	0.9936 ± 0.0009
Keno 24	0.9982 ± 0.0008	0.9944 ± 0.0008
Keno 25	1.0012 ± 0.0009	0.9952 ± 0.0009

^{235}U with all other nuclides specified as B-VI gave values for k_{eff} of 0.9907 ± 0.0016, 0.9963 ± 0.0009, and 1.0007 ± 0.0019 for the water-reflected uranium sphere, ORNL-1 and L-7 benchmarks respectively. This indicates a decrease, sometimes very small, in k_{eff} for most of the B-V and B-VI results. This seems to indicate that the B-VI evaluation for ^{235}U is more reactive, giving higher values for k_{eff}.

In the past, the CSEWG thermal data testing effort has obtained interesting results for the series of large homogeneous uranyl-nitrate solution assemblies (ORNL-1 and others) and for a series of smaller uranyl-fluoride assemblies (L-7 and others), both built at ORNL. Earlier B-V

Table 3. Revised and New Criticality Benchmarks for MCNP

	ENDF/B-V	ENDF/B-VI
Godiva CSEWG-F5	0.9953 ± 0.0011	0.9992 ± 0.0012
Jezebel CSEWG-F1	1.0051 ± 0.0018	1.0003 ± 0.0020
Jezebel-Pu CSEWG-F21	1.0041 ± 0.0011	1.0003 ± 0.0012
Jezebel-23 CSEWG-F19	0.9923 ± 0.0011	0.9926 ± 0.0010
Flattop-25 CSEWG-F22	1.0058 ± 0.0015	1.0048 ± 0.0013
Flattop-Pu CSEWG-F23	1.0088 ± 0.0015	1.0042 ± 0.0015
Flattop-23 CSEWG-F24	1.0031 ± 0.0015	1.0041 ± 0.0015
Bigten -2D CSEWG-F20	1.0031 ± 0.0010	1.0053 ± 0.0011
Thor CSEWG-F25	1.0138 ± 0.0014	1.0083 ± 0.0013
Water-Reflected Uranium Sphere	0.9967 ± 0.0019	0.9946 ± 0.0018
ORNL-1 CSEWG-T1	1.0007 ± 0.0010	0.9956 ± 0.0009
L-7 Proposed CSEWG	1.0034 ± 0.0017	1.0022 ± 0.0016

and B-VI multigroup calculations show a trend of increasing multiplication with increasing leakage (typically 0.6 to 0.7 percent between the low leakage and high leakage limits).[18] In addition, the multiplication for the low-leakage systems with B-VI gave low values for k_{eff} by approximately 0.3 percent, with B-V values being very close to unity. An analysis of the situation suggested that the resonance capture integral for ^{235}U was the source of the leakage bias and small problems in the thermal cross sections were responsible for the low multiplication. A modified evaluation is being prepared for Release 3 of ENDF/B-VI.[19]

CONCLUSIONS

The combination of MCNP4A and the ENDF60 library is now available for making criticality safety calculations. The combination of the geometrical flexibility, faithful physics modeling, and continuous-energy accuracy of MCNP with the modern cross section data of

ENDF60 provides a very powerful and defendable tool. The new library gives quite good results for a variety of critical assemblies, and the new data which will become available from Release 3 of B-VI will hopefully improve the performance of the system even more in the near future.

REFERENCES

1. "MCNP-A General Monte Carlo N-Particle Transport Code," ed. J. Briesmeister Los Alamos National Laboratory manual, LA-12625 (1993).

2. "ENDF-102 Data Formats and Procedures for the Evaluated Nuclear Data File ENDF-6," ed. P. Rose and C. Dunford, Brookhaven National Laboratory, BNL-NCS-44945 (revised 1991).

3. R. E. MacFarlane and D. W. Muir, "The NJOY Nuclear Data Processing System, Version 91," Los Alamos National Laboratory manual LA-12740-M (1994).

4. "ENDF/B-VI Data for MCNP," J. Hendricks, S. Frankle, and J. Court, Los Alamos National Laboratory Report, LA-12891 (1994).

5. "MCNP ENDF/B-VI Validation: Infinite Media Comparisons of ENDF/B-VI and ENDF/B-V," J. Court, J. Hendricks, and S. Frankle, Los Alamos National Laboratory Report, LA-12887 (1994).

6. "Photon Production Assessment for the MCNP Data Libraries," S. C. Frankle, Los Alamos National Laboratory report, to be published.

7. "Lawrence Livermore Pulsed Sphere Benchmark Analysis of MCNP ENDF/B-VI," J. Court, R. Brockhoff, and J. Hendricks, Los Alamos National Laboratory Report, LA-12885 (1994).

8. "Benchmark Analysis of MCNP ENDF/B-VI Iron," J. Court and J. Hendricks, Los Alamos National Laboratory Report, LA-12884 (1994).

9. "MCNP: Criticality Safety Benchmark Problems," J. Wagner, J. Sisolak, and G. McKinney, Los Alamos National Laboratory report, LA-12415 (1992).

10. "MCNP: Neutron Benchmark Problems," D. Whalen et al, Los Alamos National Laboratory Report, LA-12212 (1991).

11. "ENDF-202: Cross Section Evaluation Working Group Benchmark Specifications," Brookhaven National Laboratory Report, BNL 19302, (revised 1991).

12. "Los Alamos Critical-Mass Data," H.C. Paxton, Los Alamos National Laboratory report, LA-3067-MS, Rev., (1975).

13. "Reevaluated Critical Specifications of Some Los Alamos Fast-Neutron Systems," G.E. Hansen and H.C. Paxton, Los Alamos National Laboratory report, LA-4208, (1969).

14. "Critical Measurements of a Water-Reflected Enriched Uranium Sphere," C.C. Byers et al., Transactions of the American Nuclear Society, 27, pg. 412 (1977).

15. "Thermal Data Testing Memorandum 81-2," P. Rose, Brookhaven National Laboratory memorandum (1981).

16. "Critical Dimensions of Systems Containing 235U, 239Pu, and 233U," H.C. Paxton and N.L. Pruvost, Los Alamos National Laboratory Report, LA-10860-MS, 1986 Revision, pg. 131 (1987).

17. "Summary of Experimentally Determined Plutonium Array Critical Configurations," H.F. Finn et al., Lawrence Livermore National Laboratory Report, UCRL-51041 (1971).

18. "Data Testing of ENDF/B-VI," R. E. MacFarlane, Proceedings of the International Conference on Nuclear Data for Science and Technology, pg. 786 (1994) .

19. "A Modification to ENDF6 U235 To Increase Epithermal Alpha and K1," C. R. Lubitz, Proceedings of the International Conference on Nuclear Data for Science and Technology, pg. 646 (1994).

WEDNESDAY, MAY 17, 1995

SESSION IV
BENCHMARK COMPARISONS

LESSONS LEARNED FROM APPLYING VIM TO FAST REACTOR CRITICAL EXPERIMENTS*

R. W. Schaefer, R. D. McKnight and P. J. Collins

Introduction

VIM is a continuous energy Monte Carlo code first developed around 1970 for the analysis of plate-type, fast-neutron, zero-power critical assemblies.[1] In most respects, VIM is functionally equivalent to the MCNP code[2] but it has two features that make uniquely suited to the analysis of fast reactor critical experiments: 1) the plate lattice geometry option, which allows efficient description of and neutron tracking in the assembly geometry, and 2) a statistical treatment of neutron cross section data in the unresolved resonance range. Since its inception, VIM's capabilities have expanded to include numerous features[3], such as thermal neutron cross sections, photon cross sections, and combinatorial and other geometry options, that have allowed its use in a wide range of neutral-particle transport problems.

The earliest validation work at Argonne National Laboratory (ANL) focused on the validation of VIM itself.[4,5] This work showed that, in order for VIM to be a "rigorous" tool, extreme detail in the pointwise Monte Carlo libraries was needed, and the required detail was added. The emphasis soon shifted to validating models, methods, data and codes against VIM. Most of this work was done in the context of analyzing critical experiments in zero power reactor (ZPR) assemblies.

The purpose of this paper is to present some of the lessons learned from using VIM in ZPR analysis work. This involves such areas as uncovering problems in deterministic methods and models, pitfalls in using Monte Carlo codes, and improving predictions. The numerical illustrations included here were taken from the extensive documentation cited as references.

Infinite Lattice Calculations

A systematic study was executed to validate the cross section processing scheme used in ZPR analysis at Argonne National Laboratory,[6,7] with emphasis on unit cell homogenization. VIM and deterministic solutions were compared for a series of model problems, ranging from infinite homogeneous media to infinite lattices of three-dimensional plate and pin unit cells with an imposed buckling. Based on these comparisons, one dimensional modeling approximations and methods approximations were established that accurately predict cell average fluxes, reaction rates and leakage for core unit cells of typical liquid-metal fast reactor (LMR) mockups.

---

*Work supported by the U.S. Department of Energy, Reactor Systems, Development and Technology, under Contract W-31-109-Eng-38.

Even before that study was completed, difficulties were encountered in the analysis of a mockup of a different reactor concept, the gas-cooled fast reactor (GCFR). Using VIM solutions to infinite lattice problems as a reference, the standard deterministic method for treating neutron streaming in coolant channels were found to be inadequate when the channels were essentially voids, as in the GCFR. An alternative diffusion coefficient was developed to treat this situation.[8] Other problems occurred in the analysis of the steam-filled GCFR mockup, representing the postulated steam ingress accident.[9] It was found, through comparisons with VIM cell calculations, that errors caused by the narrow resonance approximation (NRA), which for the LMR and normal GCFR cells were unimportant, were large when steam was introduced. The data in Table I, taken from this evaluation of the NRA, illustrate the detailed level at which comparisons were made to diagnose problems in the calculations. Neglect of energy loss in anisotropic scattering, the "inconsistent P_1" approximation, also was found to cause an significant error in deterministic calculations of steam ingress reactivity.

Assembly Eigenvalue Calculations

A practical barrier to making criticality predictions with VIM for ZPR experiments was the difficulty of producing a detailed, three-dimensional whole core model. A high fidelity model requires many thousands of lines of input, even in plate lattice geometry, the hand production of

Table I. Errors in Deterministic (MC^2 Code) Calculations of ^{239}Pu Absorption Rate In a Normal (Dry) and Steam-Filled (Wet) GCFR Mockup.

	Dry				Wet			
	VIM		MC^2 - NRA	MC^2/RABANL	VIM		MC^2 - NRA	MC^2/RABANL
Group	$\Sigma_a\phi$[a]	% Uncertainty[b]	% Error	% Error	$\Sigma_a\phi$[a]	% Uncertainty[b]	% Error	% Error
1	1.104E-3	4.85	+0.77		1.164E-3	5.78	-1.80	
2	3.887E-3	1.60	+1.44		3.871E-3	2.04	-2.82	
3	1.128E-2	1.15	+0.98		1.043E-2	1.27	+0.86	
4	1.736E-2	0.82	-1.56		1.509E-2	1.10	+2.52*	
5	2.229E-2	0.87	-0.36		1.903E-2	0.96	-0.16	
6	4.623E-2	0.56	+0.48		3.364E-2	0.71	-0.83	
7	3.727E-2	0.45	+0.16		2.471E-2	0.57	+0.93	
8	4.673E-2	0.36	-0.49		2.704E-2	0.73	+0.07	
9	5.015E-2	0.39	-0.08		2.492E-2	0.55	+0.40	
10	4.684E-2	0.35	-1.11*		2.136E-2	0.95	-0.47	
11	4.411E-2	0.30	-0.18		1.872E-2	0.57	+2.08*	
12	3.194E-2	0.35	-0.41		1.509E-2	0.86	+0.99	
13	3.961E-2	0.31	-0.58		1.787E-2	0.75	+0.39	
14	3.154E-2	0.46	-0.13		1.737E-2	1.12	+0.23	
15	1.985E-2	0.39	+0.10		1.569E-2	0.82	-0.64	
16	2.302E-2	0.51	-1.56*	-0.56	2.141E-2	1.13	-0.79	+0.23
17	2.138E-2	0.47	-2.01*	-0.61	2.471E-2	0.94	-2.91*	-0.63
18	1.769E-2	0.67	-0.68	-0.28	2.689E-2	0.96	-3.68*	-0.70
19	1.222E-2	0.85	+0.33	-1.88*	2.836E-2	1.25	5.68*	-2.49
20	8.106E-3	1.00	+4.54*	-1.28	3.267E-2	1.00	3.58*	-1.67
21	3.265E-3	1.44	+8.82*	-2.66	2.628E-2	1.51	-0.68	-1.68
22	2.929E-3	2.00	+10.86*	+0.20	5.683E-2	1.44	+0.53	+2.54
23	2.018E-3	11.2	+55.30*	+7.48	4.071E-2	2.30	+23.29*	+3.35
24	1.569E-6	53.9	+3.12	+5.35	1.548E-2	3.42	+38.37*	+2.34

[a]Track Length Estimators.

[b]One Standard Deviation.

*More than 2 standard deviations.

which is tedious, time consuming and prone to error. Despite this, a number of ZPR assemblies were modeled successfully by hand. Reasonable compromises were made in which only representative unit cells were modeled but these were quite detailed. The task was partially automated at the ZPR 6 and 9 facilities. Ultimately, an automatic VIM input generation system, BLDVIM, was created at the ZPPR facility, which accessed the full assembly description on the ZPPR computer database. Fig. 1, which is a two-dimensional slice through one cell modeled using BT DVIM, gives an indication of the detail included in the model. This automation was important for three reasons: it made practical the modeling of assemblies in full detail, it greatly reduced the amount of labor required to produce a model and, most importantly, it offered a high degree of quality assurance, i.e., the probability of input errors was reduced markedly.

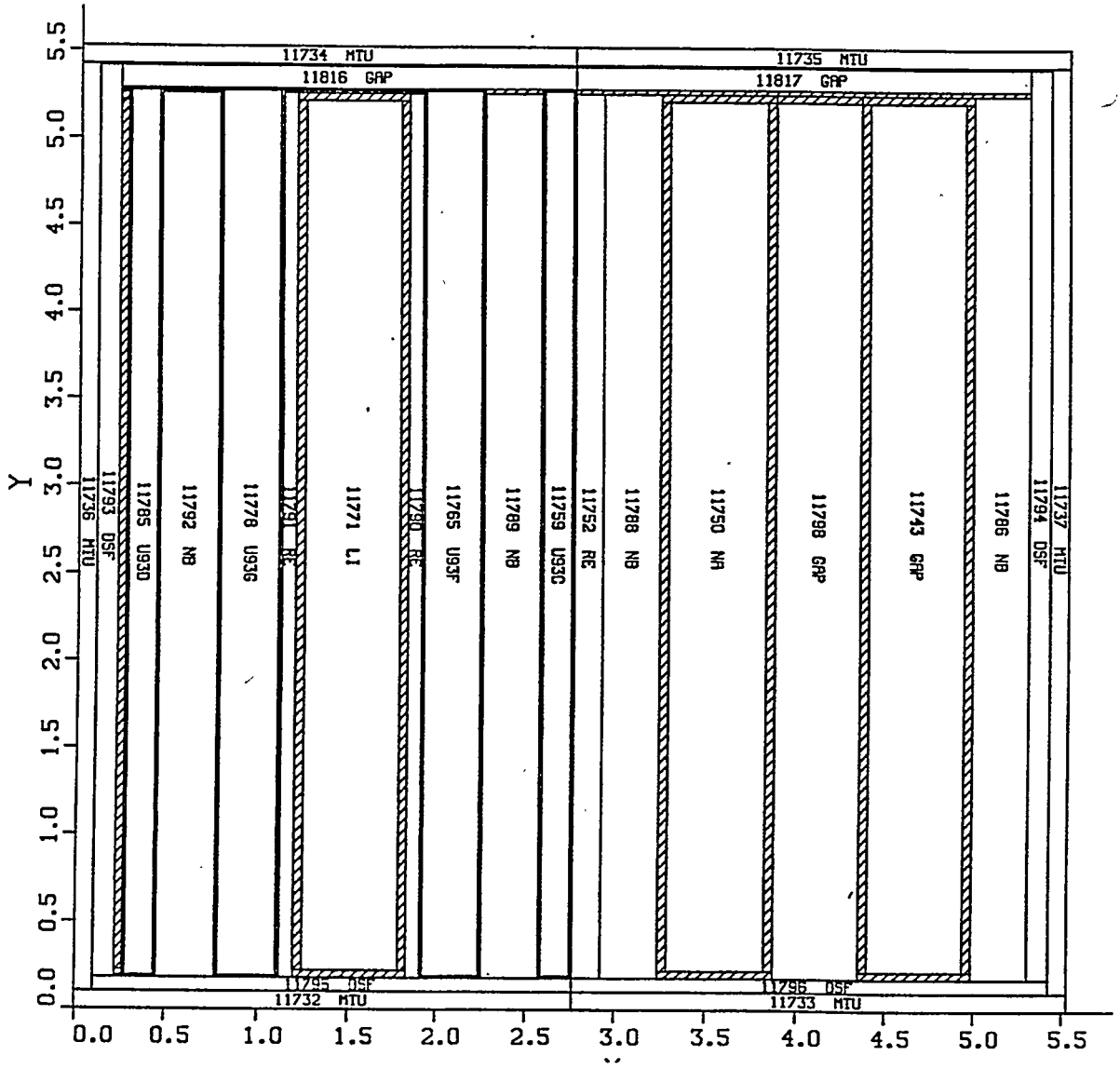

Fig. 1. XY Plane Through Model of Drawer Master 20-2-206 at Z=13.0 cm.

Probably the first benefit derived from whole core ZPR calculations with VIM was the discovery of a bug in VIM. Two sets of VIM calculations of Reactor Safety Research assemblies, produced independently by different analysts, had eigenvalue solutions that were close but uniformly discrepant beyond one standard deviation. Recognition that the results taken as a whole were statistically inconsistent precipitated an investigation that uncovered the code bug.

Problems with deterministic cross section processing codes were uncovered as a result of VIM calculations for ZPR mockups whose core compositions were dominated by iron and ^{235}U. When standard deterministic eigenvalue predictions for a critical configuration were found to be more than 3% below unity, a whole core VIM calculation was run. The VIM prediction agreed much better with experiment. This motivated comparisons between VIM and deterministic solutions in a series of related model problems. The main error was found to be neglect of resonance behavior in the ENDF/B high energy "smooth" elastic scattering cross sections of structural materials such as iron.[10] Algorithms to treat this phenomenon were implemented in the deterministic codes.[11]

How results from plate critical experiments should be applied in power reactor design depends on how well calculations account for the heterogeneity difference between the plate cells of critical assemblies and the pin cells of power reactors. Pin and plate versions of nearly the same core design were built, first in the UK[12] and later at ZPPR. VIM was used to calculate eigenvalues for these assemblies, helping to separate discrepancies into data, methods and experimental components.

In time, VIM eigenvalue calculations were made for enough ZPR assemblies that trends and biases could be observed.[13] Table II is an example from Ref. 13. Eigenvalues for mixed-oxide-fueled LMR mockups are larger by about 0.2% when computed by the standard deterministic approach compared to those from VIM. For a wider range of fast reactor compositions the discrepancy is as large as 0.5%. These errors are mostly associated with misprediction of leakage.[10] There is a 3% spread among eigenvalues computed for critical ZPR assemblies with VIM and ENDF/B Version 4 nuclear data, implying the existence of significant deficiencies in the basic ENDF/B data.

Having VIM predictions of integral parameters (primarily eigenvalues) for a wide range of fast critical assemblies makes it possible to reduce markedly the impact of deficiencies in cross section data.[14,15] Using ENDF/B Version 5 data, VIM calculations have been done for dozens of assemblies, including ones built at Los Alamos, at ZEBRA in the UK and at the ZPRs at ANL. A generalized least squares procedure has been used to adjust multigroup cross section sets within their uncertainties such that the integral parameters as a whole are predicted more accurately. As one example of the insight gained, errors in Version 5 high energy boron absorption cross sections were identified through a difference in the error in control rod worths from a hard spectrum space reactor mockup compared to those from LMR mockups.

Table II. K_{eff} Predictions for Six Assemblies Using Deterministic and Monte Carlo Methods.

Assembly	VIM Histories	$k_{eff} \pm 1\sigma$ (VIM)[a]	k_{eff}(MC²-2/SDX)[b]	k_{eff}(MC²-2/SDX) - k_{eff}(VIM)[a]
ZPR-6/7	300,000	0.9781 ± 0.0011	0.9809	+0.0028 ± 0.0011.
ZPR-9/32	200,000	0.9952 ± 0.0016	1.0005	+0.0055 ± 0.0016
ZPR-9/34	100,000	0.9817 ± 0.0026	0.9865	+0.0047 ± 0.0026
ZPR-9/36	100,000	1.0070 ± 0.0022	1.0101	+0.0030 ± 0.0022
ZPPR-11B	500,000	0.9858 ± 0.0009	0.9909	+0.0051 ± 0.0009
ZPPR-12	250,000	0.9983 ± 0.0013	0.9994 0.9983[c]	+0.0011 ± 0.0013 +0.0000 ± 0.0013

[a] Uncertainty is 1σ estimate from the VIM Monte Carlo calculation only.

[b] These MC²-2/SDX eigenvalues are reference multigroup diffusion theory calculations corrected for higher order effects (e.g., transport, streaming, mesh, etc.) of known significance.

[c] This value is calculated with three-dimensional nodal transport methods [9].

Calculating Other Assembly Parameters

As computing power increased, it became practical to compute, with adequate statistical precision, experimental quantities besides eigenvalue using VIM. VIM was used to investigate mispredictions of reaction rate distributions in a ZPR mockup of the radially heterogeneous Clinch River Breeder Reactor. Comparisons of radial reaction rate distributions from experiments, deterministic calculations and VIM calculations revealed that the discrepancies with experiment were a combination of deficiencies in the ENDF/B Version 4 nuclear data and inaccuracies in the deterministic cross section processing methods used for the mix of core and blanket plate cells in this reactor design.[16] Table III is an example from Ref. 16 showing the increasing error in nonthreshold reaction rates as radius increases that is attributable to deficiencies in the ENDF/B-IV data.

Another investigation of errors in radial reaction rate distributions lead to the discovery that the uncertainty estimates from VIM could be misleading. For radial reaction rates in the very large, radially heterogeneous assembly, ZPPR-13A, the variance was observed not to have the expected linearly inverse relationship with fission rate. This was traced to serial correlations among successive batches, caused by the use of the fission source distribution computed in the previous batch, and made important by the unusually small eigenvalue separation between the fundamental mode and the first harmonic.[17]

VIM has also been used to test the accuracy of a correction factor needed in the reduction of experimental subcritical multiplication data. Ordinarily, source importance ratios[18] can be computed accurately by standard deterministic methods but, in the case of reflector worth in the SP-100 space reactor mockup, those methods were of questionable validity. The VIM

Table III. Comparison of Reaction Rates by Radial Zone From VIM and Experiment.

	VIM Calculation/Experiment			
Zone[a]	$^{239}Pu(n,f)$	$^{235}U(n,f)$	$^{238}U(n,\gamma)$	$^{238}U(n,f)$
CB	-	1.006	1.045	0.958
F1	0.986	1.006	1.029	0.966
B1	-	1.011	1.042	0.961
F2	0.987	1.036	1.050	0.954
B2	-	1.014	1.051	0.983
F3	0.999	1.039	1.050	0.935
B3	-	1.059	1.063	0.977
F4,5	1.018	1.059	1.075	0.968
RB	-	0.995	1.042	0.935

[a] Radial zones from center, outward, (CB=central blanket; F1=fuel ring 1, etc.; B1=internal blanket ring 1, etc.; RB=radial blanket). For the three nonthreshold reactions, VIM 1σ uncertainties vary from 1.5% in CB to 0.5% in RB, and for ^{238}U fission the range is 2.5% to 1%.

calculations confirmed the suspicion that the conventionally-computed factors were less accurate than usual and allowed appropriate uncertainty estimates to be assigned to the experimental worths.

Conclusion

The VIM code was used for many years in conjunction with fast reactor critical experiments, yielding a wealth of information. Long ago the frequency and severity of deficiencies uncovered in VIM decreased to the point where it was considered to be a mature, reliable tool whose accuracy is limited only by statistical precision and the accuracy of basic cross section data. This not withstanding, it is incumbent on users always to be critical evaluators searching for evidence of code deficiencies, input errors, etc. VIM has been used to improve standard modeling and to identify errors in deterministic calculations. It has even been helpful in the discovery of errors in cross section data.

References

1. L. B. LEVITT and R. C. LEWIS, "VIM-I, A Nonmultigroup Monte Carlo Code for Analysis of Fast Critical Assemblies," AI-AEC-12951, Atomics International (1970).

2. J. F. BRIESMEISTER, editor, "MCNP - A General Monte Carlo N-Particle Transport Code, Version 4A," LA-12625, Los Alamos National Laboratory (1993).

3. R. N. BLOMQUIST, "VIM," *Proc. Int. Topl. Mtg. Advances in Mathematics, Computations, and Reactor Physics,* Pittsburgh, PA, April 28 - May 2, 1991, Vol. 5, p. 30.4 2-1, American Nuclear Society, ISBN: 0-89448-161-4 (1991).

4. R. E. PRAEL, "Cross Section Preparation for the Continuous-Energy Monte Carlo Code VIM," *Proc. Conf. Nuclear Cross Sections and Technology,* Washington D.C., March 3-7, 1975, Vol. 1, p. 447, NBS Special Publication 425 (1975).

5. R. E. PRAEL and H. HENRYSON II, "A Comparison of VIM and MC²-2 - Two Detailed Solutions of the Neutron Slowing-Down Problem," *Proc. Conf. Nuclear Cross Sections and Technology,* Washington D.C., March 3-7, 1975, Vol. 1, p. 451, NBS Special Publication 425 (1975).

6. D. C. WADE, "Monte Carlo-based Validation of the ENDF/MC²-II/SDX Cell Homogenization Path," ANL-79-5, Argonne National Laboratory (1979).

7. R. D. MCKNIGHT, "Validation Results for the SDX Cell Homogenization Code for Pin Geometry," *Nucl. Sci. Eng.,* **75**, 111 (1980).

8. E. M. GELBARD et al., "Calculations of Void Streaming in the Argonne Gas-cooled Fast Reactor Critical Experiments," *Nucl. Sci. Eng.,* **64**, 624 (1977).

9. R. W. SCHAEFER, "Calculations of Steam Worth in a GCFR Lattice," *Trans. Am. Nucl. Soc.,* **28**, 772 (1978).

10. R. D. MCKNIGHT et al., "Validation Studies of the ENDF/MC²-2/SDX Cell Homogenization Path," *Proc. Topl. Mtg. on Advances in Reactor Physics and Core Thermal Hydraulics,* Kiamesha Lake, NY, September 22-24, 1982, Vol. 1, p. 406, NUREG/CP-0034 (1982).

11. R. N. HWANG, B. J. TOPPEL and H. HENRYSON II, "Improved Algorithms for the Calculation of Resolved Resonance Cross Sections With Applications to the Structural Doppler Effect in Fast Reactors," ANL-80-104, Argonne National Laboratory (1980).

12. M. J. GRIMSTONE, J. L. ROWLANDS and J. M. STEVENSON, "Progress Report on the International Comparison of Calculations for the CADENZA Assemblies (the Pin-Plate Benchmark)," *Proc. Topl. Mtg. on Reactor Physics and Shielding,* Chicago, IL, September 17-19, 1984, Vol. II, p. 738, American Nuclear Society (1984).

13. R. D. MCKNIGHT, P. J. COLLINS and D. N. OLSEN, "The Critical Eigenvalue in LMFBRs: A Physics Assessment," *Proc. Topl. Mtg. on Reactor Physics and Shielding,* Chicago, IL, September 17-19, 1984, Vol. II, p. 750, American Nuclear Society (1984).

14. P. J. COLLINS et al., "A Data Base for the Adjustment and Uncertainty Evaluation of Reactor Design Quantities," *Proc. NEACRP Specialists' Mtg. on Application of Critical Experiments and Operating Data to Core Design via Formal Methods of Cross Section Data Adjustment,* Jackson, WY, September 23-24, 1988, p. 77, NEACRP-L-307, Nuclear Energy Agency Committee on Reactor Physics (1988).

15. P. J. COLLINS and S. E. AUMEIER, "Utilization of VIM Monte Carlo Calculations for Fast Reactor Experimental Data Analysis," these proceedings.

16. P. J. COLLINS and R. D. MCKNIGHT, "A Monte Carlo Calculation for ZPPR-11B," NEACRP-A-665, Nuclear Energy Agency Committee on Reactor Physics (1984).

17. R. N. BLOMQUIST, "Monte Carlo Neutronic Analysis of a Loosely Coupled Reactor," these proceedings.

18. S. G. CARPENTER et al., "Conclusions Drawn From Subcritical Multiplication Results in ZPPR," *Proc. Topl. Mtg. on Advances in Reactor Physics,* Gatlinburg, Tennessee, April 10-12, 1978, CONF-780401, p. 467, (1978).

MONTE CARLO ANALYSIS OF A LOOSELY COUPLED REACTOR*

Roger N. Blomquist
Argonne National Laboratory

In this paper, we discuss the difficulties encountered in Monte Carlo analysis (using VIM[1]) of the Zero Power Physics Reactor Assembly 13A, a neutronically loosely-coupled radial heterogeneous fast reactor. In particular, the fission rate statistical errors in large reactor core zones were badly underestimated, although the statistics were apparently quite good. The principal eigenvalue was not affected, however.

The reactor consists of a square array of steel lattice sites into which are slid rectangular, open-top "drawers" containing plates of fuel, structure, coolant, control, and other materials. The drawers are arranged in a radially heterogeneous pattern, so from the center outward, there are the inner blanket, the inner core, a middle blanket, the middle core, a second middle blanket, the outer core, the radial blanket, and a reflector. Each blanket consists of relatively densely packed blanket pins which are rather strongly absorbing; hence the radial decoupling among the three radial core zones.

In "well-behaved" Monte Carlo reactor calculations, i.e., in which the generations are essentially independent after convergence to the fundamental mode, the estimated variance $\sigma 2$ is proportional to 1/N, where N is the number of scores and the proportionality is a function of the dispersion of the scores. For a reactor in which the phase space is well-sampled and in which essentially no variance reduction methods are applied to the random walks, we should observe relatively lower relative variances in regions with higher fission rates. Nevertheless, in one ZPPR-13A calculation, the track-length fission rate estimates were $0.148 \pm 1.63\%$, $0.330 \pm 0.93\%$, and $0.523 \pm 1.22\%$, for the inner, middle, and outer radial cores, respectively. If, based on the number of scores, we extrapolate the one-sigma error estimate from the middle core to the outer core, we would expect an error of only 0.74%; but the observed error estimate was high by a factor of over 1.6.

An independent calculation with 240 generations of 1000 histories per generation was performed to provide data for further statistical analysis. To consider the effects of serial correlation among generations, the average estimates of the outer core fission rate over sets of 20 consecutive generations were computed, and are shown in Table 1. Between sets of generations, the fission rate undergoes remarkable shifts which are far outside of statistics (e.g., 6σ at generation 60).

To better understand these anomalies, we chose to investigate the dramatic rise in the fission rate near generation 60. Examining the fission rate for each generation showed that the overall change in the fission rate occurred because of a 10% increase between the ends of generations 63 and 64 to a level which then persisted for 17 generations. We restarted the Monte Carlo

Table 1. Outer core fission rate trends.

Generations	Fission Rate
1-20	0.138±1.1%
21-40	0.139±1.6%
41-60	0.134±1.3%
61-80	0.153±1.6%
81-100	0.147±1.7%
101-120	0.147±2.0%
121-140	0.139±1.7%
141-160	0.142±2.6%
161-180	0.152±1.3%
181-200	0.145±1.8%
201-220	0.150±1.3%
221-240	0.150±1.4%

calculation from the fission sites produced during generation 62, repeating generations 63 and 64 ten times, each time with a new random number sequence. Because the only information passed between generations is the continuation of the random number series and the fission site distribution, we could determine whether the increase in fission rate was preordained by the spatial distribution of starting particles, or whether it arose during the course of generation 63 or during generation 64. Over the ten independent repeats, the generation 63 and 64 fission rates were only 0.1372 ± 0.0023 (with a maximum of 0.148) and 0.1392 ± 0.0024 (with a maximum of 0.151), respectively. This indicated that the generation 62 fission site distribution was consistent with the previous generations, and contained no shift which could have caused the higher outer core fission rate after generation 63.

Taking the set of fission sites produced by the original generation 63, we then repeated (independently) generation 64 six times. The average fission rate estimate was 0.1508 ± 0.0042, (with a minimum or 0.137), nearly 3σ above the preceding generation. This indicated that the shift in the fission rate was indeed caused by a shift in the fission site distribution during generation 63. A comparison of the radial fission site distributions for the two generations did show a clear spatial shift; the sites produced in generation 63 were spatially much more similar to those produced in generation 64 than to those produced in the independent repeats of generation 63. The fission sites were inspected to verify that no particular sites were chosen many times, an occurrence which would have indicated a code bug or other non-physical and non-statistical problem.

Two statistical techniques were applied to fission rate tallies from two independent Monte Carlo calculations to correct for the effects of correlation: (1) generation grouping, and (2) MacMillan's method. In grouping, we lumped the tallies into groups of N generations (for N=l, 2, 4, 8, and 16), and recomputed the error estimates for the grouped data in each simulation. The effect of grouping the generations is to reduce the effects of serial correlation, since the histories in the i-th group are N generations removed from those in the i-l-th group. Table 2, which includes results from the above-mentioned calculation and a separate independent replica, shows this quite clearly; the correlation coefficients tend to zero and the error estimates increase as the group size is increased. In fact, the fluctuations noted in Table 1 are consistent with the larger error estimates resulting from grouping generations.

Table 2. Outer core fission rate statistics (grouped generations).

Run	Gens/ Batch	VIM σ	r_1	r_2	r_2/r_1	C
1	1	0.00066	0.642	0.540	0.84	3.01
1	2	0.00084	0.682	0.531	0.78	2.68
1	4	0.00111	0.632	0.340	0.54	1.93
1	8	0.00146	0.433	-0.027	—	~1
1	16	0.00190	-0.019	0.011	—	~1
2	1	0.00066	0.692	0.614	0.89	3.63
2	2	0.00086	0.731	0.503	0.69	2.39
2	4	0.00113	0.608	0.372	0.61	2.03
2	8	0.00148	0.560	0.243	0.43	1.72
2	16	0.00184	0.512	0.462	0.90	3.35

For non-independent samples, the variance of the mean is

$$\sigma^2 = E\left[\frac{\left(\sum \xi_i\right)^2}{N}\right] ,$$

where ξ_i is the deviation of the i^{th} sample from the mean. The usual calculation of the error estimate relies on the fact that the cross terms in the square of the summation cancel, which they do not when they are correlated. By making an assumption about the distribution of the higher mode eigenvalues, MacMillan[2] derived an estimate of a multiplicative factor to correct for the correlation among generations. The sums of the cross terms were shown to be the lag-n autocorrelation coefficients, so the correction factor can be given by

$$C = \sqrt{1 + \frac{1 + 2r_1}{1 - r_2/r_1}} \quad ,$$

where r_1 and r_2 are the lag-1 and lag-2 correlation coefficients, respectively, and their ratio is the eigenvalue dominance ratio. Table 2 also shows the MacMillan factors computed for the fission rate, for each group size. The erratic correlation coefficients for N=16 are probably indicative of inadequate statistics for generating the correction factors — they appear to be too unreliable to use in MacMillan's scheme.

The ZPPR-13A calculations point out a recurring feature of Monte Carlo calculations of loosely coupled systems. It is crucial to understand the effects of the higher eigenmodes on the fission source iteration process, not just because of the well-known contamination of final tallies by the fission source guess, but also because the stochastic simulation process itself can excite higher modes and produce misleading error estimates.

References

[1] R. N. Blomquist, "VIM", proc. ANS topical meeting on *Advances in Mathematics, Computations, and Reactor Physics*, April 28 - May 2, 1991, Pittsburgh, PA.

[2] D. B. MacMillan, "Monte Carlo Confidence Limits for Iterated-Source Calculations," Nucl. Sci. Eng, **50**, 73-87 (1973).

THE USE OF DETERMINISTIC CODES FOR 'SEPARATING THE WHEAT FROM THE THE CHAFF' IN BENCHMARK MODELS AND CALCULATIONS

R. Douglas O'Dell
Los Alamos National Laboratory

An important effort in the field of nuclear criticality safety is the establishing and modeling of a set of benchmark critical (or near critical) experiments and the use of these benchmark experiment models to validate and verify computer codes and cross sections. For the most part Monte Carlo codes such as MCNP and KENO.Va have emerged as the codes of choice in the U.S. Since Monte Carlo codes generally have the capability of modeling complex geometries in great detail there is a tendency to focus attention on modeling an experiment in very great detail. Indeed, it is the author's observation that so much effort is expended trying to *exactly* model unimportant details (the 'chaff') that many of the truly significant features and characteristics (the 'wheat') of the experiment can be lost in the shuffle. An obvious question now arises. How does one determine what is 'wheat' and what is 'chaff'?

This presentation will focus on the use of deterministic, or, more specifically, discrete-ordinates codes for performing sensitivity calculations in determining which details are important and which are not.

The principal advantage of discrete-ordinates codes is that they can quite precisely determine the effect on k_{eff} associated with distinct details of an experiment such as impurities, external structure, conflicting or missing information, etc.

Three different examples are used to demonstrate the value of using discrete-ordinates codes for separating the wheat from the chaff. It is also shown that, for all practical purposes, Monte Carlo codes are essentially unsuited for determining small effects on k_{eff}.

Example 1.

The first example uses an idealized model of the original Pu-239 Jezebel benchmark experiment, a sphere of delta-phase plutonium at a density of 15.61 g/cc. The Pu parts were all nickel plated (nominal 0.005 in. thick) for contamination control. We choose to try to determine the effect of this nickel clad on the exterior surface of a 17.020 kg sphere of plutonium metal. Using the ONEDANT discrete-ordinates code with three different multigroup cross section sets we find the results shown in Table 1. Included in the results is the incremental plutonium surface-mass-equivalent to the 58 g Ni plating on the sphere that can be readily determined with ONEDANT. The wall clock time to perform each of these calculations was less than 1 minute on a Sun SPARCstation 10.

Table 1. Effect of External Ni Plating on Jezebel: ONEDANT

CROSS SECTION SET	k_{eff}, No Ni	k_{eff} with Ni	Δk_{eff}	Pu Mass Equivalent
Hansen-Roach 16 Grp	1.00122	1.00227	0.00105	63 g
ENDF/B-IV 27 Grp	0.99776	0.99895	0.00119	71 g
ENDF/B-V 30 Grp	0.99362	0.99483	0.00121	72 g

For comparison with a Monte Carlo code, MCNP was used to make three independent estimates of the worth of the Ni plating. For each of the runs one million active histories were executed. The elapsed wall clock time for each run was about 40 minutes on a Sun SPARCstation 10. The results are shown in Table 2. These results show the difficulty in estimating the worth of the Ni plating using Monte Carlo. About all that can be said is that it doesn't seem to be worth very much.

Table 2. Effect of External Ni Plating on Jezebel: MCNP

Run	k_{eff}, No Ni	k_{eff} with Ni	68% Δk_{eff}	95% Δk_{eff}
1	0.99714 ± 0.00050	0.99914 ± 0.00060	0.00200 ± 0.00078	0.00200 ± 0.00156
2	0.99643 ± 0.00060	0.99794 ± 0.00059	0.00151 ± 0.00084	0.00151 ± 0.00168
3	0.99844 ± 0.00058	0.99936 ± 0.00064	0.00092 ± 0.00086	0.00092 ± 0.00173

Example 2.

For the second example we use the so-called ^{240}Pu, or "dirty" Jezebel spherical critical assembly that was comprised of plutonium with 20.1 at. % ^{240}Pu and 3.1 at. % ^{241}Pu. Because ^{241}Pu decays with a 14.4 yr half life to ^{241}Am we will determine the reactivity effect of ^{241}Am following five years of ^{241}Pu decay. Results from the ONEDANT discrete-ordinates code with two different cross section sets are shown in Table 3. Each calculation required less than 1 minute wall clock time.

Table 3. Effect of ^{241}Am Buildup in the ^{240}Pu Jezebel Assembly

CROSS SECTION SET	k_{eff}, No ^{241}Am	k_{eff} with ^{241}Am	Δk_{eff}
ENDF/B-IV 27 Grp	0.99991	0.99847	0.00144
ENDF/B-V 30 Grp	0.99537	0.99432	0.00105

For a Monte Carlo comparison, results from three independent KENO V.a pairs of calculations using ENDF/B-IV 27 group cross sections are shown in Table 4. For each of the calculations 1.8 million active histories were run and the elapsed wall clock time for each run was about 20 minutes on a Sun SPARCstation 10. Once again, Monte Carlo gives us little information other than the effect of the ^{241}Am appears to be fairly small.

Table 4. Effect of ^{241}Am Buildup in the ^{240}Pu Jezebel Assembly: KENO V.a

Run	k_{eff}, No Am	k_{eff} with Am	68% Δk_{eff}	95% Δk_{eff}
1	0.99916 ± 0.00064	0.99784 ± 0.00062	0.00132 ± 0.00089	0.00132 ± 0.00178
2	0.99935 ± 0.00063	0.99923 ± 0.00069	0.00012 ± 0.00093	0.00012 ± 0.00187
3	1.00026 ± 0.00067	0.99918 ± 0.00061	0.00108 ± 0.00091	0.00108 ± 0.00181

Example 3.

For our final example we consider a fairly common uncertainty that arises in modeling early experiments, namely an uncertainty in what kind of steel was used in an experiment. We use the SHEBA 5% enriched uranyl fluoride solution reactor as an example and determine the difference in k_{eff} assuming the tank material is pure iron instead of stainless steel 304L.

Results from the TWODANT discrete-ordinates code with ENDF/B-IV 27 group cross sections give a k_{eff} with SS304L of 1.00934 and a k_{eff} with pure iron of 1.00980 for a Δk_{eff} of 0.00046, a very small change in k_{eff}. Wall clock time for each of these calculations was about 45 minutes.

For a Monte Carlo comparison, results from two independent KENO V.a pairs of calculations using ENDF/B-IV 27 group cross sections are shown in Table 5. For each of the calculations 1.2 million active histories were run and the elapsed clock time for each run was about 3 hours on a Sun SPARCstation 10. Even with this large number of histories, the results from the Monte Carlo runs are not resolved sufficiently to give us much useful information.

Table 5. Effect of SHEBA Tank Composition on k_{eff} : KENO V.a

Run	k_{eff}, SS Tank	k_{eff}, Fe Tank	68% Δk_{eff}	95% Δk_{eff}
1	1.00868 ± 0.00071	1.00853 ± 0.00073	–0.00015 ± 0.00102	–0.00015 ± 0.00204
2	1.00706 ± 0.00067	1.01035 ± 0.00072	0.00329 ± 0.00098	0.00329 ± 0.00197
3	1.00692 ± 0.00070	1.00852 ± 0.00071	0.00160 ± 0.00100	0.00160 ± 0.00199
4	1.00830 ± 0.00066	1.00905 ± 0.00073	0.00075 ± 0.00098	0.00075 ± 0.00197
5	1.00819 ± 0.00067	1.00789 ± 0.00072	–0.00030 ± 0.00098	–0.00030 ± 0.00197

From the above examples it should be clear that discrete-ordinates codes are excellent tools for determining whether modeling details have a significant effect on the k_{eff} of the basic problem being analyzed. Many modeling features or uncertainties whose effect on the basic problem is small can be simplified or omitted without diminishing the value of the basic analysis. The use of Monte Carlo codes to calculate reactivity effects of, say 0.001 in k_{eff}, is virtually an exercise in futility since literally tens of millions of histories are likely to be required to definitively resolve such small effects. Cluttering up a model with too much neutronically-

insignificant detail tends to cloud over the essential features and characteristics of the system being analyzed. We must never lose sight of the fact that the Jezebel assemblies were fundamentally bare spheres of plutonium metal or that SHEBA is fundamentally a bare cylinder of uranyl fluoride solution.